Volume 5 DECEMBER, 1934 Number 12

PHYSICS

A Journal of General and Applied Physics

The Electrical Conductivity of Glass

Part I. The Formation of Highly Resistant Layers

H. R. KIEHL, *Pennsylvania State College*

(Received August 31, 1934)

An effort is made to distinguish more clearly between two types of phenomena which may occur in some glasses: (1) a "reversible absorption" current due to the formation of a high counter electromotive force, and (2) an "irreversible absorption" current due to the formation of a highly resistant layer in the glass. Characteristic curves showing one type of the latter which may occur under certain conditions are given. Although many observers seem to have observed both phenomena previously, considerable confusion still seems to exist in distinguishing between them. Combinations of both phenomena may be one possible cause of some of the large discrepancies in current-time behaviors reported. A study of the relatively small, slowly decreasing residual electromotive force observed upon discharging the sample shows a linear increase of this electromotive force with increase in temperature for temperatures as high as 150°C.

I. INTRODUCTION

THE vagueness and contradictory nature of the data in the literature on the conductivity of many solids, and especially on the conductivity of glass indicates the existence of variables which have not been sufficiently taken into account. A series of investigations on the behavior of some one solid insulating material whose electrical history is rather completely known should therefore be of value. It is the purpose of this series of papers to report the first results of such a series of investigations.

Glass was chosen for the first of such a series because of the many properties which it seems to have in common with other solid and liquid insulating materials as well as because of its commercial importance. A knowledge of the fundamental processes in glass may lead to important predictions concerning the behavior of these other materials.

One of the possible causes of variations in the electrical characteristics of glasses seems traceable to the presence of highly resistant layers in the glass in the vicinity of one or both electrodes. One type of layer seems to be produced by an excess of one type of ion at either one or both electrodes giving rise to a space charge which is evidenced externally by a large counter e.m.f. opposing the applied potential difference. The production of such an opposing e.m.f. causes a fall-off of current with time to a constant final value. Discharge of the sample causes a large reverse current to flow which falls off to zero in about the same time. This type of behavior has been observed by many and has been designated as the "reversible absorption current." Much concerning the nature or behavior of such layers is, however, still to be determined. Another type of layer which also causes a fall-off of current with time due probably to an actual increase in resistance of a portion of the sample without production of a very large counter e.m.f., has also been observed in glasses, by Warburg,[1] Gunthershulze,[2] Le Blanc and Kershbaum,[3] and

[1] E. Warburg, Wied. Ann. **31**, 622 (1884); **32**, 432 (1887); **35**, 455 (1889); **41**, 18 (1890); Ann. d. physik. Chemie **21**, 622 (1884).
E. Warburg and F. Tegetmeier, Wied. Ann. (1888); Ann. d. physik. Chemie **35**, 455 (1888).

[2] A. Gunthershulze, Ann. d. Physik **37**, 435 (1912).

[3] M. Le Blanc and F. Kershbaum, Zeits. f. physik. Chemie **72**, 4, 468 (1910).

others. However, little seems quantitatively known concerning the nature of this type of current decrease with time. From the observations made in the present series of studies the nature of this decrease appears in many instances to be similar to that previously mentioned when the field is applied, but the reverse currents on discharging the sample are very small in comparison. Furthermore, these layers, produced by the penetration of foreign ions from the electrode, may remain permanently "frozen" in the glass. They seem also to change permanently many of the electrical properties of the glass in which they are produced. Some of these changes have already been observed by Le Blanc and Kershbaum,[3] Gunthershulze,[2] and by Mulligan, Ferguson and Rebbeck.[4] Similar effects may possibly exist in various other types of insulating materials. The present discussion emphasizes the apparent difference between two effects which seem to have been confused by many observers, and attempts to point out the possible effect of the simultaneous action of these two phenomena in causing the many apparent discrepancies in existing time-current data.

II. Apparatus

(a) The samples of glass used for the present series of tests were rectangular microscope cover slides approximately 44 mm×50 mm in size and from 0.15 mm to 0.30 mm in thickness. In some cases circular specimens 25 mm in diameter and similar thickness were used. They were obtained from the Central Scientific Company and specified as "non-corrosive" soda-lime glass. Knowledge of the exact composition was not considered necessary for present investigations. Both sides of the glass were chemically silvered, with a layer sufficiently thick to produce good surface conductivity. Surplus silver not in contact with the electrodes was removed.

(b) The apparatus used was designed for flexibility in the study of the materials chosen, as well as in the range of voltages and temperatures used. Fig. 1 represents a cross-sectional view of this apparatus.

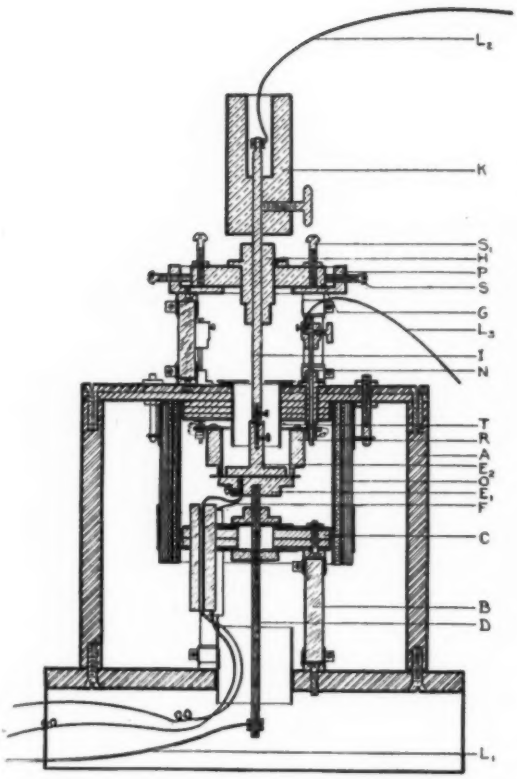

Fig. 1. Diagram of apparatus. L_1, L_2—brass lead wires, K—brass cylinder, S_1—leveling screw, H—brass bushing, P—brass ring, S—adjusting screw, G—circular brass plate, L_3—guard ring lead, I—$\frac{1}{8}$" brass rod, N—guard ring supporting rods, T—metallic electrode shield, R—guard ring, A—steel case, E_2—upper electrode, O—electric oven, E_1—lower electrode, F—copper-advance thermocouple, C—circular platform supporting lower electrode, B—Pyrex insulating post, D—$\frac{1}{8}$" threaded brass rod.

It consisted of a steel case A 20.4 cm high and 18.4 cm in length, open at front and back. Mounted on the base by three Pyrex posts B 5.6 cm high and 1 cm in diameter was a circular platform C, consisting of several layers of transite with metal facing plates. Passing through a hole in the center of the platform was a threaded brass rod D, supporting the lower electrode E_1, on which the sample was mounted. The hole in the platform C was large enough to allow lateral adjustment of the electrode, while the threaded rod D allowed vertical adjustment. The rod could be insulated from the platform by means of mica washers if necessary. The lower electrode E_1 was of brass, diameter 4.0 cm, with the surface in contact with the sample, flat and

[4] Mulligan, Ferguson and Rebbeck, J. Phys. Chem. **32**, 779 (1928); **32**, 843 (1928); **32**, 1018 (1928).

polished. Into a hole extending almost to the upper surface of the electrode E_1 was placed one junction of a copper-advance thermocouple F for measurement of sample temperatures. The thermocouple leads were led through the lower platform by Pyrex capillary tubes, further insulated with mica. With the other junction immersed in an ice bath, thermocouple electromotive forces were read by means of a type K, Leeds and Northrup potentiometer. Surrounding the platform C was a thermally insulated electrical oven O. Temperatures were manually controlled by means of a control rheostat. The oven had sufficient heat capacity to make changes in temperature take place fairly slowly. Temperatures could be kept constant to within 0.2 percent or less at 200°C. To replace the sample or make other necessary adjustments, the oven could be detached from position shown and allowed to rest on the base of the outside case.

Mounted on the top of the metal case which provided thermal insulation above the oven by means of layers of transite was a second circular platform P supported by three Pyrex posts 4 cm high. If greater insulation of this upper platform was necessary, these posts could be replaced by ones of fused quartz. This upper platform served as a support for the upper electrode E_2, to which was connected the current measuring circuit. It consisted of a brass ring on which was mounted a circular brass plate G somewhat smaller in diameter than the inside diameter of the vertical sides of the ring P. By four screws S passing through this vertical side wall, the circular plate G could be laterally adjusted and fixed. Four vertical screws S_1 allowed for leveling of the plate if necessary. Passing through a brass bushing H in the center of this plate was a $1/8''$ brass rod I fitted to allow free vertical motion with a minimum of lateral motion. To the lower end of this rod was attached the brass electrode E_2 32 mm in diameter. The junction between rod and electrode was one allowing free adjustment of this electrode to the sample at all times. Connection between electrode and rod was made with a short brass wire fastened by set screws. Where a joint of this type could be used, adjustment of the electrode by the leveling screws S_1 was unnecessary. To insure intimate contact between electrodes and sample at all times a heavy brass cylinder K was fastened to the upper end of the rod I. The surface of the electrode E_2 in contact with the silvered portion of the glass was flat and polished. Electrical connection was made to both upper and lower electrodes by means of brass leads L_1, L_2 to eliminate as much as possible any small thermal electromotive forces occurring at higher temperatures.

In order to eliminate surface leakage of currents from the measuring circuit, a guard ring R was used. This was kept in place by two vertical rods N passing through brass bushings in the top of the steel case. Vertical motion of these rods, together with flexibility of the attachment of the rods to the ring allowed for automatic adjustments of the ring to the surface of the sample. The ring was of sufficient weight to insure intimate contact at all times with the silvered guard ring on the sample. Connection of guard ring and entire metal case to the circuit beyond the measuring instruments through the proper resistance insured a minimum of potential difference between electrode E_2 and guard ring.

In order to eliminate possible effects due to the ionization of the air which might result when higher potentials were used, a metallic cylinder T was used which extended through the opening in the top of the metal case and surrounded the collecting rod, extending well within the level of the upper surface of the guard ring. The opening in the top of the case was closed with a mica covering to decrease heat losses. When necessary, the entire collecting electrode apparatus on the top of the case could be shielded by a grounded metallic shield.

For some of the earlier tests outlined below, another apparatus was used, slightly different in appearance, but embodying the same essential features as that described here.

III. The Measuring Circuit (See Fig. 2)

The circuit used was the type usually used for direct current conductivity tests, with several special arrangements for some of the tests made. The source of potential was a group of heavy duty 45 volt B batteries, which produced a steady e.m.f. as high as 560 volts with the

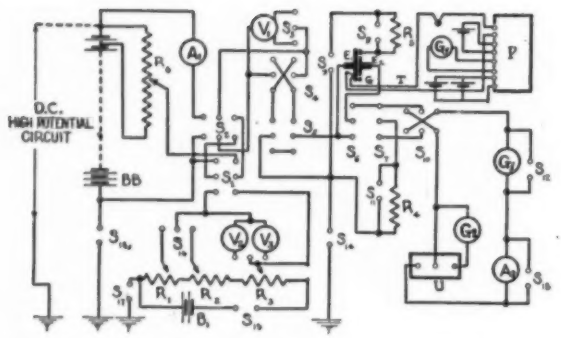

FIG. 2. Circuit diagram. E_1—lower electrode, E_2—upper electrode, BB—"B" battery potential source, A_1—milliammeter 0–10 milliamperes, A_2—milliammeter 0–1.5 milliamperes, G—guard ring, G_1—d'Arsonval galvanometer—sensitivity 1 to 2×10^{-10} amp./scale division, G_2—d'Arsonval galvanometer—sensitivity 1.9×10^{-9} amp./scale division, T, P, G_3—thermocouple and potentiometer circuit, B_1—1.5 to 6.0 volt battery, V_1—double range voltmeter—maximum range 0–600 volts, V_2, V_3—voltmeters with various ranges up to 0–15 volts, U—universal shunt, R_1, R_2, R_3—potentiometer circuit resistances for low "bucking" potentials, R_4—protective resistance 10^5 ohms, R_5—guard ring circuit resistance, R_6—potentiometer circuit resistance for high "bucking" potentials, S_5, S_6, S_7—highly insulated switches, S_1, etc.—switches for use as indicated in circuit diagram.

currents used. For higher potentials the batteries could be replaced by a high potential, kenetron rectified, direct-current source. For the present series few tests with potentials in excess of that supplied by the batteries were used. With the samples used, over-all fields as high as 2.6×10^4 volts/cm could thus be obtained.

One terminal of the high potential source was connected, through the various switches shown, to the lower electrode E_1. In series with the collecting electrode E_2 were connected three current measuring instruments G_1, G_2, A_2 and a protective resistance R_4 of 10^5 ohms. Galvanometer G_1 was either a Leeds and Northrup type R or type P d'Arsonval galvanometer with current sensitivity of 1 to 2×10^{-10} amp./scale division. Galvanometer G_2 was a type P Leeds and Northrup galvanometer of sensitivity 1.9 to 10^{-9} amp./scale division. Connected to G_2 was a universal shunt U allowing sensitivity decrease to 1.9×10^{-6} amp./division. Milliammeter A_2 had a sensitivity of 1×10^{-5} amp./division and a maximum range of 1.5×10^{-3} ampere. Switches S_{12}, S_{13} and shunt U allowed each meter to be individually short-circuited. Switch S_6 was a highly insulated switch allowing direct short-circuiting of sample. Switch S_7 was a single pole, double throw V type switch, so constructed as to keep one or both blades in contact with the terminals at all times, by which the measuring circuit could be short-circuited for convenient zero corrections on instrument readings. Reversal switch S_4 allowed reversal of polarity on the sample. A high resistance, double pole, double throw switch S_5 allowed observations of charge or discharge currents on the sample. A double range voltmeter V_1 allowed potential drops across sample and measuring circuit to be measured.

In order to measure large counter polarization e.m.f.'s by the "bucking" method, switches S_2 and S_1 together with a high resistance voltage divider circuit R_6 for small adjustments of voltage were used. This "bucking" method consisted in the sudden application of a field sufficiently large to equal the existing polarization potential, causing momentarily, no discharge current to flow through the measuring circuit. Successive trials gave the proper value of the voltage to be applied. For measurement of small slowly changing polarization e.m.f.'s which occurred, a special circuit S_1, R_1, R_2, R_3, S_{15}, S_{16}, V_2, V_3 was used. Potential difference was here supplied by batteries of constant e.m.f. from 3 to 6 volts. Adjustment of the potential difference across the sample was made until the current through the measuring instruments was zero. The value of the polarization potential was measured by means of voltmeters V_2 and V_3.

The circuit was thoroughly shielded and insulated where necessary and so constructed as to allow connection of one side of the circuit to ground at will.

IV. RESULTS

At lower temperatures (i.e., up to about 50°C) a current fall-off with time to a final constant value occurred. Short-circuiting the sample resulted in a large reverse current which fell off to zero in about the same time necessary for the original current to reach its constant value. This behavior is similar to that mentioned above and has been designated as the reversible absorption current. Although the measuring instruments used here did not allow measure-

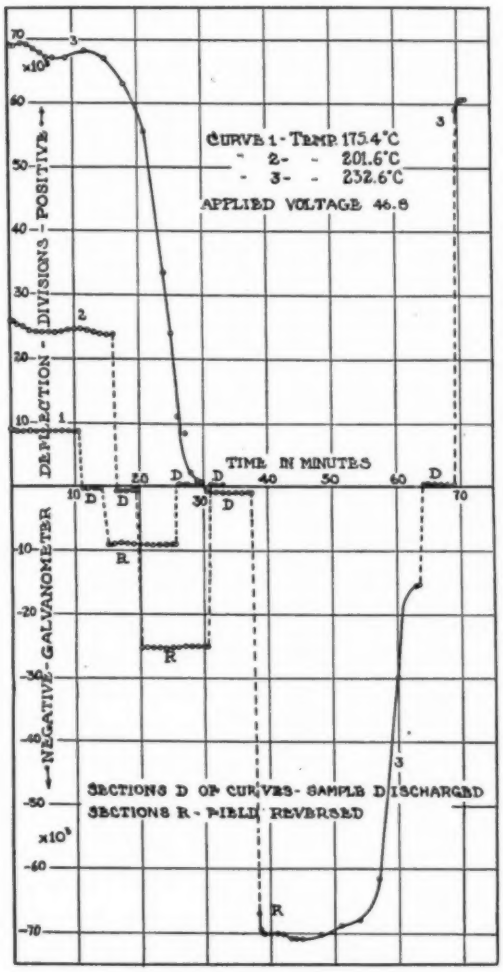
CURVE 1 - TEMP. 175.4°C
2- - 201.6°C
3- - 232.6°C
APPLIED VOLTAGE 46.8
DEFLECTION - DIVISIONS - POSITIVE
NEGATIVE - GALVANOMETER
TIME IN MINUTES
SECTIONS D OF CURVES - SAMPLE DISCHARGED
SECTIONS R - FIELD REVERSED

FIG. 3.

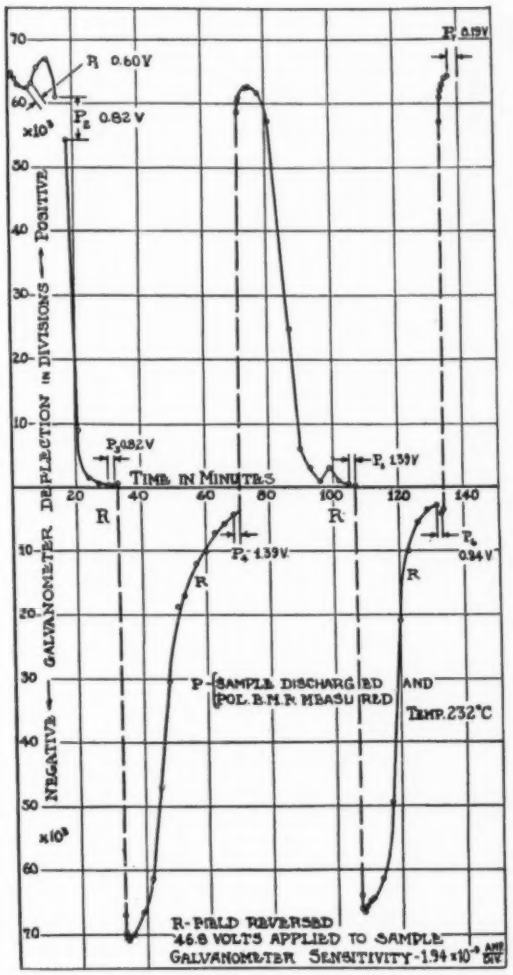

FIG. 4.

ments of current immediately after the application or removal of the field, measurements could be made sufficiently rapidly at room temperature to account for polarization potentials of from 85 to 95 percent of the applied voltage.

As the temperature was increased these original changes became smaller and were finally no longer visible, no doubt due to the slowness of the instruments. The current remained constant over considerable periods of time (Fig. 3, curves 1 and 2). Discharge currents now were small and corresponded to polarization voltages of several volts maximum value. These currents fell off very slowly with time, existing for days before a zero value was reached. They were no doubt similar to those observed by Mulligan, Rebbeck and Ferguson,[4] and thought by them to be chemical in nature. Reversal of the applied potential yielded a reverse current of a magnitude as determined by the applied potential and the polarization potential.

At higher temperatures a second type of behavior becomes increasingly apparent. The constant current is followed by a decrease with time to a new approximately constant value (Fig. 3, curve 3). At higher temperatures or higher fields, this fall-off begins more quickly after the application of the field. This type of behavior noticeably differs from that observed at low temperatures, when the sample is short-circuited, as a discharge of the sample here shows no large reverse current at least fifteen seconds after the sample was short-circuited.

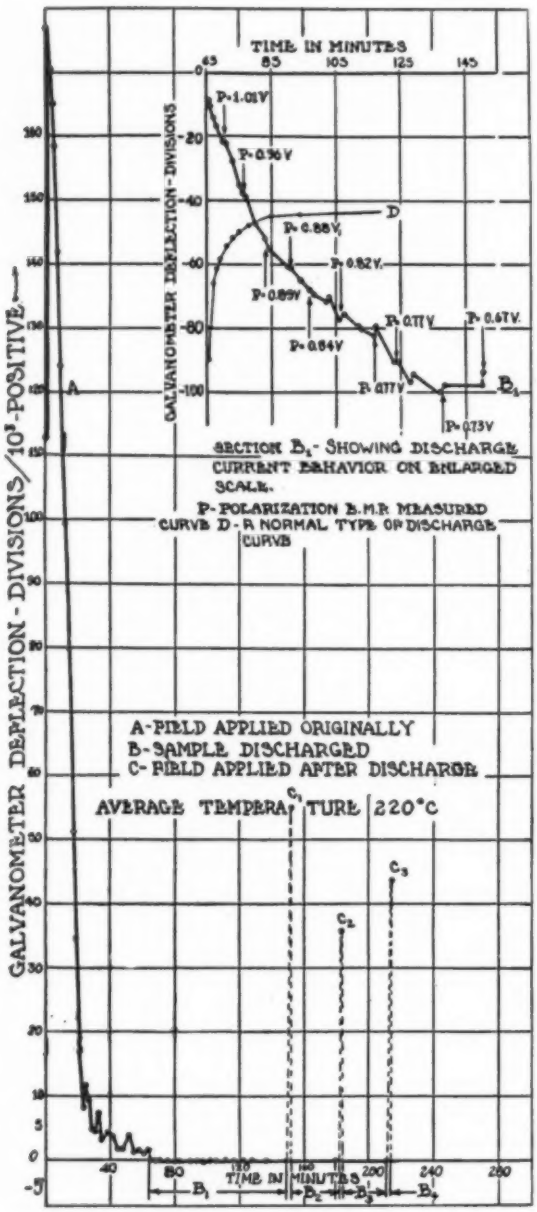

FIG. 5.

With the measuring instruments used, the behavior in shorter times after short-circuiting of the sample could not be observed with certainty. It seems unlikely, however, that this decrease of current with time when the field is applied is due to the production of a large polarization e.m.f., but rather that it is due to the forming of a highly resistant layer only.

Reversal of the applied field causes a current of equal magnitude in the opposite direction which also shows a similar time behavior (Fig. 3, curve 3, R). Continual reversal has been observed here and by other investigators to cause a breakdown of the sample.

On another similar sample (Fig. 4) the polarization was measured by the "bucking" method at various times during the formation of the layer. At no time could an appreciable polarization increase be measured as the current decreased with time. If a greater polarization e.m.f. existed when the current reached the new approximately constant value after the formation of the layer, it must fall off in less than 15 seconds to the small value which was observed with the measuring circuit. If time as great as twenty minutes or more were necessary for its production, it would seem unlikely that it should fall off to a very small fraction of its value in less than 1/100 of this time. Fig. 4 shows values of measured polarizatiom e.m.f. at various times after application and reversals of the field. It will be noticed also that re-applications of the field after these tests resulted in a current similar in magnitude to that observed previous to the "bucking" test. This points also to a pure resistance increase in the glass.

A somewhat different phenomenon is observed for discharge currents of samples into which relatively large amounts of the electrode material were forced at higher temperatures. Instead of having a fall-off of the discharge current with time as is usually observed, a steady increase of discharge current with time was observed. This increase occurred until a maximum value was reached, after which a decrease in current occurred. Section B_1 (curve B_1) of Fig. 5 shows on an enlarged scale a portion of a discharge current of this type. Curve D shows the type of discharge current usually observed. Measurements of the polarization e.m.f. (points P, curve B_1), made while the increase was taking place show a decrease in polarization e.m.f. with time. This gives evidence of an apparent elastic relaxation and decrease in resistance of the sample which seems to occur in these cases. Application of the field once more showed, in some cases, an increase in the charging current over that observed immediately before the sample was discharged. (See C_1, C_2, C_3, Fig. 5.)

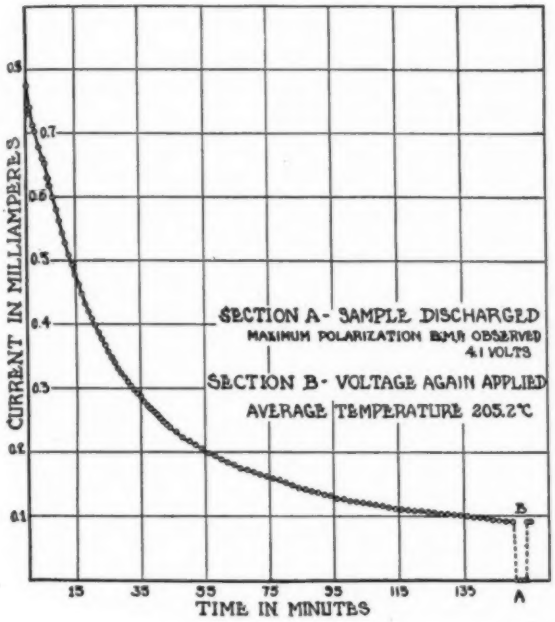

FIG. 6.

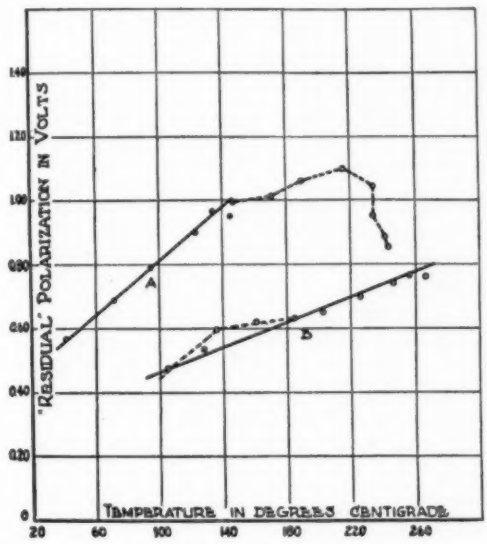

FIG. 7.

A second electrolysis at higher temperatures or with a higher applied field will cause a noticeable change in the time-current relation, as should be expected. Fig. 6 shows the relation between current and time for such a second impregnation of a sample which had previously been electrolyzed at 220°C with application of a field of 2.2×10^3 volts/cm in which the behavior was essentially of the type shown by Figs. 3, 4, 5.

Mulligan, Ferguson and Rebbeck[4] showed that the small, slowly changing polarization e.m.f.'s observed on many samples were chemical in nature. The e.m.f.'s observed here during the slow discharges of the sample described above were of the same order of magnitude as those observed by them. Additional evidence is perhaps added to that of these observers by the observations made here on the variation of this residual e.m.f. with temperature. At a time, and over a range in temperature in which this fall-off of e.m.f. with time was very slow, its variation with the temperature could be observed. By applying an external e.m.f. to the sample of sufficient size so as to cause no discharge current to flow through the measuring circuit, and slowly increasing the temperature of the sample, this residual e.m.f. was found to show a linear increase with temperature. This occurred up to a temperature of about 150°C when apparently internal diffusion in the sample caused a rapid decrease of the e.m.f. Results on one such specimen are shown in Fig. 7, curve *A*. Curve *B* shows the results of a later run on the same sample, after the polarization e.m.f. had decreased to a lower value. The linearity below 150°C seems to strengthen the assumption concerning the electrolytic nature of this type of polarization.

The author wishes to express his indebtedness to Dr. W. R. Ham, Dr. W. P. Davey and Dr. D. C. Duncan for their valuable advice and aid in this work; also to Dr. J. T. Littleton and Dr. E. M. Guyer of the Corning Glass Works for valuable criticisms in the preparation of the manuscript.

The Electrical Conductivity of Glass

Part II. Current Increase Phenomena with Highly Resistant Layers

H. R. KIEHL, *Pennsylvania State College*

(Received August 30, 1934)

With the production of certain types of highly resistant layers in some glasses, increases of current with time are observed, similar to those reported qualitatively by several earlier investigators. The nature of these current increases have been studied quantitatively and found to follow, for the cases here studied, the relationship, $\log (I_m - I_t) = \log a_1 - b_1 t$, where I_m is the maximum value of the current, I_t is the current at any time t after application of the field, and a_1 and b_1 are constants. The time T for the current to reach its maximum value seems related to the applied voltage by the equation $T = K_1/V - K_2$. The values of the constants K_1 and K_2 seem to decrease with increase in temperature. The time for the current to reach its maximum value decreases rapidly with increase in glass temperature. The possible importance of the phenomena observed in an explanation of the processes involved in the conductivity of glass is suggested, and the need for further investigation is emphasized. No theoretical explanation is given because of the apparent necessity for further investigations.

I. INTRODUCTION

A BEHAVIOR, different from that usually observed in insulating materials, has been observed in glass by some investigators. Under certain conditions, with application of the field, the current increases more or less rapidly with time to reach a maximum value; at which it may remain constant for varying periods and then decrease in value. Gunthershulze[1] reports such a current increase when certain electrode materials are used. Heydweiller and Kopfermann[2] report a similar behavior. Schiller,[3] in his study of the conductivity of glasses under high fields, reports such current increases in some cases. Hubmann,[4] in studying conductivity processes in extremely thin glass samples with fields as high as 10^6 volts/cm, also observes a marked increase for some specimens.

Little seems, however, to be quantitatively known concerning these current increases. Hubmann observes that such processes begin immediately with application of the field, and that the maximum value of the current is noticeably influenced by the type of electrodes used. He further observes that the time necessary for the current to reach the maximum value is decreased with increase of field, and suggests the possibility of reciprocal relationship between this time and the applied field. The ratio of the maximum current to the current at the beginning of the increase does not seem to increase rapidly with increase in field strength.

During the series of studies made on the properties of highly resistant layers, some of which were reported previously,[5] similar current increase phenomena were observed. A certain amount of quantitative information was obtained on this type of behavior. The tests are not complete, but represent only a small part of the total information necessary for a complete understanding of the process. No theoretical explanations will, therefore, be attempted until such further data are available. Whether this same behavior would be noted for other types of glass or for different electrodes cannot be stated from the data at present available.

II. APPARATUS

The apparatus and electrical circuit used were the same as those described previously.[5]

III. PROCEDURE

The type of tests made during the entire series of observations may be briefly outlined as follows. Starting with a sample to which a field had not been previously applied (i.e., an "unimpregnated" sample), the values of the final constant current corresponding to a definite

[1] A. Gunthershulze, Ann. d. Physik **37**, 435 (1912).
[2] A. Heydweiller and F. Kopfermann, Ann. d. Physik **32**, 739 (1910).
[3] H. Schiller, Ann. d. Physik **81**, 32 (1926).
[4] H. Hubmann, Ann. d. Physik **9**, 733 (1931).
[5] H. R. Kiehl, preceding paper in this issue.

group of increasing voltages were observed. The temperature of the sample was kept constant while these observations were made. The sample was short-circuited after each application of the field, and the discharge currents observed. On following days succeeding similar runs at higher temperatures were made. The sample was short-circuited and cooled to room temperature between runs. Temperatures were increased for successive runs until values were reached at which highly resistant layers formed too rapidly for the initial constant value of the current to be observed.[5] Impregnation was then allowed to continue until the current had reached an approximately constant value. The sample was then allowed to cool to room temperature, and was short-circuited until a new series of runs similar to those made on the unimpregnated sample were made on succeeding days. Succeeding impregnations were made following this series of tests, and studies made on the changes produced. In all tests except during the actual impregnation, the applied field was removed before a noticeable change in resistivity due to impregnation occurred. At no time during the observations was the direction of the field reversed.

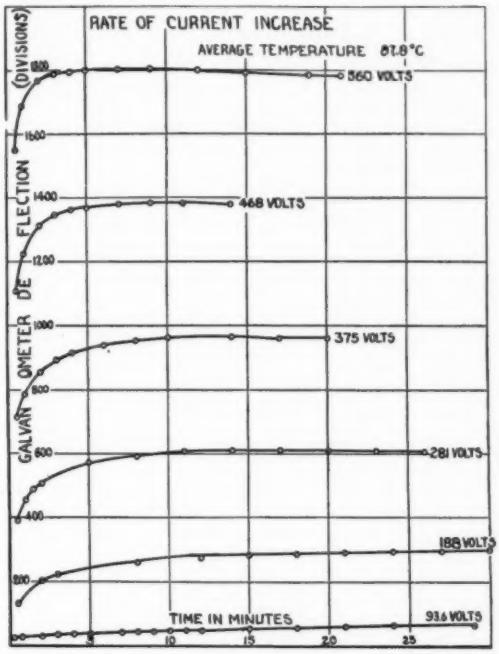

FIG. 1.

IV. RESULTS

For unimpregnated samples the current increase, if present at all, occurred very slowly. Because of this absence or extreme slowness of the current increase, and because of our desire to avoid as much as possible impregnation of the sample, no observations of current increase rates were made on the unimpregnated sample. However, after the first impregnation involving a charge of 2.7×10^{-2} coulombs, a marked current increase occurred with time, similar to that reported by Hubmann[4] on some samples.

(1) General nature of the currents

Starting at a relatively low value, the current increased rapidly with time at first, approaching a maximum value more slowly as time progressed. Fig. 1 shows such increase in current, with constant temperature, for different potential differences applied to the sample. At the lower temperatures or fields the current appeared to remain approximately constant at this maximum value for a considerable period of time. This constant value of the current was then followed by a decrease in current with time. As the temperature of the sample was increased, the period of existence of this maximum current at the constant value decreased, and the fall-off became more marked. In all of the present tests, the sample was short-circuited when the current had reached its maximum value, in order to avoid further possible impregnation of the sample. Quantitative observations of the phenomena were many times rendered difficult by small erratic variations in current due to other sources which occurred.

After a second impregnation involving a charge of 2.0 coulombs on the same sample, the current increase phenomena were no longer observed. Tests made on other samples, in which thinner impregnated layers were used, seemed to indicate that the time for the current to reach its maximum value showed a marked increase with decrease in the layer thickness. It is therefore possible that the increase may have occurred too rapidly to be observed with the instruments available when thicker layers were used.

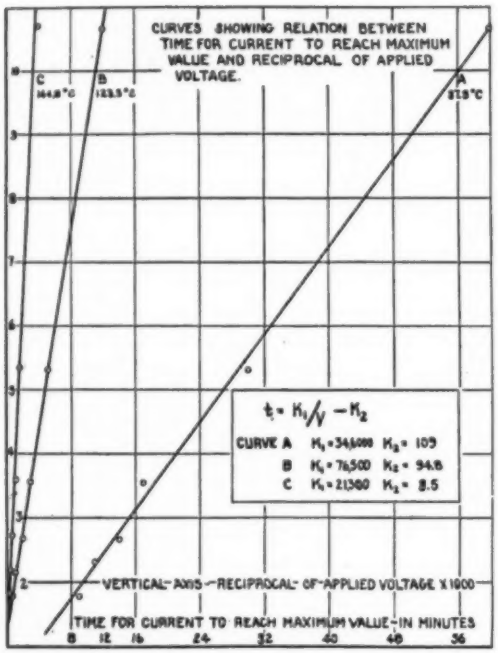
CURVES SHOWING RELATION BETWEEN TIME FOR CURRENT TO REACH MAXIMUM VALUE AND RECIPROCAL OF APPLIED VOLTAGE.
C
B
A
$t = K_1/V - K_2$
CURVE A $K_1 = 346000$ $K_2 = 109$
B $K_1 = 76500$ $K_2 = 94.8$
C $K_1 = 21360$ $K_2 = 8.5$
VERTICAL AXIS—RECIPROCAL OF APPLIED VOLTAGE X 1000
TIME FOR CURRENT TO REACH MAXIMUM VALUE IN MINUTES
8 12 16 24 32 40 48 56

FIG. 2.

(2) Relation between time necessary for current to reach its maximum value and the applied voltage

For a constant temperature the time necessary for the current to reach the maximum value seemed to verify the relationship suggested by Schumann. For the samples studied, this time was found to be inversely proportional to the voltage applied, and could be expressed by the equation $T=K_1/V-K_2$ where T is the time necessary to reach the maximum value; V is the applied voltage, and K_2 and K_1 are constants. Fig. 2, curves A, B, C, show typical relationships of this type. This value of the constants K_1 and K_2 decreased rather rapidly with increase in temperature. Values of K_2 and K_1 for curves A, B, C are shown in Table I.

Observations at various fields show that this relationship seems valid only to definite minimum value of the field; below this value the time of current increase becomes noticeably decreased. In the present sample this critical value seemed to occur between fields of 4.4×10^3 volts/cm and 2.2×10^3 volts/cm. Present data are not sufficient to indicate the complete behavior at these lower fields.

TABLE I. *Values of K_1 and K_2 for curves A, B and C of Fig. 2.*

Temperature	K_2	K_1
87.8°C	109.0	346×10^3
123.5°C	94.8	76.5×10^3
144.8°C	8.5	21.3×10^3

(3) Time of current increase and temperature

With increase in temperature the time necessary for the current to reach the maximum value decreased rapidly until it occurred too quickly to be observed with the instruments available. Data are yet insufficient to indicate quantitatively the relationship between this time and the temperature of the sample. Fig. 3, curves A, B, C serve, however, to indicate the general nature of the behavior. One might expect this decrease to be logarithimic, if the increases in current are related directly to the velocity of diffusion of the moving charges. Further work is being done on the study of this behavior.

(4) The relationship between current and time

The relationship between the increasing current and the time over which this increase occurs seems to be expressed, for the samples studied by the relation $\log\ (I_m-I_t)=\log\ a_1-b_1t$ where I_m

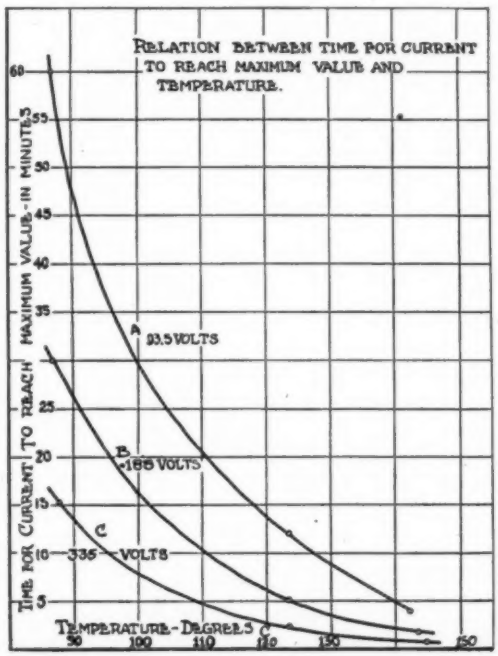
RELATION BETWEEN TIME FOR CURRENT TO REACH MAXIMUM VALUE AND TEMPERATURE.
TIME FOR CURRENT TO REACH MAXIMUM VALUE IN MINUTES
A 93.5 VOLTS
B 185 VOLTS
C 335 VOLTS
TEMPERATURE-DEGREES C
90 100 110 120 130 150

FIG. 3.

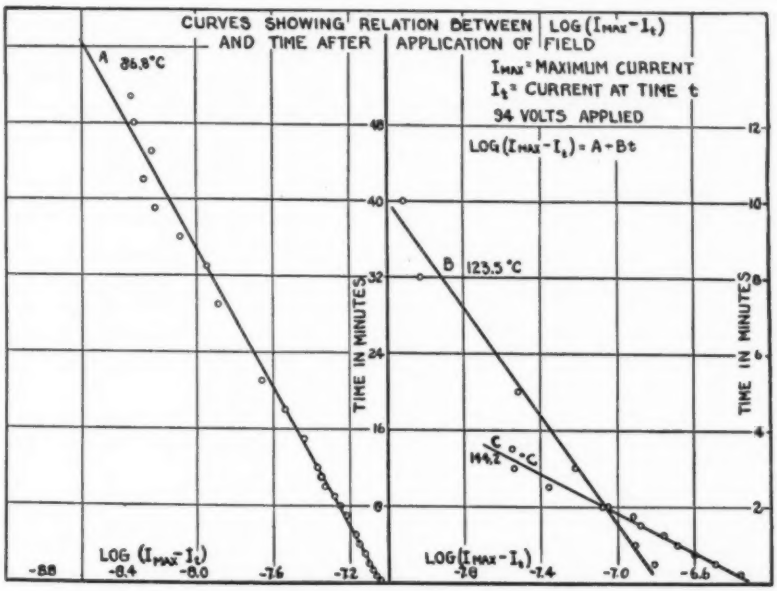
CURVES SHOWING RELATION BETWEEN LOG (IMAX - It)
AND TIME AFTER APPLICATION OF FIELD
IMAX = MAXIMUM CURRENT
It = CURRENT AT TIME t
94 VOLTS APPLIED
LOG (IMAX - It) = A + Bt
A 86.8°C
B 123.5 °C
C 144.2 °C
TIME IN MINUTES
TIME IN MINUTES
LOG (IMAX - It)
LOG (IMAX - It)

FIG. 4.

represents the maximum value of the currents observed, I_t the current at any time t after application of the field and a_1 and b_1 are constants. Fig. 4, curves A, B, C represent typical relationships. The agreement appears remarkably good when one considers the difficulty encountered in getting an accurate value of I_m in many cases. The value of the constant a_1 seems to increase with increase in applied field, at least for the values of the field used. The value of b_1 also shows a marked increase with increase in field.

With increase in temperature an increase in the values of both a_1 and b_1 seems to occur.

Calculation of the values of I_0, the current when $t=0$, for several temperatures from the equation above, shows in all cases a nonlinear relation between I_0 and the field applied, at least for the lower values of the fields used. If this nonlinear relation is due to the existence of polarization e.m.f.'s as assumed in the Joffé theory, they must have been produced in a very small period of time after the application of the field and before the current increase began. The apparatus available did not, however, allow the validity of this assumption to be tested.

Apparently contrary to the results of Hubmann, the ratio of I_0/I_m seems to indicate a definite decrease as the applied field increases. This ratio also decreases with increase in temperature of the sample. Schumann,[6] in discussing theoretically the effects of thin discrete charged layers upon the current-time phenomena, predicts an increase in current with time. The nature of this increase does not seem at first inspection to be that observed in this case. A possible difference in the conditions obtaining here from those in the case proposed by Schumann may be an explanation of the variation observed. A satisfactory explanation of the entire phenomenon observed seems only available after further information concerning the variables involved in the process is obtained. The results of Hubmann seem to indicate that the type of the glass and the type of the electrodes used may influence to a marked extent the behavior of the current increase phenomena. These effects should be investigated. Variations of the behavior of the current with voltage, temperature and thickness of layer and sample must be investigated further.

The author again wishes to express his indebtedness to Dr. W. R. Ham, under whose direction the work was done, and to Dr. D. C. Duncan and Dr. W. P. Davey, as well as to Dr. J. T. Littleton and Dr. E. M. Guyer of the Corning Glass Works, for kind interest and for the many helpful suggestions given.

[6] W. O. Schumann, Archiv. f. Elektrotechnik **27** (3), 155 (March 15, 1933).

The Mechanism of Division of Small Liquid Systems Which Are the Seats of Physico-Chemical Reactions

N. RASHEVSKY, *Department of Physiology, University of Chicago*

(Received July 12, 1934)

In continuation of a previous investigation, the mechanism of division of small liquid droplets, which are the seats of physico-chemical reactions, is being studied now not from thermodynamical, but from the kinetic point of view. Thermodynamical considerations give us conditions under which the whole drop is less stable, than its two halves. It does not say however anything about the degree of stability. The present investigation makes this next step, and shows under what conditions a drop becomes so unstable, that an infinitesimal deformation will lead to a division. The critical sizes calculated here are close to those calculated by thermodynamical method. The importance of "release phenomena" and "valve action" in the cases considered is pointed out.

IN a previous paper[1] we have studied the thermodynamical conditions for the spontaneous division of a small drop, which either absorbs some substances from the outside, or secretes some substances from inside. Due to the variation with the radius of the drop of the difference between outside and inside concentrations, a division of the drop in two is followed above a certain radius by a decrease of free energy, and can therefore happen spontaneously. The critical size, above which this may happen, happens to be of the same order of magnitude as that of living cells.

This previously studied thermodynamical condition for spontaneous division is however found upon closer inspection to be a *necessary*, but not sufficient one. The drop above the critical size is in a relatively stable condition, due to its spherical symmetry. A division of the drop corresponds therefore to a transition from one, relative minimum of free energy, to another one, absolute minimum. And though this second minimum may lie lower, a truly spontaneous transition from one state into another will not take place, if there is a maximum between the two minima, an energy threshold, which has to be overcome by some external disturbance. In case of a low threshold a very small disturbance will bring about the transition of the system from one state of equilibrium into the other. But, even for a very large difference in the energy levels of the two minima, the threshold between them may be so high, that a very large disturbance is required to bring about the transition. Such a transition may never occur. A truly *spontaneous transition* will happen only when the maximum between the two minima disappears, and the upper minimum degenerates into an inflection point with horizontal tangent. Physically speaking, a truly *spontaneous* division of a drop will occur when any infinitesimal deviation from the spherical shape will produce such a distribution of forces along the surface of the drop, which will tend to increase *this deviation*.

Furthermore the following consideration must be kept in mind in dealing with those problems. In homogeneous and simple heterogeneous systems, dealt with in usual thermodynamics, the geometrical structure does not play any essential part. Such systems actually change their configuration spontaneously in the direction of decreasing free energy. This is, however, not always so with systems possessing a definite structure. A simple example will illustrate this. Consider a receptacle divided by an air-tight partition into two compartments, and let the partition have an opening, closed by a one-way valve, that is, a valve which opens in only one direction. If there is an excess of gas pressure on that side of the partition on which the valve opens, this excess of pressure will keep the valve closed. In spite of the fact that the equalization of pressures on both sides is accompanied by the decrease of free energy, such an equalization will never occur spontaneously. Under no condition in such a system will there occur a spontaneous transition to a state of smaller free energy.

In inorganic systems such valve actions play a very little part or no part at all. In biological phenomena, to which this present investigation is closely related, they are frequently of prime importance.

[1] Rashevsky, Physics **2**, 303 (1932).

Let us now consider what forces are active in a drop, such as considered previously, in which various physico-chemical reactions occur. First of all, due to the existence of concentration gradients, gradients of osmotic pressure will be produced, which in their turn will produce a force equal per unit volume to

$$f_0 = -\text{grad } p = -(RT/M)\,\text{grad } c \qquad (1)$$

the notations being the same as before.

Since we have a discontinuity of concentrations at the cell boundary, a pressure

$$p_0 = (RT/M)(\alpha c_e - c_i) \qquad (2)$$

will be produced. c_e and c_i denote the outside and inside concentrations, respectively. The constant α is introduced to take into account the difference of heats of solutions of a substance inside and outside of the drop. For in the absence of any reactions we have $c_i = \alpha c_e$.[1]

Besides the osmotic forces there are, however, other forces proportional to the gradients of the concentration and having the same order of magnitude as the osmotic ones. If the dissolution of one substance in another is accompanied by the liberation of heat, it means that work is done when a molecule of the solute is brought into the solvent. In other words it means that there is a force of attraction between each molecule A of the solvent and each molecule B of the solute. We shall not deal here in detail with the theory of those forces, but shall only roughly estimate their order of magnitude, which will show that in general they may be of prime importance in producing a mechanical instability of the drop.

Let the force between two molecules A and B be given by

$$f = K/r^n. \qquad (3)$$

Let the gradient of concentrations be everywhere along the x-axis, so that c is a function of x only, and consider the attraction on a molecule A of all molecules B, which lie between the planes x and $x+dx$. By using as center the base of the perpendicular dropped from the point occupied by A on the plane x, draw in that plane two concentric circles with radii r' and $r'+dr'$. The attraction of all the molecules B contained in the ring-shaped region limited by the above two planes and by the cylindrical surfaces r' and $r'+dr'$ is given by

$$\frac{Nc(x)}{M}\frac{2\pi K r' dr' dx}{r^n}\frac{x}{r} = \frac{Nc(x)}{M}\frac{2\pi K x dr dx}{r^n}, \qquad (4)$$

where $r^2 = x^2 + r'^2$, N denotes Avogadro's number and $c(x)$ the concentration of B. The force of attraction due to all molecules B lying between the planes x and $x+dx$ is equal to

$$\frac{2\pi KNc(x)xdx}{M}\int_x^\infty \frac{dr}{r^n} = \frac{2\pi KNc(x)dx}{M(n-1)x^{n-2}} \qquad (5)$$

and the force of attraction due to all molecules B lying to the right of the molecule A is given by

$$\frac{2\pi KN}{M(n-1)}\int_d^\infty \frac{c(x)dx}{x^{n-2}} = \frac{2\pi KNc(d)}{M(n-1)(n-3)d^{n-3}} + \frac{2\pi KN}{(n-1)(n-3)M}\int_d^\infty \frac{dc/dx}{x^{n-3}}dx. \qquad (6)$$

d denotes the smallest distance to which two molecules can approach and is given by[2]

$$d = (M_1/\rho_1 N)^{\frac{1}{3}} \sim 10^{-8}\text{ cm}, \qquad (7)$$

where M_1 and ρ_1 are, respectively, the molecular weight and the density of the solvent. The second integral of the right-hand side of (6) may be written

$$\overline{dc/dx}\int_d^\infty \frac{dx}{x^{n-3}} = \frac{\overline{dc/dx}}{(n-4)d^{n-4}},$$

where $\overline{dc/dx}$ denotes the mean value of dc/dx in the region from $x=d$ to $x=\infty$. If c remains everywhere finite, and dc/dx tends therefore at infinity to zero, then this term is negligible as compared with the first term of the right-hand side of (6).

A similar expression like (6) is obtained for the force due to all molecules B lying to the left of A, only we must take now $c(-d)$ instead of $c(d)$. The resultant force is therefore equal to

$$g = \frac{2\pi KN}{M(n-1)(n-3)d^{n-3}}[c(d) - c(-d)] = \frac{4\pi KN}{M(n-1)(n-3)d^{n-4}}\frac{dc}{dx}. \qquad (8)$$

[2] A. Gyemant, *Grundzüge der Kolloidphysik*, Vieweg, 1925.

The constant K can be estimated as follows. The force (3) is derived from a potential and we have:

$$\varphi = -\frac{1}{n-1}\frac{K}{r^{n-1}}. \tag{9}$$

We also have approximately $\varphi(d) \sim \lambda$, where λ is the heat of solution per molecule. Hence

$$K \sim (n-1)d^{n-1}\lambda. \tag{10}$$

Introducing this into (8) and remembering that there are d^{-3} molecules A per unit volume, we find for the force acting per unit volume of the solvent the expression

$$f_s = \frac{4\pi N\lambda}{M(n-3)} \text{ grad } c_i = \Gamma \text{ grad } c_i. \tag{11}$$

$N\lambda$ is the heat of solution per gram-mol and is usually of the order of magnitude of 10^{10} ergs; n being anywhere between 5 and 8,[2] we see that the force given by Eq. (11) is of the same order of magnitude as that given by Eq. (1).

If the drop is bound by a membrane of a small but finite thickness δ we have inside of the membrane

$$dc/dr = (\alpha c_e - c_i)/\delta$$

and therefore there is a force acting normally to the membrane and equal per unit volume to

$$-\Gamma'(\alpha c_e - c)/\delta,$$

which corresponds to a pressure per unit area of

$$p_s = -\Gamma'(\alpha c_e - c_i).$$

Γ' will in general be different from Γ. The minus sign is used because the pressure is negative (directed outwards) when $\alpha c_e > c_i$.

There are also other forces acting on each element of volume of the drop. One is due to the fact that there are forces of attraction between two reacting molecules, which combine to form a new molecule, as well as forces of repulsion between two molecules, which are formed as a result of a spontaneous breakdown of a more complex molecule. Under circumstances these forces may be comparable with the above discussed. Their order of magnitude can be estimated in a similar way from the heat of reaction. We arrive at expressions of a similar type to (11). And we shall therefore consider Γ and Γ' as being the sums of the constants corresponding to both types of forces. Another force is due to the circumstance that in each element of volume a number of molecules disappears due to the reaction. This "absorption" of the molecules is also accompanied by the "absorption" of their momentum, and thus produces a force. A still different force is due to the flow of the diffusing substance and is of hydrodynamical nature. Both these forces are easily calculated and shown to be vanishingly small, as compared with the above ones.

We thus have for the total force acting on a unit of volume

$$f = (\Gamma - RT/M) \text{ grad } c_i \tag{12}$$

and for the total pressure

$$p = (RT/M - \Gamma')(\alpha c_e - c_i). \tag{13}$$

The force (12) is derived from a potential φ thus:

$$f = -\text{grad } \varphi; \quad \varphi = -(\Gamma - RT/M)c_i. \tag{14}$$

Consider an infinitesimal elongation of the drop. This deformation will produce a rearrangement of concentrations inside and outside of the drop, and the distribution of forces will now no more possess spherical symmetry. In order that the resulting forces would now tend to increase that infinitesimal elongation, it is necessary that along the surface of the deformed drop forces would be directed from the equator to the poles. This requires that at the surface the sum of the potential φ and of the total pressure would be larger in the equatorial region than in the polar region of the drop. Or

$$\begin{aligned} -(\Gamma - RT/M)c_{ei} + (RT/M - \Gamma')(\alpha c_{ee} - c_{ei}) \\ + P_e > -(\Gamma - RT/M)c_{pi} \\ + (RT/M - \Gamma')(\alpha c_{pe} - c_{pi}) + P_p, \end{aligned}$$

which can also be written:

$$\begin{aligned} -(\Gamma - \Gamma')(c_{ei} - c_{pi}) + \alpha(RT/M - \Gamma')(c_{ee} - c_{pe}) \\ > P_p - P_e, \end{aligned} \tag{15}$$

where P_e and P_p denote, respectively, the cappillary pressure at the equator and the poles. c_{ei} and c_{ee} denote the equatorial values of c_i and c_e, and c_{pi} and c_{pe} are the polar values of those quantities.

The study of an arbitrary infinitesimal de-

formation presents great difficulties and we shall therefore restrict ourselves to a deformation which leaves the deformed drop a figure of revolution, the equation of the meridian section being:

$$R=R_0+\Delta_0\cos 2\theta. \tag{16}$$

In the following we shall use the abbreviation:

$$\Delta_0\cos 2\theta=\Delta. \tag{17}$$

A simple calculation shows that in such a deformed drop $dc/d\nu$, ν denoting the normal to the surface, differs from dc/dR only by quantities of the order of Δ_0^2. Therefore we can everywhere write dc/dR instead of $dc/d\nu$.

For the concentrations in a spherical drop we have[3]

$$c_i'=\alpha c_0'+\frac{q}{3h}R_0+\frac{\alpha q}{3D_e}R_0^2+\frac{q}{6D_i}(R_0^2-R^2) \text{ inside}$$

$$\text{and} \qquad c_e'=c_0'+\frac{qR_0^3}{3D_e}\frac{1}{R} \text{ outside.} \tag{18}$$

These expressions satisfy respectively the differential equations

$$D_i\Delta^2c_i'+q=0 \quad \text{and} \quad D_e\Delta^2c_e'=0. \tag{19}$$

At the boundary of the deformed cell, we have:

$$\begin{aligned}[c_i']_{R_0+\Delta}&=\alpha c_0+\frac{qR_0}{3h}+\frac{\alpha qR_0^2}{3D_e}-\frac{qR_0\Delta}{3D_i},\\ [c_e']_{R_0+\Delta}&=c_0+\frac{qR_0^3}{3D_e}\frac{1}{R_0+\Delta}=c_0+\frac{qR_0^2}{3D_e}-\frac{qR_0\Delta}{3D_e}\end{aligned} \tag{20}$$

and

$$\begin{aligned}&\left[D_i\frac{dc_i'}{dR}-h(\alpha c_e'-c_i')\right]_{R_0+\Delta}\\ &\quad=\left[\frac{\alpha hR_0}{3D_e}-\frac{D_i+hR_0}{3D_i}\right]q\Delta=-A\Delta,\\ &\left[D_e\frac{dc_e'}{dR}-h(\alpha c_e'-c_i')\right]_{R_0+\Delta}\\ &\quad=\left(\frac{\alpha hR_0}{3D_e}+\frac{2D_i-hR_0}{3D_i}\right)q\Delta=-B\Delta.\end{aligned} \tag{21}$$

That is, (18) does not satisfy the boundary conditions of the diffusion problem in a deformed drop, which it does in a spherical one. Let us put for the deformed drop

$$c_i=c_i'+c_i^*; \quad c_e=c_e'+c_e^* \tag{22}$$

and try to determine c_i^* and c_e^* so that both the differential equations

$$D_i\nabla^2c_i=-q; \quad \nabla^2c_e=0 \tag{23}$$

and the boundary conditions

$$D_i\frac{dc_i}{dR}-h(\alpha c_e-c_i)=0; \quad D_e\frac{dc_e}{dR}-h(\alpha c_e-c_i)=0 \tag{24}$$

would be satisfied at the *deformed* boundary. In view of (19) and (21) we can satisfy (23) and (24) by putting $\nabla^2c_i^*=0$; $\nabla^2c_e^*=0$ and at the boundary

$$\begin{aligned}&D_i\frac{dc_i^*}{dR}-h(\alpha c_e^*-c_i^*)=\\ &\qquad-\left[D_i\frac{dc_i'}{dR}-h(\alpha c_e'-c_i')\right]=A\Delta\end{aligned} \tag{25}$$

and similarly

$$D_e(dc_e^*/dR)-h(\alpha c_e^*-c_i^*)=B\Delta.$$

To satisfy the differential equations we can put

$$c_i^*=\sum_0^\infty a_nR^nP_n(\theta); \quad c_e^*=\sum_0^\infty b_nR^{-n-1}P_n(\theta), \tag{26}$$

where $P_n(\theta)$de notes the n-th zonal harmonics. Introducing (26) into the boundary conditions of (25), we find, neglecting quantities of second and higher orders in Δ_0

$$\begin{aligned}&\sum_0^\infty S_nP_n(\theta)=A\Delta_0\cos 2\theta;\\ &\sum_0^\infty Q_nP_n(\theta)=B\Delta_0\cos 2\theta\end{aligned} \tag{27}$$

with

$$\begin{aligned}S_n&=(D_inR_0^{n-1}+hR_0^n)a_n-h\alpha R_0^{-n-1}b_n,\\ Q_n&=hR_0^na_n-[D_e(n+1)R_0^{-n-2}+h\alpha R_0^{-n-1}]b_n,\end{aligned} \tag{28}$$

or putting $x=\cos\theta$

$$\begin{aligned}&\sum_0^\infty S_nP_n(x)=A\Delta_0(2x^2-1);\\ &\sum_0^\infty Q_nP_n(x)=B\Delta_0(2x^2-1).\end{aligned} \tag{29}$$

[3] N. Rashevsky, J. Gen. Physiol. **15**, 289 (1932).

We have

$$S_n=\frac{2n+1}{2}\int_{-1}^{+1}(2x^2-1)P_n(x)dx \qquad (30)$$

and a similar expression for Q_n.

The coefficients thus calculated are found to have the values:

$$\begin{aligned} &S_0=-\tfrac{1}{3}A\Delta_0; \quad Q_0=-\tfrac{1}{3}B\Delta_0; \\ &S_2=\tfrac{4}{3}A\Delta_0; \qquad Q_2=\tfrac{4}{3}B\Delta_0. \end{aligned} \qquad (31)$$

all others being equal to zero. Since according to (15) we are interested only in the difference of the values at the equator and the poles, we need to know only a_2 and b_2, for the 0-th terms of (26) do not contain θ. Putting $n=2$ into (28) and introducing values (31) we find after somewhat elaborate but elementary calculations

$$\begin{aligned} a_2&=\frac{4B}{3hR_0^2}\Delta_0+\left(\frac{3D_e}{hR_0^6}+\frac{\alpha}{R_0^5}\right)b_2; \\ b_2&=\frac{4hqR_0^5-8BD_iR_0^4}{18D_iD_e+6D_ih\alpha R_0+9D_ehR_0}\Delta_0. \end{aligned} \qquad (32)$$

For future references we give also the expressions for a_0 and b_0:

$$\begin{aligned} a_0&=-[\alpha R_0q/3D_e+A/3h]\Delta_0; \\ b_0&=-(qR_0^2/3D_e)\Delta_0. \end{aligned} \qquad (32')$$

Remembering that, for θ as argument, $P_2(0)=1$ and $P_2(\pi/2)=-1/2$ we find:

$$\begin{aligned} c_{ei}^*-c_{pi}^*&=-(1/2)a_2(R_0-\Delta)^2-a_2(R_0+\Delta)^2 \\ &=-(3/2)a_2R_0^2 \qquad (33) \end{aligned}$$

$$c_{ee}^*-c_{pe}^*=-b_2/2R_0^3-b_2/R_0^3=-3b_2/2R_0^3.$$

We omit here terms in Δ_0, because both a_2 and b_2 already contain the infinitesimal quantity Δ_0 as factor.

We now have:

$$\begin{aligned} c_{ei}-c_{pi}&=(c_{ei}'+c_{ei}^*)-(c_{pi}'+c_{pi}^*)=(c_{ei}'-c_{pi}') \\ &+(c_{ei}^*-c_{pi}^*)=2qR_0\Delta_0/3D_i-3a_2R_0^2/2, \qquad (34) \end{aligned}$$

$$c_{ee}-c_{pe}=2qR_0\Delta_0/3D_e-3b_2/2R_0^3. \qquad (35)$$

For infinitestimal deformations (lim $\Delta_0=0$) expressions (34) and (35) represent an exact solution of our problem. However, on account of the rather complex structure of a_2 and b_2 their use would complicate the final formulae tremendously. Using, however, $D_i\sim10^{-7}$ cm^2 min^{-1}, $D_e\sim10^{-5}$ cm^2 min^{-1}, $h\sim10^{-4}$ cm min^{-1} and $a\sim10^{-4}$g cm^{-3} min^{-1}, which values are suggested by biological considerations, we find that if R_0 is of the order of magnitude of 10^{-3} cm, the second terms of the right hand sides of (34) and (35) are considerably smaller than the first ones. We have therefore approximately:

$$c_{ei}-c_{pi}=2qR_0\Delta_0/3D_i;\ c_{ee}-c_{pe}=2qR_0\Delta_0/3D_e. \qquad (36)$$

Now we must calculate the capillary pressure P. It is given by

$$P=\gamma(1/\rho_1+1/\rho_2), \qquad (37)$$

γ being the surface tension and ρ_1 and ρ_2 the principal radii of curvature. The radius of curvature of the meridional section of the deformed drop is given by[4]

$$\frac{1}{\rho}=\frac{R^2+2R'^2-2R''}{[(R^2-R'^2)^3]^{\frac{1}{2}}} \qquad (38)$$

with $R'=-2\Delta_0\sin 2\theta$; $\quad R''=-4\Delta_0\cos 2\theta$. (39)

At the pole we have

$$\begin{aligned} \frac{1}{R_1}=\frac{1}{R_2}=\frac{1}{\rho_p}&=\frac{(R_0+\Delta_0)^2+4(R_0+\Delta_0)\Delta_0}{(R_0+\Delta_0)^3} \\ &=\frac{1}{R_0}+\frac{3\Delta_0}{R_0^2} \qquad (40) \end{aligned}$$

and therefore

$$P_p=2\gamma(1/R_0+3\Delta_0/R_0^2). \qquad (41)$$

At the equator we have

$$\begin{aligned} &1/R_1=1/\rho_e; \\ &1/R_2=1/(R_0-\Delta_0)=1/R_0+\Delta_0/R_0^2 \end{aligned} \qquad (42)$$

and

$$1/\rho_e=1/R_0-3\Delta_0/R_0^2, \qquad (43)$$

which gives

$$P_e=2\gamma(1/R_0-\Delta_0/R_0^2), \qquad (44)$$

$$P_p-P_e=(8\gamma/R_0^2)\Delta_0. \qquad (45)$$

---

[4] Geiger-Scheel's Handbuch der Physik, Vol. 3, p. 157. J. Springer, Berlin, 1928.

Introducing (36) and (45) into (15) we obtain:

$$-2(\Gamma-\Gamma')qR_0/3D_i + 2\alpha(RT/M-\Gamma')qR_0/3D_e > 8\gamma/R_0^2. \quad (46)$$

In order that (46) could be satisfied at all, we must have

$$q[\alpha(RT/M-\Gamma')/D_e-(\Gamma-\Gamma')/D_i]>0. \quad (47)$$

This is a relation between the various physico-chemical constants of the drop, which must be satisfied in order that a truly spontaneous division should occur. If this relation is satisfied, then (46) will be satisfied for sufficiently large R_0, and the critical value of R_0, above which this happens and above which the drop becomes unstable, is given by:

$$R^*=\left(\frac{12\gamma}{q[\alpha(RT/M-\Gamma')/D_e-(\Gamma-\Gamma')/D_i]}\right)^{\frac{1}{3}}, \quad (48)$$

which is obtained by equating the two sides of (46).

Using the above estimated values for Γ and Γ', remembering that α is of the order of unity and taking for γ the value used previously[1], we again find R^* to be of the order of magnitude of 10^{-3} cm. This also justifies our use of the approximation (36).

It is interesting to see what effect the osmotic forces alone would produce. This we can find by putting $\Gamma=\Gamma'=0$, $\alpha=1$. But then (47) can be satisfied only when $q>0$, that is, only when the substance is produced in the drop and diffuses outside. Eq. (48) reduces in this case to

$$R^*=(12\gamma MD_e/qRT)^{\frac{1}{3}}. \quad (49)$$

For $q<0$ the osmotic forces will be such as to always tend to restore the spherical shape of the drop. They will never lead to a spontaneous division of the drop, in spite of the fact that such a division would be, as we have seen, above a certain size always accompanied by a decrease of the free energy. We have here a close analogon to the above discussed valve action.

Equation (49) gives the same order of magnitude for the critical size as the previously derived equation.[1] It differs however from the latter in many peculiar respects. One is that the critical size at which a real instability occurs depends only on D_e, and becomes infinite with the latter. If we would use instead of (36) the exact expression (34) and (35) the critical radius would involve also D_i, but it still would become infinite for $D_e=\infty$. On the other hand the radius, calculated previously, above which the division is accompanied by a decrease of free energy, remains finite even for infinite D_e, since our previous calculations were made only for that case. For $D_e=\infty$ we find the valve action to be present both in case of positive and negative q.

Another difference between (49) and our former equations is that (49) does not contain c_0, whereas the energy liberated during the division, depends, according to reference 1, on c_0. This paradoxon is also easily illustrated by a purely mechanical example. Consider again a container partitioned in two air-tight compartments. The partition has no openings at all. We see that if a certain excess of the pressure on one side of the partition will cause a breakdown of the latter, this breakdown will be determined solely by the difference of pressures on both sides of the partition, but not by their absolute values. But the decrease of free energy caused by the process of equalization of pressures, which will result after the breakdown of the partition, will depend on the absolute values of those pressures.

We have entirely neglected here the forces, which might be produced by the electrical charges, present in every disperse system. Those will be investigated in a separate paper.

Furthermore it must be emphasized, that even the above conditions of instability do not yet form absolutely general sufficient conditions for a spontaneous *complete* division of a drop. For as we have seen,[5] drops, which are the seats of physico-chemical reactions may under certain circumstances possess a non-spherical, oblong shape of stable equilibrium. The instability of a spherical drop discussed in this paper may lead not only to a complete division, but to a formation of such non-spherical configurations, which however will probably occur in exceptional cases. Nothing more definite can be said about it until the very difficult general mathematical theory of such non-spherical equilibria is developed.

---

[5] Rashevsky, Physics **1**, 143 (1931).

Stabilizing Arcs by Electrode Surfacing

C. G. SUITS, *Research Laboratory, General Electric Company, Schenectady, N. Y.*

(Received July 27, 1934)

The effect of electrode surfacing on arc stability is studied for arcs between copper and silver electrodes in air at atmospheric pressure. For the copper arc it is shown that the random fluctuations in arc voltage and light intensity may be reduced to a very small value by giving the anode surface a high polish. Observations of the spectrum and volt-ampere characteristic are described. For the silver arc partial stability of arc voltage and light is obtained by electrode polishing.

1. INTRODUCTION

MANY of the difficulties of studying arcs at high pressures are due to the irregular and erratic nature of all of the associated phenomena. In the copper arc in air at one atmosphere, for example, the arc voltage, arc light, arc position, and probably other quantities partake in this fluctuation. There are a number of excellent methods for stabilizing arcs with respect to position,[1, 2] and there are described below some new experiments which bear on the problem of stability of arc voltage and light intensity. It is shown that by employing electrode surfaces of high polish it is possible to stabilize the copper arc and partly to stabilize the silver arc.

2. NATURE OF ARC INSTABILITY

If an arc is formed between copper electrodes at atmospheric pressure in the current range 10 ± 9 amperes, it will be found that for constant current the arc voltage suffers an irregular and erratic fluctuation of from 15–45 percent of the mean value. The rapidity of these fluctuations is generally such that they may be resolved by a magnetic oscillograph, although for some electrode materials periodicities of several hundred thousand cycles have been found. The lowest frequency components may be observed on an ordinary laboratory voltmeter shunted across the arc.

The causes of this phenomenon are not entirely clear, but some pertinent facts are available. It is commonly supposed that in metallic arcs, as for example the mercury arc, the variations in arc voltage correlate with the movements of the cathode spot, which is in turn a result of the pressure developed from vaporization of the cathode material. We have proven that no large part of this voltage variation is due to movements of the cathode spot for the copper and silver arcs by taking high speed movies of these arcs with sound movie equipment. As the arc appearance is photographed, the arc voltage is simultaneously recorded on the sound track. When the movie is projected on the screen, the arc voltage is put on the sound amplifier system in synchronism with the screen image, so that any correlation between arc appearance and arc voltage can be detected. We have some fine records in which a 3 mm copper arc is rapidly oscillating between two points on the electrode surface, and when these films are projected, we find no significant correlation with arc voltage. In another series of photographs of a silver arc, which occupies a fixed position on the electrodes but is rapidly fluctuating in light intensity, we find a correlation between arc light and arc voltage, an increase in light intensity being accompanied by a decrease in voltage. These and other observations suggest as a hypothesis that the changes in arc voltage are related to the various critical potentials of the arc gas and electrode vapor, but a test of this possibility awaits more comprehensive data.

3. COPPER ARC WITH POLISHED ELECTRODES

The effect of electrode surface on arc voltage is quite striking and is shown by Fig. 1, where arc current, of a substantially constant value (1.95 ± 0.05 amperes d.c.), and arc voltage are recorded as a function of time for three different degrees of surfacing of copper electrodes. The degree of polish is a good criterion of the constancy of the arc voltage, and it can be seen that for the best

[1] A. Lotz, Zeits. f. tech. Physik **5**, 187 (1934).
[2] E. Traub, Ann. d. Physik **18**, 169 (1933).

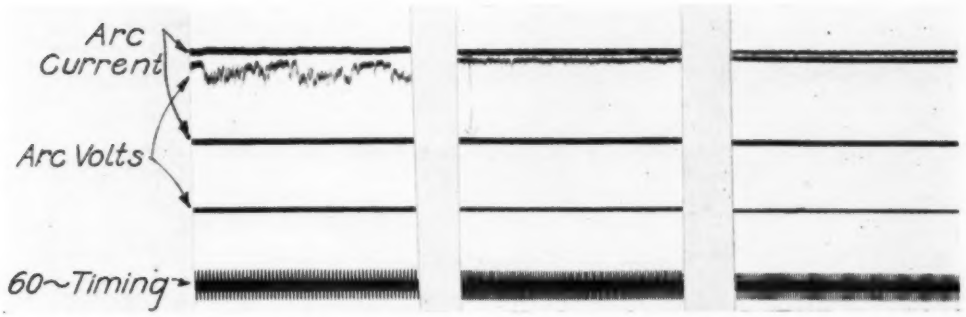

FIG. 1.

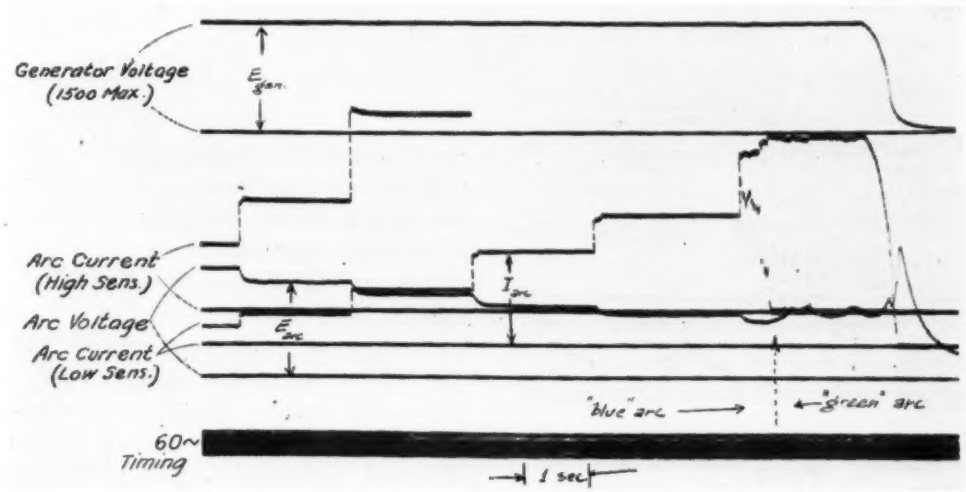

FIG. 2. 3 mm copper arc in air at atmospheric pressure; highly polished 12 mm dia. electrodes.

obtainable polish (rouge on a high speed chamois buffer) the arc voltage fluctuation is reduced to a very small value.

A volt-ampere characteristic, obtained by an automatic oscillographic method for a 3 mm copper arc between highly polished copper electrodes, is shown as Fig. 2. In this method a commutator successively short-circuits portions of the current limiting resistance in such a manner that the arc current increases in uniform steps, each of a relatively constant value. A low sensitivity galvanometer records the high current steps, while the high sensitivity galvanometer allows the low currents to be read with accuracy. The arc voltage thus decreases in uniform steps, during each of which the voltage is nominally constant. (A low period galvanometer is used for arc voltage so that high frequency components are absent.) The highly polished electrode surface is effective in removing gross fluctuations almost completely. It is also effective in changing the visual appearance of the arc, the color being blue instead of the characteristic green of the copper arc. Examination of spectrograms reveals that the green arc has strong copper lines superimposed on a faint banded spectrum of nitrogen. The blue arc is characterized by a strong band spectrum of nitrogen upon which are superimposed faint blue copper lines 3248 and 3274, and very faint copper lines 5106, 5153, 5218 and 5782. The exposure was, of course, identical for both records. The blue arc is evidently a nitrogen arc with faint traces of copper vapor.

The unexpected performance of one polished

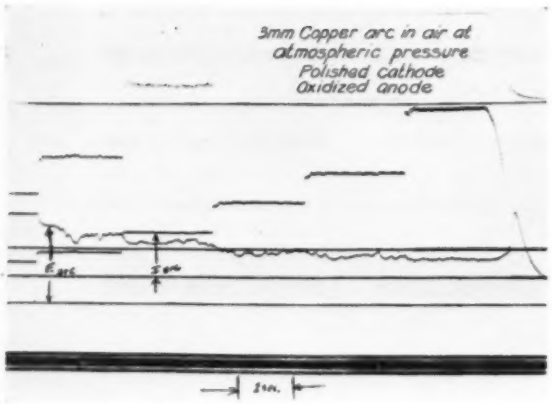

FIG. 3.

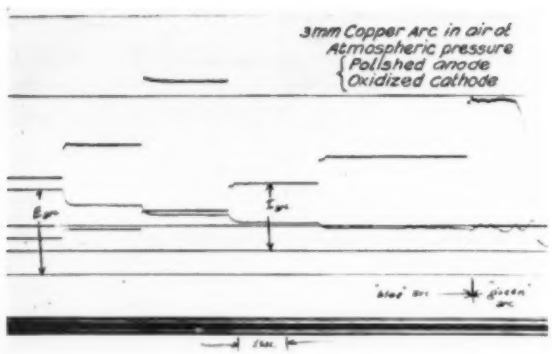

FIG. 4.

electrode and one oxidized electrode is shown in Figs. 3 and 4. In Fig. 3, the cathode was polished and anode oxidized, which resulted in a fluctuating arc voltage identical in appearance with that found for two oxidized electrodes. The polished anode-oxidized cathode case, as in Fig. 4, shows, however, an arc voltage trace as smooth as that found for two polished electrodes. Evidently the polished anode alone is effective in this phenomenon. This does not necessarily prove that the seat of the voltage fluctuation is at the anode; it may reside at the cathode, dependent upon the absence or presence of metal vapor supplied by the anode. That the effect is present and unmistakable can be regarded as established by the oscillograms.

There is the possibility of electrode contamination by the polishing method. The chief evidence that the emery and rouge were not present in the

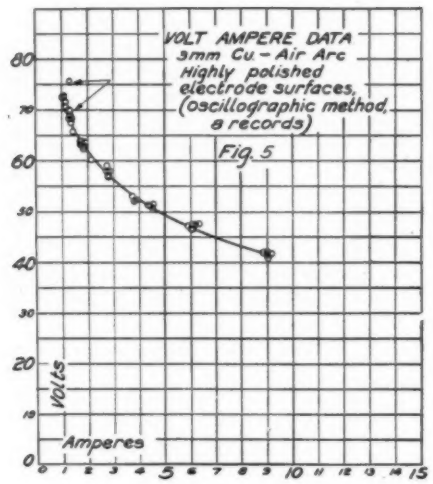

FIG. 5.

arc is found in the spectrographic data. For the polished electrode case all the lines which may be detected are due to copper, while all the prominent bands are those of nitrogen.

We have in no case found polished electrodes entirely free from markings of some kind after burning, for example, at 2 amperes for 15 seconds. The anode may, however, have very superficial traces of having been used, such as a sooty deposit which rubs off readily, but no pitting that can be observed with low magnification. All polished electrodes used for cathodes have had positive evidence of burning, pitting and some oxidation.

This type of arc (polished Cu electrodes) is extremely reproducible and constant in its characteristics, as shown, for example, in Fig. 5 where all points from eight oscillographic records have been plotted. The spread is extremely small, particularly when it is remembered that these points are read directly from the oscillograms and do not represent averages.

4. Silver Arc with Polished Electrodes

Silver, with many physical properties similar to copper, might be expected to perform similarly as electrode material. Fig. 6 represents the typical volt-ampere record for highly polished silver electrodes taken for a 3 mm arc at atmospheric pressure. The arc voltage is characterized by a relatively constant portion (in any given current step) with occasional large, rapid decreases in

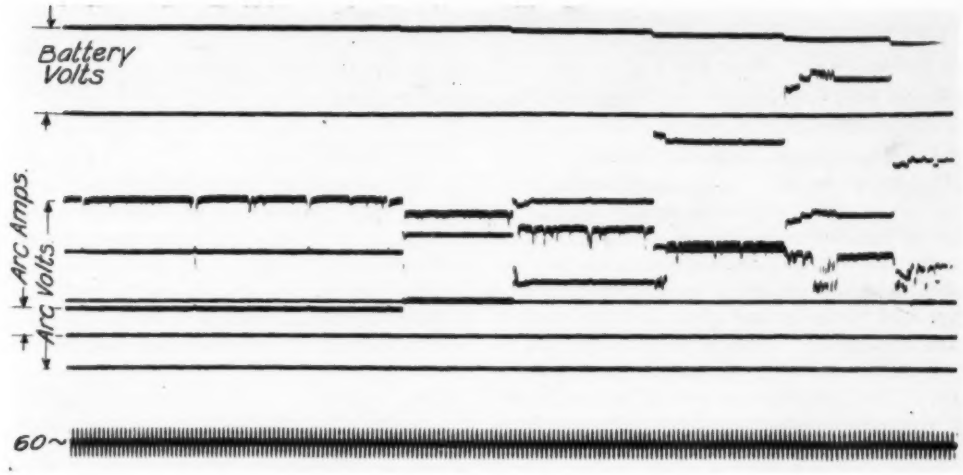

FIG. 6. 3 mm silver arc in air at atmospheric pressure; highly polished electrodes.

voltage. The arc is visually blue during the time the voltage is constant, and assumes a brilliant white appearane when the voltage dips occur. That the arc light intensity increases during the periods of the voltage decrease has been determined by a number of methods. In the steady state, however, the light output increases with arc watts, indicating that the mechanism of light production during the transients is different from the steady state.

In the case of silver, evidence of the arc voltage jumping between two definite levels at a single value of current is found. This can be observed in several current steps of Fig. 6, and is particularly suggestive in the last two steps. Without providing some sort of a voltage-operated shutter arrangement, it is not possible to observe the spectrum in these two stages. Data for plotting the volt-ampere characteristic are not sufficiently numerous for the low voltage condition represented by the voltage dips. The high voltage state is very definite and yields the arc characteristic

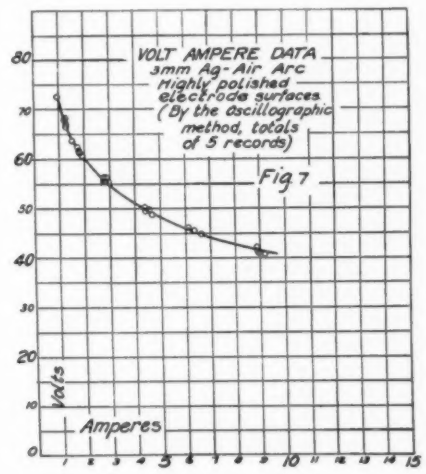

FIG. 7.

of Fig. 7, where data from five oscillographic records are plotted. The extremely small spread indicates a high experimental accuracy and a constant and reproducible type of arc phenomenon.

Glass-to-Metal Seals

ALBERT W. HULL AND E. E. BURGER, *General Electric Company, Schenectady, N. Y.*

(Received September 4, 1934)

The problems of sealing are adhesion and strain. The simplest, but perhaps not the only means of *adhesion* is a firm layer of metal oxide. *Strains* can be avoided if, and only if the *thermal expansions of metal and glass are the same.* This postulate is thoroughly tested. Equations are derived for the stresses in cylindrical seals, in terms of the difference in expansion of metal and glass, and the stresses thus calculated are compared with those observed photoelastically in carefully annealed test seals. Such tests are carried out on all the important sealing materials. These tests include accurate *contraction coefficient* measurements of glass and metals, (Fig. 8); graphical exhibition of axial stresses by photographs through crossed Nicols and a quartz wedge, (Figs. 9 and 10); and numerical evaluation of all the stresses, both theoretical and experimental, (Table VII). Two new sealing alloys are described: *fernichrome* (Fe 37 percent, Ni 30 percent, Co 25 percent, Cr 8 percent) which matches standard lead glass; and fernico (Fe 54 percent, Ni 28 percent, Co 18 percent) which matches Corning glasses G-71 and G-705 A O. The unique feature of these alloys is that their *expansion characteristics are curved* in such a manner that they match those of the glasses mentioned with considerable fidelity. The seals made with these combinations are found to be practically free from strain.

1. INTRODUCTION

THE *art* of sealing metals to glass is old. It has long been one of the accomplishments of the skilled glass blower. For lamps and radio tubes this skill, and the empirical machine-technique which has developed from it, have thus far been considered satisfactory. These methods are not satisfactory for tubes for power conversion purposes, even those of today, and still less for new developments. A *science* of seal-making is needed. The data presented in this paper are a contribution toward such a science.

2. GENERAL PRINCIPLES

The requirements of a glass-to-metal seal are easily defined. They are:

(1) The glass must "wet" the metal.

(2) The stresses resulting from thermal expansion and contraction must not exceed the tensile strength of the glass.

The necessary and sufficient conditions for fulfilling these requirements may be stated here in advance of the evidence:

(1) Any glass will wet and adhere to any *clean, gas-free* metal, provided the metal is covered with an *adherent layer of oxide*, and the temperature is raised to the point where this oxide partially dissolves in the glass.

(2) Properly annealed seals will be strain-free at all temperatures if, and only if, the coefficients of expansion of glass and metal are the same over the whole temperature range from room temperature up to the annealing point.

3. WETTING

The affinity of clean, pure metals for glass is generally assumed to be very small. If a bead of glass is laid on a sheet of metal and placed in a hydrogen furnace, the glass will not spread over the metal at any temperature, and there will be little, if any, adhesion. This might be attributed to a superficial reduction of the glass by the hydrogen, though it is true of glasses that show no trace of reduction; but the same results are obtained in pure nitrogen and in pure carbon dioxide, provided the metal surface is unoxidized. It is quite different if the metal surface is oxidized. The glass then spreads readily in N_2 and CO_2, even climbing against gravity as much as a centimeter on a vertical metal plate, and the adherence between metal oxide and glass is strong. If the oxide is so thin, or the heating so prolonged, that all of the oxide is absorbed, adherence may again become weak. If, on the other hand, the oxide is too thick, the adherence of metal oxide to metal will be weak. Such over-oxidized seals are characterized by very slow leakage of air along the interface between oxide and metal.

The function of an adherent oxide layer is well illustrated by the behavior of molybdenum. Molybdenum has been considered an unsatis-

factory sealing metal, because glass does not readily stick to it. The reason is that the wire usually becomes coated with a thick, non-adherent, semi-liquid oxide. But if the access of oxygen is limited, for example by surrounding the wire with a closely-fitting sleeve of the glass, excellent adhesion is obtained. If, on the other hand, oxygen is entirely excluded, no adhesion is obtained under ordinary conditions. It is thus evident that the problem of adherence is a problem of oxidation. The methods and tests of oxidation will not be discussed in this paper.

The metal oxide represents a phase that is soluble in both metal and glass, and hence is qualified to act as a cement, and is the easiest means of obtaining adherence, but we believe it is not the only means. The tenacity with which clean metals adhere to each other, and the facility with which mercury wets iron and glass in vacuum when sufficiently clean, suggest that glass might adhere to clean metal. We have recently obtained evidence of such adherence. It seems probable that an important factor in such pure wetting is congruence between the metal lattice and the molecular dimensions of the glass. Platinum may or may not be an example of adherence without oxide, since it is known to be covered with an exceptionally stable layer of oxide.

Gas bubbles between metal and glass weaken the bond. Such bubbles most commonly come from dissolved gas in the metal, and a few seconds of heating at the temperature at which the seal is to be made will usually de-gas the metal sufficiently to avoid them. But, for some metals, a much longer treatment is needed. For example, nickel, which is notorious for bubbling, cannot be de-gassed by any practical treatment in a flame, but makes excellent seals if pre-fired for 15 minutes at 1200°C in air, nitrogen, hydrogen, or vacuum. The degassing thus produced is permanent, and the metal may be allowed to lie around without danger of reabsorbing gas.

Bubbles may come, however, from oxidation of impurities in the metal, particularly carbon. Superficial carbon can be burned off, though with difficulty and at the risk of over-oxidation. For example, a lead pencil mark on a metal sheet results in a row of large bubbles at the glass-metal interface, if ordinary sealing technique is used; but the carbon mark can be burned off and bubbling prevented by one minute of preheating in an oxyhydrogen flame. A much longer treatment, of the order of an hour at 1100–1200°C, is needed when carbon has penetrated the metal, as, for example, in the case of metal which has been heat-treated in hydrogen in a carbon boat.

4. Measurement of Thermal Expansion

The stress resulting from thermal strain can be calculated from the relative thermal expansion of glass and metal, and can be checked by photoelastic measurements on the finished seals. Such calculations and measurements constitute the remainder of this paper.

Since complete expansion data were not available, we have obtained these data for all the important sealing combinations. The simple but sensitive method used in these measurements has been described elsewhere,[1] and need not be discussed here, except to note that each glass specimen was compared directly with a metal of nearly the same expansion, instead of with quartz, thus obtaining a smaller difference between sample and standard, and allowing a higher scale sensitivity. In the following figures, it is the *difference in expansion* between the glass and adjacent metals to which attention is directed, and which is accurately represented. This difference determines the stresses when the two are joined. The total expansions, which are shown in Figs. 1 and 5 because they give a better idea of the shape of the expansion curves, were obtained by adding the measured differences to the known or separately determined expansions of the metals.

Expansion measurements were made during both heating and cooling. The two never agree precisely, but the differences are slight after good annealing. *The curves shown throughout the paper are those taken during cooling*, at the rate of one degree per minute, unless otherwise specified. They were found to be reproducible and independent of previous history, as compared to heating measurements which are very sensitive to previous history. The cooling measurements are the ones desired in this case. They represent, nearly, the contractions which the glass will

[1] E. E. Burger, G. E. Rev. **37**, 93 (1934).

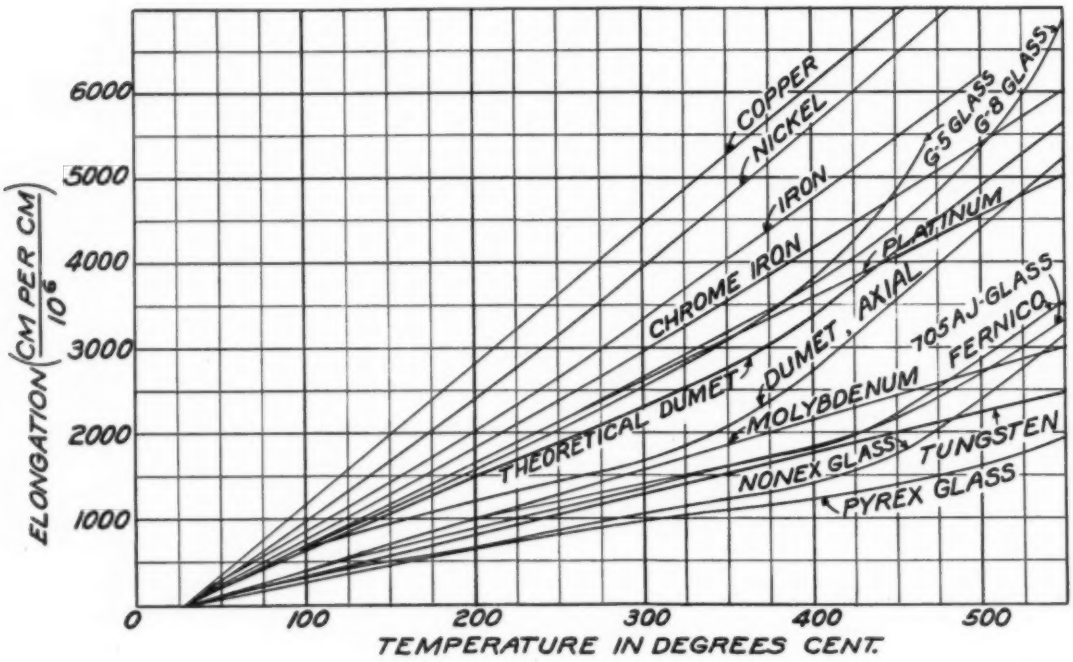

FIG. 1. Thermal expansion, in cm per cm of length, of common glasses and metals. Note the shape of the glass curves.

actually suffer in the ordinary lehr annealing, and are therefore a measure of the stresses that will remain in annealed seals. Subsequent heating never reaches the point where these stresses are released.

Fig. 1 gives the total thermal expansion, in cm per cm of length, of a few of the more important glasses and metals. They are shown together for purposes of comparison; the individual combinations will be shown later. It will be noted that Cu, Fe and Ni are higher in expansion than any standard glass, probably higher than any practical stable glass; and Pyrex is lower than any known metal or alloy. The important feature to be observed, however, is the shape of the glass curves. The rate of expansion increases rapidly as the softening point is approached. We have sought in vain for a glass without this "transition" in its expansion.[2] Whatever its physical cause, it is a stable, reproducible characteristic of well-annealed glasses, at least for such rates of heating and cooling as are used in practice.

The significant fact about the transition in the glass expansion is that it occurs at a temperasure considerably (between 50 and 100°C) below the lowest practical annealing temperature, so that it is impossible to "match" the glass expansion, over the range from room temperature to the annealing point, with the nearly linear expansion of pure metals. The best that can be done is to find combinations of metal and glass which match at zero and at the annealing point. Many such combinations are shown and discussed in the following pages.

There is one exception. We have found an alloy of iron, nickel, and cobalt, (54 percent Fe, 28 percent Ni, 18 percent Co), designated as *Fernico*, which has a "transition" in its thermal expansion almost identical with that of a standard hard glass (Corning G-71). The transition occurs at the temperature at which ferromagnetism is lost (Curie point). The magnetic transformation is accompanied by a threefold increase in the rate of thermal expansion; *viz.*, from 4.75×10^{-6} to 14.25×10^{-6} cm per cm per degree centigrade. The significance of this particular

[2] Turner and Winks (J. Soc. Glass Tech. **14**, 84 (1930)) reported a glass with no transition point in its expansion. Dr. Louis Navias, of our laboratory, has kindly reproduced this glass for us, using pure chemicals and a platinum crucible; and we find that, when completely annealed, it shows the same transition as other glasses.

alloy is that it has the lowest expansion of any of the ternary Fe-Ni-Co series whose magnetic transformation point is high enough to match the "transition" in the expansion of a corresponding glass. This alloy is discussed in Sections 11 and 12. A similar alloy containing chromium (37 percent Fe, 30 percent Ni, 25 percent Co, 8 percent Cr), which matches standard lead and line-glasses more closely than any other known sealing material, is also described in Sections 11 and 12.

5. Calculation of Stresses in Seals

Simple cylindrical wire seals (Fig. 2) were chosen for study, since their stresses can be calculated in terms of the difference in expansion of glass and metal. These calculations will apply with good approximation to all wire seals, for the important stresses are those near the wire, and these are but little affected by glass more than two wire diameters away.

Assume a seal, of the form shown in Fig. 2, to be strain-free at some temperature t_0, and to be heated or cooled to a temperature, t. Let δ be the difference in the free expansions of unit lengths of glass and metal between t_0 and t.

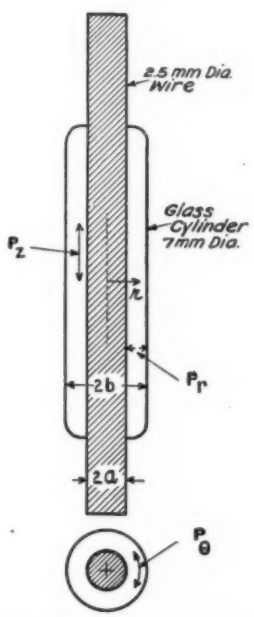

Fig. 2. Simple cylindrical seals used for tests. The stresses in these seals, due to difference in expansion of glass and metal, can be calculated from the expansion data, and can be measured by photoelastic means.

$$\delta = (k_{\text{glass}} - k_{\text{metal}})(t - t_0),$$

where k = mean expansion coefficient between t_0 and t.

The resulting stresses in the glass at any distance r from the axis will be:[3]

Radial stress,
$$p_r = -\left[\frac{E_2\delta}{1+\alpha+\alpha\beta R}\right]\left[\frac{a^2}{b^2} - \frac{a^2}{r^2}\right], \quad (1)$$

Tangential stress,
$$p_\theta = -\left[\frac{E_2\delta}{1+\alpha+\alpha\beta R}\right]\left[\frac{a^2}{b^2} + \frac{a^2}{r^2}\right], \quad (2)$$

Axial stress,
$$p_z = -\left[\frac{E_2\delta}{1+\alpha+\alpha\beta R}\right]\left[2\sigma\frac{a^2}{b^2} + \frac{1+\alpha+\alpha\beta R}{1+\beta R}\right]; \quad (3)$$

where
E_1 = elasticity (Young's modulus) of wire,
E_2 = elasticity (Young's modulus) of glass,
σ = Poisson's ratio, assumed equal for wire and glass,[4]
a, b = radii of wire and glass, respectively,
$R = E_2/E_1$, $\alpha = (a^2/b^2)(1-2\sigma)$, $\beta = b^2/a^2 - 1$.

It will be noted that the radial stress is positive (tension), when δ is positive, for all values of a/b and r (since a/r must always be greater than a/b), and decreases from a maximum value at the surface of the wire to zero at the surface of the glass; while the tangential and axial stresses are negative (compression), when δ is positive, and are likewise maximum at the wire, the axial stress being constant over the cross section, and the tangential decreasing in the ratio $(a^2+b^2) : 2a^2$ from the wire to the surface of the glass.

The important stresses are therefore those at the surface of the wire. These have been calculated for a number of different ratios b/a of glass to wire diameter, using the elastic constants:[5]

[3] The derivation of the fundamental equations from which these expressions are obtained is given in the paper immediately following this, by Dr. H. Poritsky.

[4] Values of Poisson's ratio for glasses given in the Int. Crit. Tab. vary from 0.22 to 0.27, which is slightly smaller than the value (0.30) for most metals. A calculation for a single case of $a/b = \frac{1}{3}$, using $\sigma_2 = 0.25$, $\sigma_1 = 0.30$, gives stresses only 2 percent different from those for $\sigma_2 = \sigma_1 = 0.30$. We have, therefore, used $\sigma_2 = \sigma_1 = 0.30$ in the following calculations.

[5] The value taken for E_1 is that of 25 percent nickel steel. It represents the important sealing metals, *viz.*, molybdenum, chrome-iron alloy, and fernico, with sufficient accuracy, since the stresses in the glass are not very sensitive to the value of E_1, provided it is large compared with E_2. The value 0.65×10^6 for glass is a mean of the

TABLE I. *Stress at surface of wire ($r=a$) per unit difference of expansion, δ, between metal and glass, as function of ratio b/a of glass diameter to wire diameter. Positive stresses are tension; negative, compression. When δ is negative, the signs of all stresses are opposite to those given in the table.*

b/a	p_r (kg/cm² per unit difference of expansion)	p_θ	p_z
∞	$+0.566\times10^6$	-0.566×10^6	0×10^6
5	+ .538 × "	− .585 × "	−0.080 × "
4	+ .523 × "	− .592 × "	− .123 × "
3	+ .492 × "	− .615 × "	− .204 × "
2.5	+ .458 × "	− .634 × "	− .277 × "
2	+ .403 × "	− .672 × "	− .392 × "
1.73	+ .353 × "	− .705 × "	− .482 × "
1.41	+ .255 × "	− .765 × "	− .630 × "
1.29	+ .200 × "	− .800 × "	− .700 × "
1.195	+ .147 × "	− .831 × "	− .766 × "
1.118	+ .096 × "	− .865 × "	− .820 × "
1.053	+ .047 × "	− .896 × "	− .877 × "
1.025	+ .023 × "	− .910 × "	− .903 × "
1.000	0	− .925 × "	− .925 × "

TABLE II. *Stress per unit difference of expansion, δ, between metal and glass, at distance r from center of wire, as function of r/a, for $b/a=2.5$ (b = radius of glass cylinder, a = radius of wire). Positive stresses are tension; negative, compression. When δ is negative, signs of all stresses are reversed.*

r/a	p_r (kg/cm² per unit difference of expansion)	p_θ	p_z
1	$+0.458\times10^6$	-0.634×10^6	-0.277×10^6
1.1	+ .363 × "	− .537 × "	− .277 × "
1.2	+ .292 × "	− .467 × "	− .277 × "
1.3	+ .236 × "	− .411 × "	− .277 × "
1.4	+ .191 × "	− .365 × "	− .277 × "
1.5	+ .155 × "	− .329 × "	− .277 × "
1.6	+ .126 × "	− .301 × "	− .277 × "
1.7	+ .1015 × "	− .276 × "	− .277 × "
1.8	+ .0812 × "	− .256 × "	− .277 × "
2.0	+ .0490 × "	− .224 × "	− .277 × "
2.2	+ .0251 × "	− .200 × "	− .277 × "
2.5	0	− .175 × "	− .277 × "

$$E_1(\text{metal}) = 1.8 \times 10^6 \text{ kg/cm}^2,$$
$$E_2(\text{glass}) = 0.65 \times 10^6 \text{ kg/cm}^2,$$
$$\sigma_1 = \sigma_2 = 0.30.$$

They are shown in Fig. 3 and Table I. The variation of the stresses with distance r from the center of the wire has been calculated for the case of a ratio of glass diameter : wire diameter $= b/a = 2.5$. These stresses are given in Table II and Fig. 4.

6. Examples of Analysis of Stresses in Seals: Chrome-Iron *vs.* Lime Glass

As examples of the method of analysis of stresses in seals made with various sealing materials, we may take the combination of a 26 percent chromium-iron alloy[6] and the two "lime" glasses which most nearly match it in thermal expansion. The first, designated G-8, is "standard" lamp glass; the second, G-6, is a special glass made by the Corning Glass Works. Fig. 5 shows the relative thermal expansion of these three materials. In addition, there is shown, cross-hatched, the "annealing range" of the two glasses, defined as follows: the upper edge is the "annealing temperature" at which 90 percent of the strain can be removed in 15 minutes; the lower edge, called the "strain-point," requires 4 hours to reduce strains to 10 percent. At intermediate temperatures the annealing time doubles approximately for every 8°C.

The curves show that G-6 glass has exactly the same expansion as the chrome-iron metal at all temperatures from zero to 400°C; but above this temperature it expands more rapidly than the metal, until at 498°C, the "annealing temperature," the difference in expansion of unit lengths of metal and glass is $\delta = 550\times10^{-6}$. If a seal between this metal and glass could be annealed at 400°C, it would be a perfect match, and would remain strain-free as it cooled. This is not, however, a practical annealing temperature. Let us assume that the annealing is carried out in such a way that the glass "sets," strain-free, at the annealing temperature (498° C), and does not flow appreciably below this temperature. Metal and glass will then start together, strain-free, at P (Fig. 5(a)). The glass will tend to contract along the curve PQ, parallel to the curve designated "G-6"; while the metal, if free, would contract along the nearly straight line PO. This difference in unit contraction, *viz.*, $\delta = -550\times10^{-6}$ cm/cm, is prevented by the stresses which are set up, and is a measure of these stresses. The numerical values of the stresses may be obtained by multiplying by δ the values in Fig. 3, which are the stresses for $\delta = 1$. It is seen that the glass, if more than 5 wire diameters thick, will be subjected to a tangential tension at the surface of the wire of $0.58\times10^6\times550\times10^{-6} = 320$ kg/cm² $= 3.2$ kg/mm², and a radial compression of nearly the same magnitude; if very thin, it will suffer a tensile stress, both tangentially and axially, of $0.9\times10^6\times550\times10^{-6} = 500$ kg/cm². These values are greater than the tensile strength of glass, even in the form of smooth glass tubes (see Section 9).

Returning to Fig. 5, let us analyze the curve for G-8 glass. We note that the G-8 glass, though

commonest values (0.6 to 0.7) quoted in I. C. T. from Winkelmann and Schott. Values for sealing glasses were not available.

[6] The Allegheny Steel Company makes an alloy of approximately this composition under the name Allegheny No. 55.

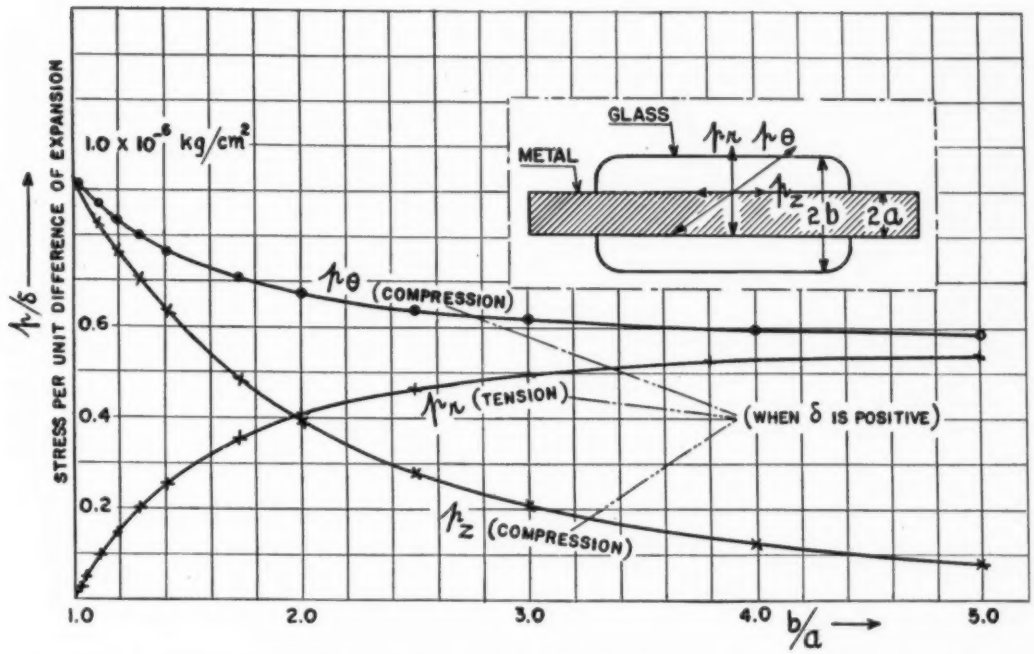

FIG. 3. (Top.) Stress in cylindrical seal at surface of wire ($r=a$) per unit difference of expansion, δ, between metal and glass, ($\delta=\{k_{\text{glass}}-k_{\text{metal}}\}\{t-t_0\}$) as function of ratio b/a of glass diameter to wire diameter. When δ is negative, the signs of stresses are the reverse of those indicated, *viz.* tension in place of compression, and *vice versa*.

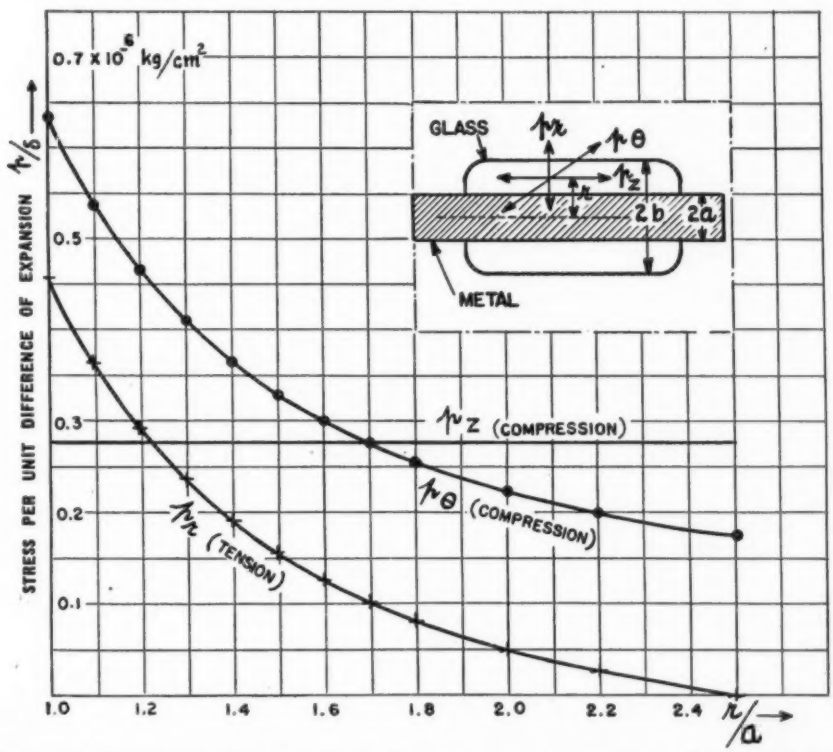

FIG. 4. (Bottom.) Stress per unit difference of expansion, δ, between metal and glass, at distance r from center of wire, as function of r/a, for $b/a=2.5$. $\delta=(k_{\text{glass}}-k_{\text{metal}})(t-t_0)$ is assumed positive. When δ is negative, the signs of all stresses are reversed.

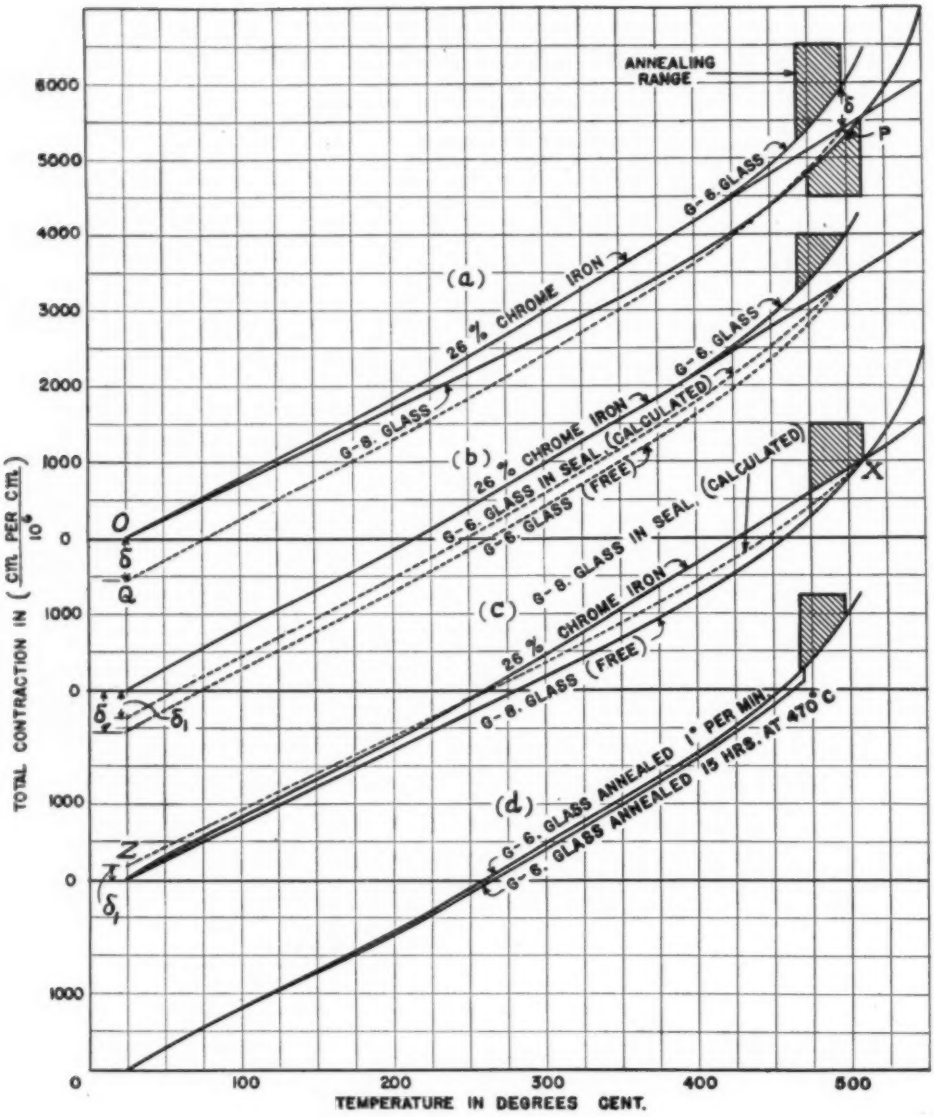

FIG. 5. (a) Thermal expansion of 28 percent chrome-iron compared with two lime-glasses. The cross-hatched areas represent the annealing range for the two glasses. (b) Effect of viscous flow during cooling of G-6-chrome iron seal. The lower dashed curve represents the observed contraction of a free glass rod during cooling at 1°C per minute, the upper, the calculated contraction when sealed to chrome-iron, corrected for flow. The net difference δ_1 between glass and metal determines the stress. (c) Same for G-8-chrome-iron seal. (d) Contraction of G-6 glass after 15 hour anneal at "strain temperature." The glass is changed by the anneal, so that its contraction coefficient is decreased.

it expands less than the metal at intermediate temperatures, catches up with it at the annealing temperature (510°C). If a seal were made with this glass and metal, and annealed at such a rate that the glass reached equilibrium and ceased to flow at the annealing temperature, then glass and metal would start cooling, strain-free, with the same relative length as at room temperature, and when cooled to room temperature would again be free from stress. During the cooling, however, and during any subsequent heating, the glass would have to pass through a region, at about 400°C, where $\delta = +425 \times 10^{-6}$, and would suffer a radial tension at the wire surface of 2.5 kg/mm².

The stresses will be very different if annealing

is carried out at a lower temperature, e.g., by holding the temperature for several hours at the "strain-point." In this case, if we take the values of δ at the strain-point as a measure of the stresses, the G-6 glass and the G-8 glass, when cooled to room temperature, will show tensile stresses at the surface of the wire of 1.4 kg/mm² and 1.7 kg/mm², respectively, (assuming thick glass), the G-8 being the more strained.

In the above discussion we have, for simplicity, postulated two definite annealing conditions. Neither of these conditions can be quite realized because of plastic flow during the annealing process. The correction for flow will now be considered.

7. Correction for Plastic Flow During Cooling

We have assumed above, as one typical case, a rate of annealing such that plastic flow of the glass neutralizes all stresses above the annealing temperature, but that no appreciable flow takes place below this temperature. This condition can be very nearly attained, at the risk of local strains in the glass, by rapid cooling. But the contraction of the glass would be different, at this rapid rate of cooling, from the values which we obtained with a rate of 1 degree per minute, as shown in Figs. 1, 5(a), etc., so that these curves do not apply. Moreover, the photoelastic methods which we have used do not apply to such strained seals. On the other hand, cooling at a uniform rate of 1°C per minute allows time for some flow below the annealing temperature, the amount of which must be calculated and allowed for. Analysis shows that with slow cooling the glass continues to flow, *under the large stresses caused by the difference of contraction*, for a long time after passing the annealing temperature. This reduces the difference δ between glass and metal, and hence the stresses.

Calculation of plastic flow during anneal

(For a more rigorous treatment, see the following paper by Dr. H. Poritsky.)

The amount of flow below the annealing temperature can be calculated from the expansion curves of metal and glass and the annealing data furnished by the glass makers, *viz.*, from the "annealing temperature" and "strain-point," which are defined as the temperatures at which 15 minutes and 4 hours, respectively, are required to remove nine-tenths of the strain.

We assume Maxwell's linear law of flow[7] in response to stress p,

$$dp/dt = E\,dS/dt - kp; \text{ where } S \text{ is the strain.} \quad (4)$$

From the logarithmic mobility law[8, 9] and the annealing data, it can be shown that k, the rate of flow per unit stress, varies with temperature according to:[9]

$$k = k_0 e^{\log 16 (T - T_0)/(T_A - T_S)}, \quad (5)$$

where T_A and T_S are the "annealing temperature" and "strain-point," respectively, and k_0 is the value of k at T_0. If we take T_0 as the "annealing temperature," k_0 is given by integration of Eq. (4) with $dS/dt = 0$ (temperature constant): $\log p/p_0 = -k_0 t$, whence, by definition of the annealing temperature, $\log 1/10 = -k_0 \times 15$ (t minutes); giving $k_0 = 0.153$.

Substituting $T - T_0 = -rt$, where r = rate of cooling in degrees per minute, (5) becomes:

$$k = k_0 e^{-2.773\, rt/(T_A - T_S)}. \quad (6)$$

Both the stresses and the strains are proportional to δ, the difference in unit expansion of glass and metal. Hence Eq. (4) may be written: $d\delta/dt = \alpha r - k\delta$, or, by (6),

$$d\delta/dt = \alpha r - k_0 e^{-brt}\delta, \quad (7)$$

where r = rate of cooling in degrees/minute; $\alpha = -\partial\delta/\partial T$ = rate of increase of strain with decrease of temperature, assumed linear; $b = 2.773/(T_A - T_S)$ is a constant of the kind of glass. The solution of Eq. (7) is:

$$\Delta = -(\alpha e^x/b)\int e^{-x}dx/x,$$

---

[7] J. C. Maxwell, Phil Mag. (4) **34**, 129 (1868).

[8] Littleton and Roberts, J. Opt. Soc. Am. **4**, 224 (1920).

[9] Twyman's law (J. Soc. Glass Tech. **1**, 61 (1917)), that the mobility doubles for each n (approximately 8) degrees rise in temperature, may be expressed by

$$k = k_0 2^{(T - T_0)/n}.$$

If, in place of a twofold increase in mobility, we take 16-fold (annealing time 4 hours cf. 15 min.) and the corresponding temperature interval $T_A - T_S$, this becomes

$$k = k_0 16^{(T - T_0)/(T_A - T_S)},$$

or

$$k = k_0 e^{\log 16 (T - T_0)/(T_A - T_S)}.$$

which can be expanded and integrated term by term, giving:

$$\Delta = e^{(x-x_0)}\delta_0 - (\alpha e^x/b)[\log x/x_0 - (x-x_0) + (x^2-x_0^2)/2\cdot 2! - (x^3-x_0^3)/3\cdot 3! + \cdots], \quad (8)$$

where $x=(k_0/br)e^{-brt}$ and $x_0=k_0/br$ and δ_0 is the value of δ at $t=0$.

If there were no flow ($k=0$), the difference in expansion would be given by (7) with $k=0$, *viz*:

$$\delta = \alpha rt + \delta_0. \quad (9)$$

Hence the amount of flow is:

$$\delta - \Delta = \alpha rt + [1-e^{(x-x_0)}]\delta_0 - (\alpha e^x/b)[brt - (k_0/br)(1-e^{-brt}) + (1/2\cdot 2!)(k_0/br)^2(1-e^{-2brt}) - (1/3\cdot 3!)(k_0/br)^3(1-e^{-3brt}) + \text{etc.}]. \quad (10)$$

Thus, for example, for seals cooled at the rate of 1°C per minute, let us assume $\delta=0$ at the annealing temperature and calculate the amount of flow of the glass during the next 30 minutes (supposing α constant over this range of temperature). For a glass with an annealing range of 40°C, we have

$$r=1, \quad k_0=0.153, \quad b=0.0693, \quad t=30,$$

and Eq. (10) gives $\delta-\Delta=12.4\alpha$, or, since by (9) $\delta=30\alpha$, $\delta-\Delta=0.41\delta$.

The amount of flow is seen to be proportional to δ, and equal to 0.41δ for the first 30°C below the annealing temperature; that is, the net difference between glass and metal at 30°C below the annealing temperature is not the value δ given by the free-contraction curves of glass and metal, but only 0.59δ.

The 30° interval, assumed for illustration, is too long for the assumption of a constant value of α, and too short to include the total amount of flow. The flow is appreciable for at least 50° below the annealing temperature. We have obtained a close approximation to this total flow by calculating a from the tangents to the glass and metal curves at each 10°C below the annealing temperature and applying Eq. (10) successively to these 10 degree intervals. Fig. 5(b) shows the net difference, thus calculated, between G-6 glass and chrome-iron, when cooled at 1° per minute. The difference, δ_1 after reaching room temperature, is -350×10^{-6} cm per cm. A seal thus annealed will therefore be subject (see Fig. 3) to a tangential tensile stress, if more than 5 wire diameters thick, of $350\times10^{-6}\times0.58\times10^6=200$ kg/cm² $=2.0$ kg/mm²; if only 2.6 times the diameter of the wire, as in the case of the test samples discussed in Section 12, it should show tensile stresses of 0.91 and 2.2 kg/mm² in the axial and circumferential directions, respectively, and a radial compression of 1.6 kg/mm². If very thin, it will suffer tension, both tangentially and longitudinally, of 3.1 kg/mm².

The corrected cooling curve of G-8 glass and chrome-iron, cooled at 1° per minute, is shown in Fig. 5(c), (curve X–Z). The difference, δ, on reaching room temperature is only 160×10^{-6} cm/cm, and the corresponding maximum tensile stress, if the glass is thick, is a radial stress of 0.95 kg/mm². If the glass is 2.6 times the diameter of the wire, as is the case of the test samples discussed in Section 12, the seal should show a radial tensile stress of 0.80 kg/mm², and a compression in the axial and tangential directions of 0.45 and 1.1 kg/mm², respectively.

The observed stresses in test samples (see Table VII, Section 12) are of the right sign but somewhat larger than predicted in the case of G-8 glass, and smaller for G-6 glass. We believe the agreement is within the limit of our knowledge of the annealing data and elastic constants.

8. Change in Glass Produced by Long Anneal at "Strain-Point"

In the case of long anneal at the "strain temperature," we have assumed that the glass would reach equilibrium at this temperature, and would then contract along the curves represented in Fig. 1. This is not quite true. Littleton[10] and others have called attention to the fact that glass cooled at ordinary rates is not in chemical equilibrium, and if allowed to stand for a long time at any one temperature will change its characteristics. Hence we may expect the glass to contract in a slightly different manner after the long anneal. Fig. 5(d) shows this contraction for G-6 glass. The corresponding curve for 705 A O glass is shown in Fig. 8. These curves represent the contraction when the glass was

[10] J. T. Littleton, J. Ind. and Eng. Chem. **25**, 748 (1933); J. Am. Ceramic Soc. **17**, 47 (1934).

cooled uniformly at 1° per minute to the strain point, held at the strain temperature for 15 hours, and then cooled at 1° per minute to room temperature. It will be noted that the contraction in cooling from the strain point to room temperature is less in each case after the long anneal than when continuously cooled, the difference being approximately 120×10^{-6} cm/cm.

In cooling to room temperature the G-6 chrome-iron seal, after long anneal at the "strain point," will therefore be subject only to a net differential unit contraction $\delta_1=78\times10^{-6}$, and the resulting axial stress, for glass/wire ratio $b/a=2.60$, will be only 0.2 kg/mm². The corresponding values for the 705 A O-fernico seal are $\delta_1=25\times10^{-6}$, $p_z=0.05$ kg/mm². Reference to Table VII, Section 12, and to photographs 3b and 17b of Figs. 9 and 10, will show that these predicted values are in excellent agreement with the stresses observed photoelastically in test seals annealed in this manner.

Long-anneal curves for the other glasses have not been obtained. We have applied an approximate correction, assuming that they behave similarly to G-6 and 705 A O, by subtracting 120×10^{-6} from the observed unit contraction of the glass between the strain point and room temperature. The values of "calculated" stress given in Table VII include this correction.

TABLE III. *Maximum inner pressure and tension in cylindrical glass tubes.* (From *Tensile Strength of Glass, etc.*, H. K. Onnes and C. Braak, Amsterdam Roy. Akad. Sci. pp. 890–897, 1907–8.)

No.	Diameter outside (b) (mm)	Diameter inside (a) (mm)	b/a	Pressure at breaking atmospheres	Max. stress in glass at breaking kg/mm²
Series a, thick wall					
1	9.3	3.5	2.66	340	5.38
2	8.8	4.0	2.20	280	4.91
3	8.7	4.2	2.07	230	4.21
4	9.4	3.2	2.94	270	4.10
5	9.2	3.0	3.07	380	5.70
6	9.7	4.2	2.31	370	6.30
7	10.4	4.0	2.60	240	3.83
8	12.8	5.8	2.21	260	4.54
9	17.6	5.0	3.52	290	4.19
Series b, capillary					
10	7.4	1.00	7.40	510	6.74
11	6.8	1.00	6.80	420	5.57
12	7.5	0.27	27.78	460	5.93
13	6.5	0.35	18.57	500	6.46
				540	6.97
14	6.7	0.24	27.92	800	10.33
				1100	14.21
15	6.7	1.08	6.20	530	7.08
16	5.9	0.70	8.43	680	8.94
17	5.8	0.46	12.61	1200	15.61
18	5.9	0.62	9.52	820	10.74
19	5.3	0.46	11.52	920	11.99
20	5.5	0.46	11.96	1060	13.80
21	6.6	1.00	6.60	660	8.78
22	7.2	1.40	5.14	520	7.07
23	6.4	1.35	4.74	520	7.13
Series c, thin wall					
24	3.8	2.42	1.57	283	7.12
25	5.6	4.00	1.40	193	6.09
26	6.4	4.78	1.34	221	7.84
27	6.9	3.91	1.76	329	7.06
28	7.4	5.11	1.45	179	5.21
29	7.9	5.46	1.45	157	4.57
30	3.5	2.26	1.54	261	6.78
31	6.8	5.13	1.32	203	7.52
32	7.4	5.19	1.43	201	6.04
33	6.8	5.78	1.18	66	3.83
34	3.8	2.42	1.57	377	9.49
35	3.8	2.50	1.52	277	7.36
36	6.0	4.37	1.37	179	5.96
37	6.8	5.17	1.31	159	6.02
38	6.8	4.85	1.40	169	5.33
39	7.3	5.62	1.30	109	4.22
40	7.8	7.31	1.067	54	7.60

9. STRENGTH OF GLASS

Table III, taken from a paper by Kamerlingh Omnes and C. Braak[11] gives a few values of maximum stress in glass tubes at breaking. If one were to choose from this table a "safe" stress, it would have to be considerably less than 4 kg/mm², since one sample broke as low as 3.8 kg/mm². Winkelmann and Schott (quoted in Int. Crit. Tab. 2, p. 93) give the "tensile strength of glass" as 3.6 to 8.5 kg/mm². Hence a "safe" value, allowing a factor of not quite two below the lowest observed break, may be taken as 2 kg/mm².

The maximum stresses at the edges of the glass in glass-metal seals will be considerably greater than our measured values at the center. These edge-effects are hard to calculate. We may assume that the edge/center ratio will not be greater than for holes in stressed sheets, *viz.*, 3/1. This would give a value for the maximum safe stress in seals, at the center, of 0.67 kg/mm². We shall take the edge factor as only 2/1, and assume that the strength of glass in seals is the same as in tubes; which gives 1 *kg/mm² as the maximum permissible measured stress in seals.*

10. PHOTOELASTIC MEASUREMENT OF STRESSES

We have studied the stresses in typical seals, of the form shown in Fig. 2, by observing the phase difference which they produce in the components of plane polarized light, polarized at 45° to the direction of the stress. The arrangement of apparatus is shown in Fig. 6. A condensed beam of nearly parallel light from an incandescent source passes through a polarizing Nicol prism and falls upon the seal *S*, which is immersed in

[11] Kamerlingh Onnes and C. Braak, Amsterdam Roy. Akad. Sci. pp. 890–897, 1907–8.

a liquid of nearly the same index of refraction as the glass. Suitable liquids for this purpose are mixtures of benzol and alcohol, or of "halowax" and Russian mineral oil. The Nicol 1 is set at 45° to the vertical. The second Nicol 2, used as an analyzer and set at 90° to Nicol 1, gives a dark field, which is not affected by the glass seal S provided it is free from stress; but if S is stressed, it will advance or retard the phase of the vertical component of the polarized light more than the horizontal component, so that the light passing through the glass will not be extinguished by the analyzer. Fig. 7(*a*) shows two seals photographed in this way, the one badly stressed and the other approximately free from stress. A photograph on the same film through an absorption wedge, exposed for the same length of time as the seal, is included for calibration of development and printing. In the photographs shown, the unstressed seal (2) (barely visible) was exposed five times as long as the badly stressed seal (1); an exposure of the same length as (1) was too faint to be seen at all.

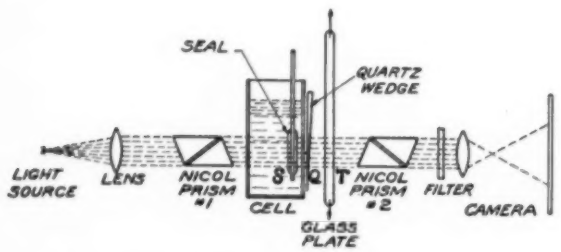

FIG. 6. Arrangement for photoelastic measurement of stresses in seals. T and Q are used alternatively. When the glass plate T is used, it is stretched with a known tension until it just neutralizes the effect of stress in S; when the quartz wedge Q is inserted, photographs are obtained like Fig. 7(c), in which the displacement of the horizontal dark lines is proportional to the stress.

These stresses in the glass may be measured by interposing in the light path a narrow glass plate T (Fig. 6) under tension, and gradually increasing the tension until the effect of the stress in S is just neutralized, as evidenced by extinction of the light. In case the axial component of stress in S is a compression, the stretched member T must be placed parallel to S; when S is under axial tension, T is placed at right angles to S. We have found this a sensitive and reliable method of measuring the stresses in seals. If T is the same thickness as the sample S, and of the same kind of glass, then the tension in T, which produces extinction of the light transmitted by S, is numerically equal to the axial stress in S.* Having thus determined the axial stress, we can read off the other stresses from Fig. 3. We measured the stresses in a large number of samples by this method. Actually we used the same tension member T for all the tests, and calibrated this glass for the different photoelastic constants of our glass samples, determined by the method next to be described. The measurements of stress made in this manner are given in Table IV.

TABLE IV. *Measurements of axial stress p_z in seals, by comparison (neutralization) with a stretched plate of 705 A O glass, of thickness $t=0.66$ cm and width $w=1.27$ cm. $p_z=(\lambda_1/\lambda)(t/d)(W/tw)$. Values of λ taken from Table V. (λ_1 = constant of comparison plate = 2.43.) Negative values of W designate stretching force applied at right angles to axis of seal.*

Glass	Metal	Anneal	Diameter of glass d	Photoelastic constant of seal λ	Stretching force on T for neutralization W	Stress in T	Axial stress in seal p_z
			cm	deg. × cm/kg	kg	kg/cm²	kg/cm²
G-5	Chrome-iron	1°/min.	0.676	1.94	48.8	58.2	−71.5
G-5	Fernichrome	406°C	0.744	"	24.7	29.5	−32.8
G-6	Chrome-iron	1°/min.	0.661	1.82	−26.5	31.6	+42.4
G-6	Chrome-iron	475°C	0.760	"	−15.7	18.7	+21.8
G-8	Chrome-iron	1°/min.	0.665	1.68	44.2	52.7	−76.0
G-8	Chrome-iron	475°C	0.700	"	60.3	72.0	−98.8
G-8	Fernichrome	1°/min.	0.670	"	28.6	34.1	−48.7
705 A J	Molybdenum	475°C	0.618	2.45	76.8	91.7	−97.2
705 A J	Fernico	1°/min.	0.750	"	48.3	57.6	−50.4
705 A J	Fernico	475°C	0.670	"	54.1	64.5	−63.2
705 A O	Fernico	1°/min.	0.682	2.43	−21.7	25.9	+25.1
71	Fernico	475°C	0.678	2.23	0	0	0
71	Molybdenum	1°/min.	0.746	"	−21.7	25.9	+25.0

A much more convenient method of exhibiting and measuring the stresses is to place a quartz wedge in the light path, as shown in Fig. 6.† The field of view with crossed Nicols is then brightly illuminated, since the doubly refracting

* This method measures, strictly speaking, not the axial stress but the ratio of axial stress to that at right angles to the axis and to the line of vision. It turns out, very fortunately, that the integrated components of radial and tangential stress, which make up the stress at right angles to the axis, exactly neutralize each other (see discussion on next page, and the accompanying paper by Dr. Poritsky) so that both this method and the following one give the axial stress uniquely.

† This elegant method was suggested to us by Dr. J. T. Littleton, of the Corning Glass Works, who has made similar tests on seals ground with flat surfaces parallel to the wire and normal to the light beam. The use of a quartz wedge for measuring stress in rectangular glass plates has been described by C. V. Boys (Nature **98**, 150 (1916)) and adopted by a number of investigators. The possibility of using this method with cylindrical rods and seals, and of determining uniquely all the stresses in a glass seal from a single photoelastic measurement, is based on the mathematical analysis of Dr. H. Poritsky (see accompanying paper).

quartz advances one component of the polarized light more than the other; but the field is crossed by horizontal dark lines, corresponding to relative phase retardations of 1, 2, etc., wave-lengths. In the photographs here shown the quartz wedge is placed so that the first two dark bands are in the field of view. If a stressed sample S is now placed in front of the wedge, a different thickness of quartz will be required to give integral wave-lengths of retardation for the light coming through S, and the horizontal dark lines will be displaced upward or downward according as the stress is tension or compression. Fig. 7(b) shows photographs taken in this manner of the same two samples as are shown in Fig. 7(a). A filter F (Wratten No. 62 Green) gave sufficiently monochromatic light, and proved more convenient than a sodium lamp.

We were unexpectedly fortunate in discovering that the displacement of the dark line depends only on the *axial component* of stress in S. Analysis shows (see accompanying paper by Dr. Poritsky) that when a symmetrical cylindrical seal of the type used (Fig. 2) is viewed at right angles to the axis of the cylinder the *integrated* effects of radial and tangential stresses exactly neutralize each other, so that *the phase displacement of the light is due solely to the axial stress and is proportional to this stress.* We have checked this in a variety of ways. In our first tests we used circularly polarized light and found the results to be identical with those of plane polarized light, polarized at 45° to the axis of the sample. A second check is the semi-elliptical shape of the displaced dark line of zero phase difference, when the quartz wedge is used and the seal is inserted in the light path. The displacement of the line should be proportional to the thickness $2y$ of glass traversed, and equal to $2y$ multiplied by $\lambda/2\pi$ (where λ is the phase displacement in radians per unit stress per unit path), times the stress p, times the distance h between successive lines of zero phase difference of the quartz wedge alone: $z = 2y(\lambda/2\pi)ph$. The displaced dark line will therefore be an ellipse of eccentricity $(1-\lambda^2p^2h^2/\pi^2)^{1/2}$ which becomes a circle when the stress is $p = \pi/\lambda h$. The shapes of the lines in Fig. 7(b) and in Figs. 9 and 10, and the close similarity of the shapes shown by seals and by glass rods under pure axial compression, are in excellent agreement with this prediction.

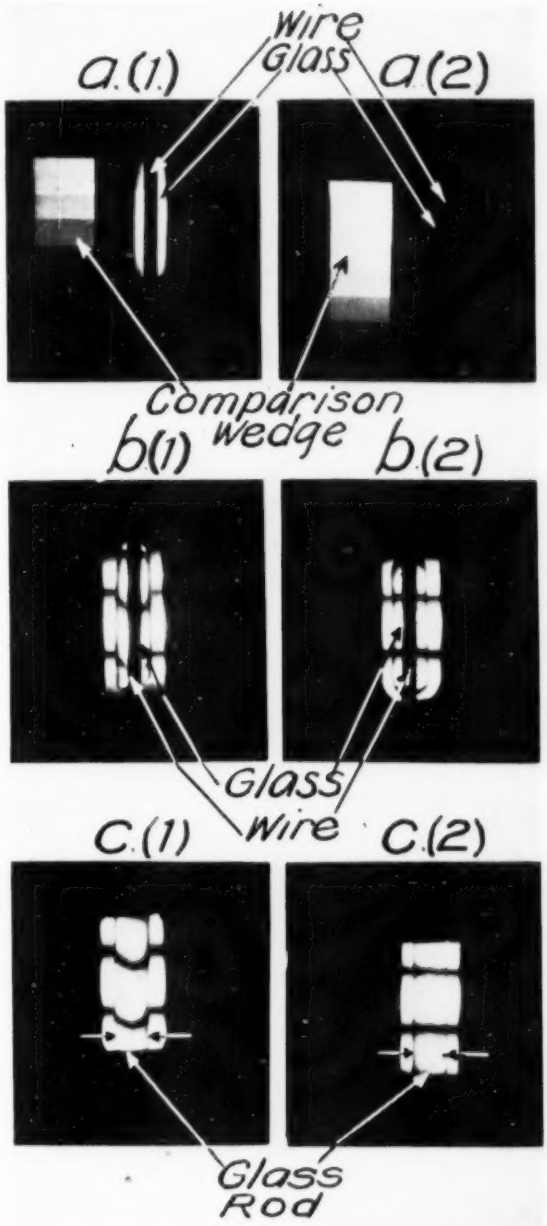

FIG. 7. (a) Typical photographs of strained glass seals, [2.5 mm wire (vertical) surrounded by glass cylinder 7 mm in diameter×30 mm long] between crossed Nicols. (1) G-5 glass and 26 percent chrome-iron; (2) G-5 glass and "fernichrome." Stepped light wedge at left of seal shows length of exposure. Seal (2), barely visible, was exposed five times as long as (1). (b) Photographs through crossed Nicols and quartz wedge of same seals as in (a). (c) Photographs through crossed Nicols and quartz wedge of G-5 glass rod, 7 mm in diameter, (1) loaded with 20.6 kg weight; (2) unstrained.

Thus, with proper calibration, the displacement of the dark lines in Fig. 7(b) may be used as a measure of the axial stress in *S*. We have obtained the calibration directly by placing a glass rod of the same diameter and kind of glass as *S* in the position of *S*, and loading it with weights, thus applying a known axial compression. Fig. 7(c) shows two such photographs of a rod of the same glass as was used in (a) and (b), (1) loaded with 20.6 kg; (2) with no load. Comparing the photographs of seal and rod, we obtain the stress in the seal by dividing this weight by the cross section of the glass rod, and multiplying by the ratio of the displacements of the dark line in sample and comparison rod, respectively.

If rods of different kinds of glass and different diameters are loaded with different weights, the displacements of the dark line are proportional to the weights and to the photoelastic constants of the glass, and inversely as the diameters. These data give the photoelastic constants λ of the glass, in degrees phase displacement per unit stress per unit thickness of glass traversed, *viz.*:

$$\lambda = 90\pi dz/hW.$$

In this way we have obtained the calibrations mentioned under method 1. Table V gives the

TABLE V. *Photoelastic constants of sealing glasses.*

Kind of Glass	Diameter d	Weight W	Displacement of dark line z	Distance between successive dark lines h	Photoelastic constant $\lambda = 90\pi dz/hW$
	cm	*kg*	*cm*	*cm*	*degrees per kg/cm² per cm thickness*
G-5 (Lead)	0.622	20.6	0.185	0.815	1.94
G-8 (Lime)	0.561	"	0.178	"	1.68
G-6	0.606	"	0.178	"	1.82
G-705 A J	0.603	"	0.242	"	2.45
G-71	0.625	"	0.212	"	2.23
G-705 A O	0.291	10.0	0.242	"	2.43
G-702 P (Nonex)	0.313	"	0.206	"	2.23
G-702 E J (Pyrex)	0.622	20.6	0.233	"	2.44
G-371 B N (Uranium)	0.608	"	0.231	"	2.36
184	0.645	10.0	.099	"	2.22

data for these calibrations, and the values thus obtained of the photoelastic constants λ.

Stress photographs, similar to Fig. 7(b), of all the seals which we have studied are shown in Figs. 9 and 10. The longitudinal stress in the glass in these seals can be estimated at a glance and also measured quantitatively from these photographs. It is equal to the maximum displacement z of the dark line, divided by the distance, h, between successive lines, times 360 over the photoelastic constant λ (in degrees), divided by the maximum thickness ($0.95\times$diameter) of glass traversed:

$$p_z = (z/h)\times 360/\lambda \times 0.95d = 380z/h\lambda d.$$

11. Sealing Metals

Platinum

The oldest sealing metal is platinum. Its expansion is shown in Fig. 1. Because of its cost, it has only historical value and will not be discussed further.

Dumet

In 1913, B. E. Eldred invented a platinum substitute, known as Dumet.[12] It consists of a core of iron-nickel alloy surrounded by a sheath of copper. The two parts are first assembled as a large rod and cylinder, respectively, and firmly welded together. They are then swaged and drawn to the required size. As used in lamp manufacture, the core metal contains approximately 42 percent nickel, and the proportion of copper in the finished wire is between 20 and 25 percent by weight. This wire has been extensively used for leading-in wires in lamps and vacuum tubes ever since its invention.

Dumet has very unusual characteristics. Calculation shows that its thermal expansion coefficient should, if there were no plastic flow of the copper, be different in the longitudinal and radial directions, *viz.*, $k_1+0.209(k_2-k_1)$ and $k_1+0.191(k_2-k_1)$, respectively, where k_1 and k_2 are the coefficients of core metal and copper, respectively. Using average values of k_1 and k_2, the longitudinal expansion coefficient comes out about 2 percent higher than the radial. The calculated expansion coefficients, both longitudinal and radial, turn out to be considerably lower than those of lead (G-5) glass. Neither of these calculated expansions agrees at all with those observed experimentally; the observed longitudinal expansion is found to be much smaller, and the radial much larger, than the calculated values, the difference between longitudinal and radial being about 40 percent, and of the opposite sign to that

[12] U. S. Patent No. 1,140,136.

calculated. These differences are accounted for by plastic flow of the copper under the stresses due to the difference in expansion between it and the core metal. The copper is subject, during cooling, to axial and tangential tension and radial compression (and *vice versa* during heating), which would produce precisely the results observed, if these stresses exceed the flow-point of the copper.

Calculation of expansion coefficients of Dumet. We assume a Dumet wire of the following composition: Core, radius a, of 42 percent nickel-iron alloy, comprising 75 percent of wire by weight; copper sheath, outer radius b, comprising 25 percent of wire by weight. The physical constants of 42 percent nickel-iron, taken from data by Guillaume[13] and Chevenard, and those of copper, from Int. Crit. Tab. are, respectively: $E_1=1.50\times10^6$ kg/cm²; $\sigma_1=0.31$; ρ_1 (density) $=8.15$ g/cc; $E_2=1.25\times10^6$; $\sigma_2=0.35$; $\rho_2=8.92$. For the wire specified this gives $b^2/a^2=1.30$.

With these constants the stress equations for concentric cylinders (see accompanying paper by Dr. Poritsky) give, for the outer (copper) cylinder,

$$p_r=+0.255\times10^6\delta,$$
$$p_\theta=-1.78\times10^6\delta,$$
$$p_z=-1.50\times10^6\delta.$$

Inserting the value of δ for the temperature range 20–300°C, *viz.* $\delta=3000\times10^{-6}$, these become:

$$p_r=+765 \text{ kg/cm}^2,$$
$$p_\theta=-5340 \text{ kg/cm}^2,$$
$$p_z=-4500 \text{ kg/cm}^2.$$

The coefficients of thermal expansion in the axial and radial directions, respectively, come out (see Poritsky, following paper):

Axial Expansion
$$=\{e_z+k_2(T-T_0)\}/(T-T_0)=k_1+0.209(k_2-k_1),$$

Radial Expansion
$$=\{u_b/b+k_2(T-T_0)\}/(T-T_0)=k_1+0.191(k_2-k_1).$$

e_z = elastic elongation (strain) in z direction; u_b = total radial elastic displacement at b; u is defined by $e_r=\partial u/\partial r$.

Table VI gives the average expansion coefficients between 20° and 300°C, calculated from the above equations, using $k_1=6.1$, $k_2=16.2$; and for comparison the observed values for 4 samples of a Dumet wire of 1.25 mm diameter:

TABLE VI.

Sample No.	Axial expansion Calc.	Axial expansion Obs.	Radial expansion Calc.	Radial expansion Obs.
476	8.2×10^6	6.8×10^{-6}	8.0×10^6	9.9×10^{-6}
486	"	6.1	"	8.0
496	"	6.6	"	10.0
506	"	6.6	"	9.1

It is evident that during heating the copper flows under the large axial and tangential compressive stresses and the radial tensile stress, thus making the net axial expansion less and the radial more than calculated. The resultant expansion under these conditions will be such as to leave the copper stressed to just its flow point, and is a measure of the flow point. A comparison of the experimental (axial) curve in Fig. 1 with the curve of 42 percent nickel-iron (not shown) gives $\delta_{max}=100\times10^{-6}$ for the range 20–450°C. The critical yield strength of the copper in the sheath is therefore $(p_z)_{max}=1.50\times100=150$ kg/cm². We may use this as a measure of the maximum force which copper can exert on a glass seal. Using this value, we can calculate the stress in Dumet-glass seals. Since the tension in the copper differs so little from that in the glass, a sufficient approximation is obtained by first applying the equations of Section 5, on the assumption that the glass extends to the core, and then correcting for the additional stress of 150 kg/cm² in the copper. In this way we obtain, for a Dumet wire of 2.0 mm diameter surrounded by G-5 glass of 7.0 mm diameter, axial stresses of 135 and 108 kg/cm², for seals cooled at the rate of 1 degree per minute and annealed at strain point, respectively. These values are in satisfactory agreement with those observed experimentally (see Table VII, Section 12).

Dumet is thus a very bad match, from the standpoint of coefficient of expansion, for the lead-glass with which it is used, and Dumet lead-glass seals should be badly strained. This is found to be true (see cuts 2a and 2b, Fig. 9, and Table VII). However, the low yielding point of copper sets a limit to the stress which it can exert. If the wire is small enough, this limit will be below the breaking strength of glass. Experience shows that seals made with Dumet wires of more

[13] Trav. et Mem. Bur. Int. Poids. et Mesures, 17, 1927.

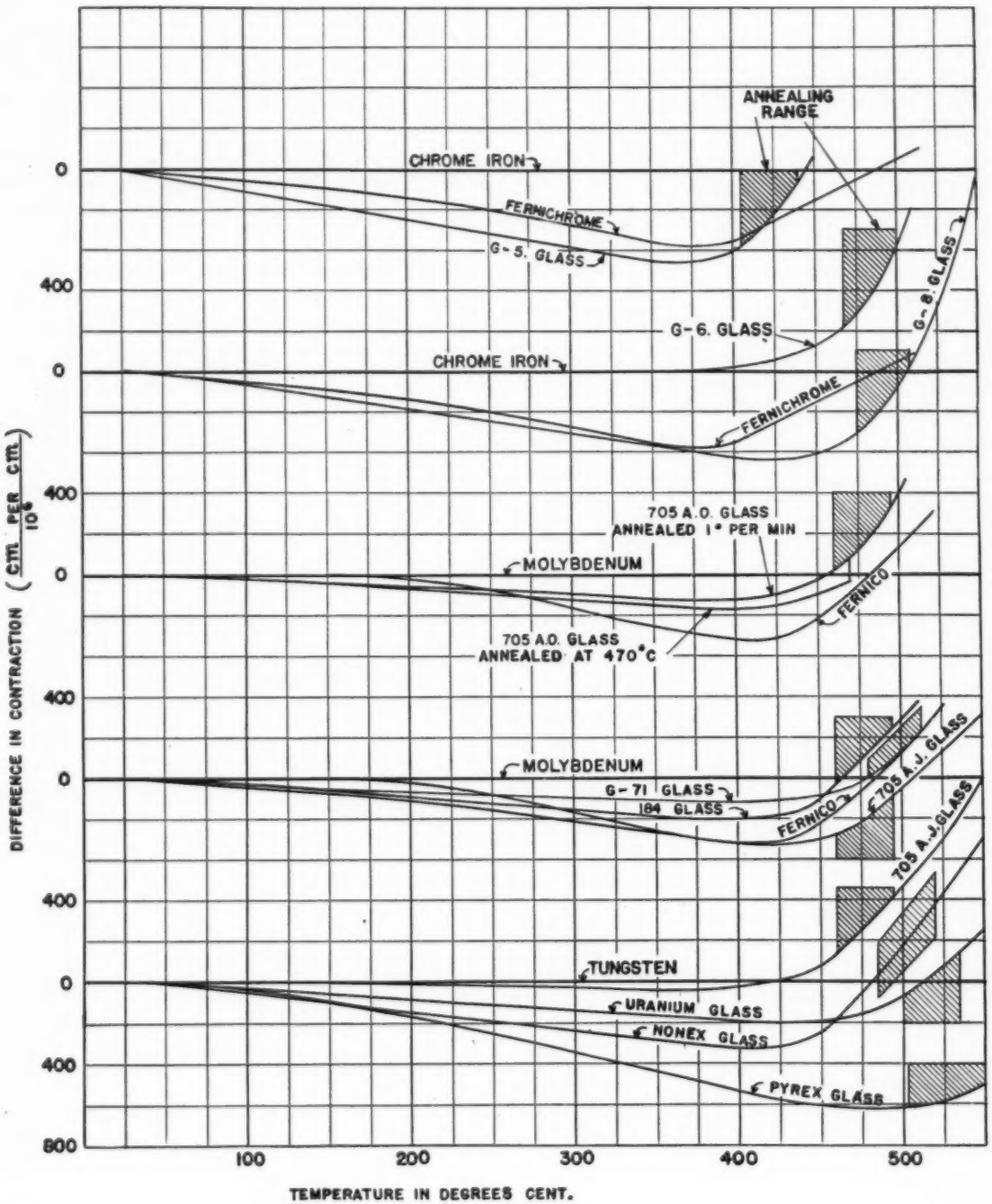

FIG. 8. Relative contraction of principal sealing glasses and metals, when cooled at rate of 1° per minute. Cross-hatched areas represent annealing range of temperature. Ordinates are the *differences* in contraction, per unit length of sample, between the metal taken as standard (axis horizontal) and the glasses and other metals nearest to it in expansion. These differences, in conjunction with the annealing conditions, determine the stresses in seals.

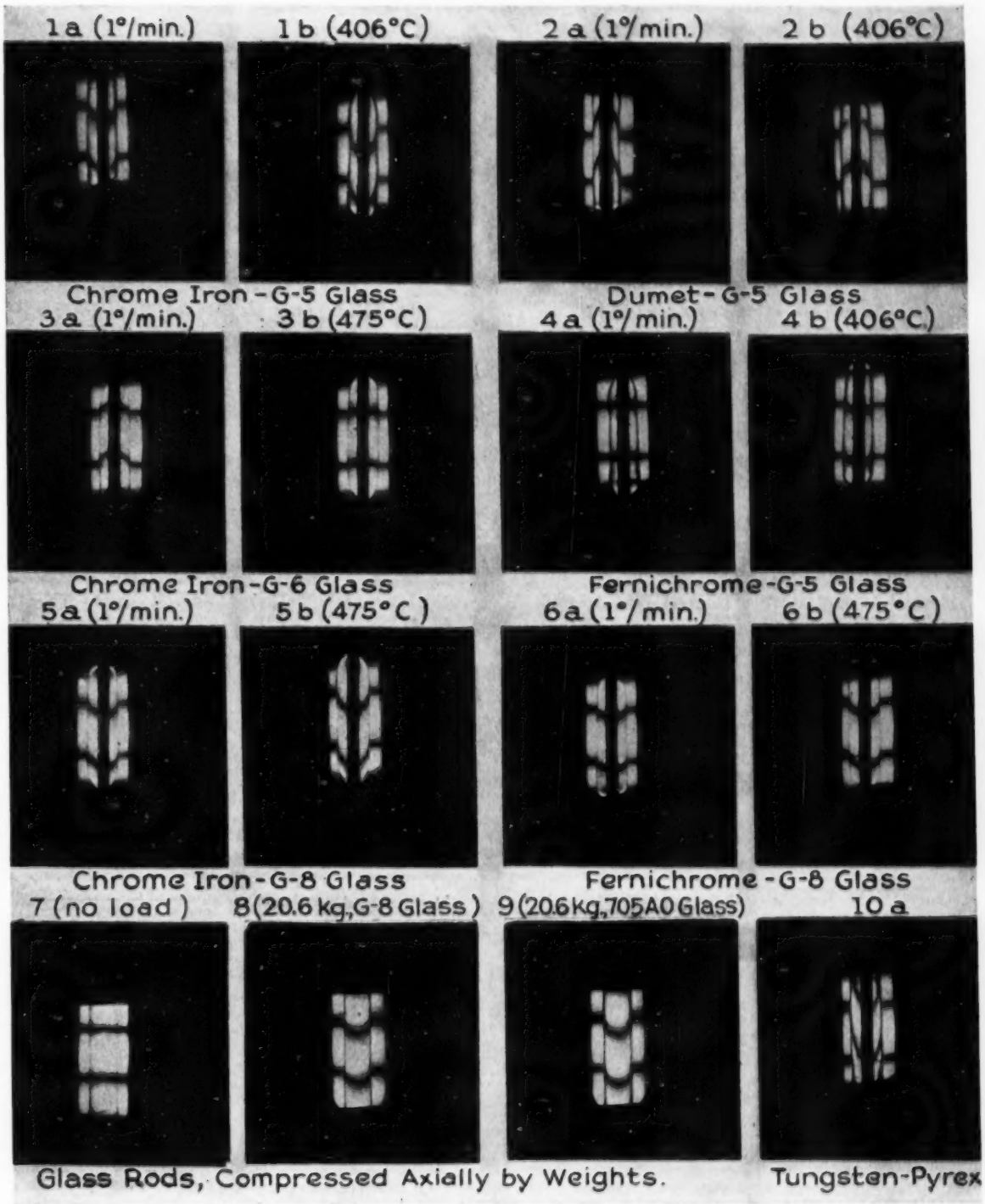

FIG. 9. Photographs of soft-glass seals (2.5 mm wire, vertical, surrounded by glass tube 7 mm in diameter×30 mm long) viewed through crossed Nicols and quartz wedge. Displacement of horizontal dark lines measures axial stress in glass, *upward being tension, downward compression*. Photo No. 7 shows glass rod unstrained, and 8 and 9 rods of G-8 and 705 A O glass compressed axially by wt. of 20.6 kg. Note that 705 A O has larger deflection, which means larger photoelastic constant.

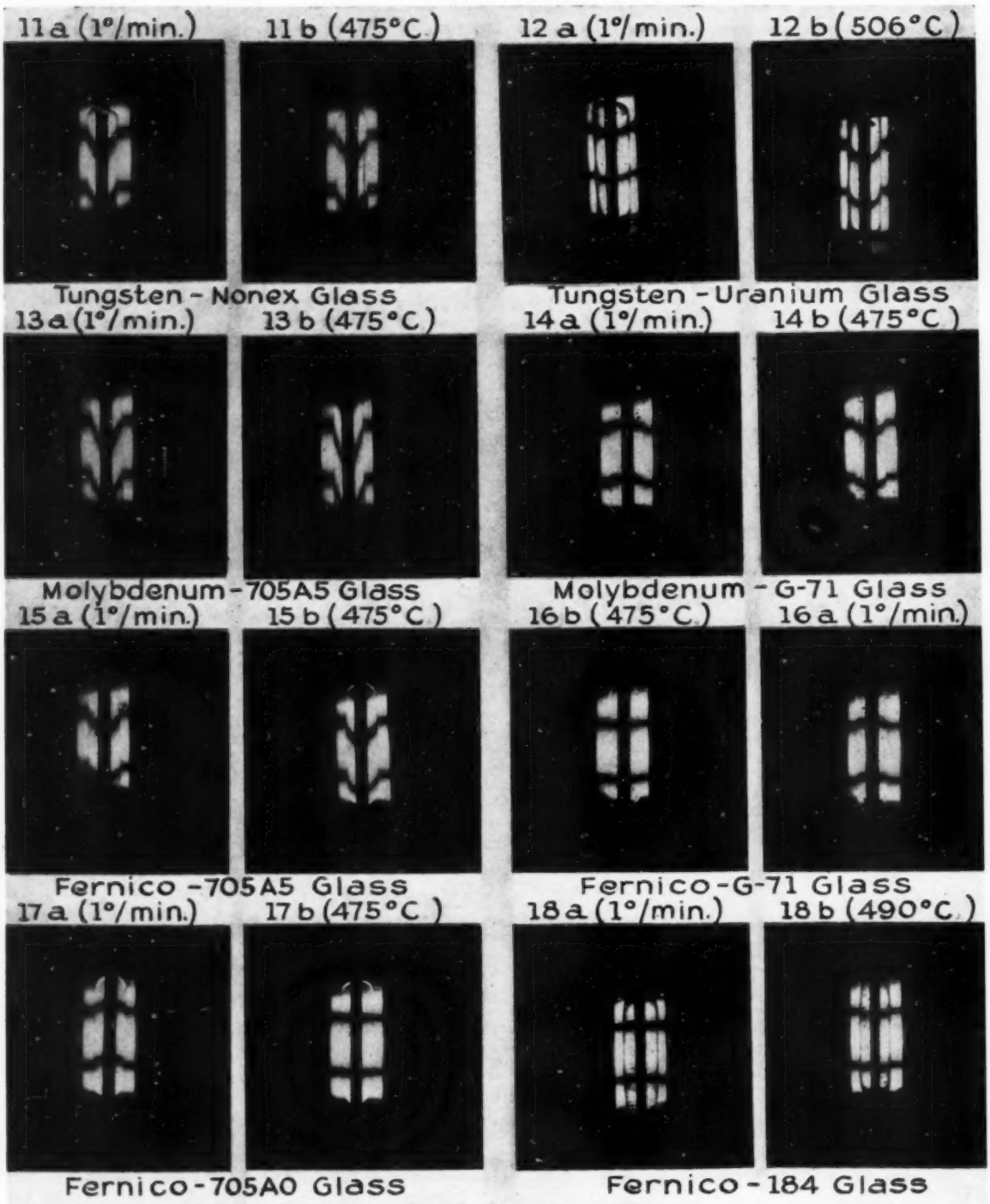

FIG. 10. Photographs of hard-glass seals (2.5 mm wire, vertical, surrounded by 7 mm glass tube 3 cm long) viewed through crossed Nicols and quartz wedge. (a) Seals cooled 1°C per minute; (b) seals annealed 15 hours at "strain" temperature. Displacement of horizontal dark lines shows, quantitatively, axial stress in glass; upward displacement means tension, downward compression. (*Correction:* titles under cuts 13 and 15 should read "705 A J Glass."

than 1 mm diameter usually break, but that wires of 1 mm or less are fairly satisfactory. The high conductivity of the copper makes it possible to use Dumet wire of 0.8 mm diameter for currents up to 20 amperes.

Chrome-iron

Chromium-iron alloy, containing 26 to 28 percent chromium, has been extensively used in Europe for sealing with lime and lead-glasses. The chrome-iron lime-glass expansion curves have already been discussed in Sections 6–8. The observed stresses in test seals are given in Table VII and shown graphically in Fig. 9. Chrome-iron is easily wetted by both lead and lime-glass, and is remarkably free from danger of over-oxidation. It is not, however, a good match for standard lead and lime-glasses if the seals are to be annealed.

Fernichrome

We have recently found an alloy consisting of iron, cobalt, nickel, and chromium (37 percent Fe, 30 percent Ni, 25 percent Co, 8 percent Cr), which we have designated as "fernichrome," that matches lead and lime-glasses much more closely than does the 26 percent chrome-iron. Its expansion characteristic, shown in Fig. 8, is curved so that it very nearly matches the shape of the glass curves. Photographs a(2) and b(2) in Fig. 7, and 4a of Fig. 9 show that lehr-annealed seals between this alloy and standard lead-glass are remarkably stain-free.

Tungsten

Tungsten has been used for sealing to hard glass since 1915.[14] It has good electric conductivity and a fairly adherent oxide, so that adherence to glass is easily obtained. It can be used in considerably larger sizes than Dumet, *viz.*, up to 5 mm diameter or even greater. It has been, until recently, the only practical sealing material for currents greater than 20 amperes (except "Housekeeper" seals—see "Copper," below). The glass which is generally used with tungsten, namely, G-702P, or Nonex, is not ideally adapted to the purpose if the seals are to be slowly cooled, as shown by photographs 11a and 11b, Fig. 10. The best tungsten sealing glass which we have found is Corning G-371 B N (photograph 12a, Fig. 10).

Molybdenum

Molybdenum is occasionally used for seals and is destined to be more used in the future. The relative thermal expansion of molybdenum and 705 A J glass is almost identical with that of tungsten and Nonex, and molybdenum has the advantage of being cheaper and less susceptible to cracks or fibrous defects. Molybdenum sealing, however, requires very careful technique in order to avoid over-oxidation.

Fernico

We have found an alloy[15] of iron, cobalt and nickel (54 percent Fe, 28 percent Ni, 18 percent Co), which we have designated "fernico," that has a remarkable thermal expansion characteristic. Its average expansion is nearly identical with molybdenum, but it has the unique feature of a "transition point" in its expansion characteristic, at which the rate of expansion increases by a factor of 3. It has been noted above that all known glasses have such a transition in their expansion. The unique feature of fernico is that this transition comes at the same temperature as that of certain standard glasses, and that the increase in the rate of expansion is also approximately the same as that of the glasses. Hence it is possible to find a glass whose expansion matches that of fernico with a high degree of accuracy *over the whole range from zero to the softening point.* Fig. 8 shows curves of a number of glasses which approach closely to this match, and photographs 16 to 18, Fig. 10, show how well actual sealing tests confirm the predictions of the expansion curves.

Copper

In 1923, W. G. Housekeeper published a remarkable paper[16] on "The Art of Sealing Base Metals Through Glass," which has had a profound influence on vacuum tube development. Briefly stated, Housekeeper's method consists in making the metal so thin that it will yield

[14] U. S. Patent No. 1,154,081.

[15] The thermal expansion of the iron-nickel-cobalt series has been studied by H. Scott, Trans. A. I. M. E., Inst. of Metals Div., pp. 506–538, 1930; and by H. Masumoto, Sci. Rep. Tohoku Imp. Univ. **20**, 101 (1931).

[16] W. G. Housekeeper, J. A. I. E. E. **42**, 954 (1923).

before the glass does. Theory and practice prove that by this method any glass may be sealed to any metal, regardless of expansion coefficients, provided they will stick to each other; and that there is no limit to the size of seal that may be made. Such seals are used today on all large power tubes. A familiar example is the six inch diameter ring seal between Pyrex or Nonex glass and the copper cylinder of the 100 kw Pliotron tube.

Copper is the metal used almost universally for Housekeeper seals, principally because of its high ductility and low yield point; and practice is tending rapidly toward the use of *Pyrex glass and copper*. Although copper appears to be the best metal for this use, it has the following weaknesses:

The seals are mechanically weak, because of the thinness of copper that is required to keep the stress on the glass within safe limits. (This limitation would be the same for any "Housekeeper" seal, whatever metal is used.) For example, the average breaking strength of a number of 3/4 inch diameter thin edge copper-Pyrex seals, tested in a steel tensile-strength testing machine, was 400 lbs., as compared to 1150 lbs. for chrome-iron-G-6 seals of the same diameter but thick edges (not Housekeeper).

Thin copper is easily oxidized to the degree that it becomes porous. This is a prolific source of factory shrinkage during the sealing-in and exhaust processes. Recently some life-failures from this cause have been observed in power tubes during operation.

The thin copper is subject to fatigue failure if repeatedly heated and cooled, since it must flow at each heating and cooling (else the glass must break). Tests on 14 copper seals (3/4 inch diameter), heated and cooled successively to 400°C and 50°C, gave an average life, due to combined fatigue and oxidation, of 290 cycles of operation, as compared to 1100 cycles for similar seals of invar, and over 5000 cycles for flat butt seals of similar diameter of fernico and 705 A J glass. Similar tests of fernico and 705 A O glass are expected to yield much longer life.

Copper cannot be electrically welded to iron, and vacuum-tight silver soldering is difficult and subject to amalgamation by mercury.

Copper is attacked, slowly, by mercury.

Because of these limitations, iron-nickel alloys, such as invar, are being used to some extent in place of copper.

12. Analysis of Seals

The relative expansions of these sealing materials and the glasses* which most nearly match them are shown in Fig. 8. These measurements were taken *during cooling* at the rate of 1° per minute. In calculating the stresses from these curves, we have made correction for the plastic flow of the glass that takes place during the annealing process, as explained in Sections 7 and 8. Uncertainty of the annealing data used for these corrections is the largest source of error in the calculated stresses. The expansion curves were taken with samples of the same glass and metal which were used for the experimental seals. The measurements are reproducible within about ±2°C, which is considerably more accurate than the reproducibility of glass and metal. The stresses calculated from these curves are given in Table VII, columns 6, 8 and 10.

Figs. 9 and 10 show photographs of all the seals which we have studied, taken through crossed Nicols and a quartz wedge, as explained in Section 10. The displacement of the horizontal dark bands in these photographs is a direct measure of the longitudinal stress in the seals, this stress being positive, i.e., tension, when the displacement is upward, and compression when the displacement is downward. The photographs are arranged in pairs, marked a and b. In group a, the seals were annealed by cooling from above the annealing temperature to below the lowest flow temperature at a uniform rate of 1° per minute. This corresponds approximately to standard lehr annealing practice for seals and other parts of vacuum tubes. In group b, the seals were held for 15 hours at the "strain point."

In comparing the a and b seals of each pair, it will be observed that whenever the deflection is upward the a sample shows a larger deflection, i.e., greater stress, than its b mate; while the reverse is true when the deflection is downward. An upward deflection, representing axial tension

* All of these glasses are made by the Corning Glass Works, except "184," which is an experimental glass made in this laboratory.

TABLE VII. *Observed and calculated stresses at surface of wire in experimental cylindrical seals (form shown in Fig. 2), when annealed as indicated and cooled to room temperature. Positive stresses represent tension, negative compression. The maximum safe tension is approximately 1 kg/mm².*

Metal	Glass	Anneal	Axial stress p_z			Radial stress p_r		Circumferential stress p_θ		Maximum tensile stress
			Obs.			Obs.	Calc.	Obs.	Calc.	Obs.
			Method 1 kg/mm²	Method 2 kg/mm²	Calc. kg/mm²	(Ave.) kg/mm²	kg/mm²	(Ave.) kg/mm²	kg/mm²	kg/mm²
Chrome-iron	G-5	1°/min.	−0.71	−0.65	−0.60	+1.28	+1.13	−1.70	−1.50	1.28
"	"	406°C		−1.20	−1.35	+2.15	+2.40	−2.90	−3.25	2.15
Dumet	"	1°/min.		+1.10	+1.35	−3.63	−4.35	+3.87	+4.75	3.00
"	"	406°C		+1.00	+1.08	−2.98	−3.22	+3.58	+3.86	2.50
Fernichrome	"	1°/min.		+0.06	+0.12	−0.11	−0.21	+0.14	+0.28	0.14
"	"	406°C	−0.33	−0.26	−0.34	+0.69	+0.79	−0.86	−1.00	0.69
Chrome-iron	G-6	1°/min.	+0.42	+0.62	+0.91	−0.93	−1.62	+1.26	+2.20	1.26
"	"	475°C	+0.22	+0.17	+0.16	−0.48	−0.39	+0.59	+0.49	0.59
"	G-8	1°/min.	−0.76	−0.75	−0.45	+1.39	+0.83	−1.86	−1.11	1.39
"	"	475°C	−0.99	−1.02	−1.01	+2.09	+2.10	−2.71	−2.73	2.09
Fernichrome	"	1°/min.	−0.49	−0.41	−0.33	+0.84	+0.62	−1.12	−0.83	0.84
"	"	475°C		−0.65	−0.91	+1.26	+1.76	−1.66	−2.31	1.26
Tungsten	G-702 P (Nonex)	1°/min.		−0.84	+0.16	+1.27	−0.24	−1.82	+0.35	1.27
"	"	475°C	−0.87	−0.91	−0.53	+1.60	+0.93	−2.16	−1.26	1.60
"	Uranium	1°/min.		−0.18	0	+0.48	0	−0.59	0	0.48
"	"	506°C		−0.56	−0.38	+1.31	+0.89	−1.64	−1.11	1.31
"	Pyrex	1°/min.		−1.98	−1.36	+4.80	+3.30	−6.00	−4.15	4.80
Molybdenum	G-705 A J	1°/min.		−0.90	−0.42	+2.15	+1.01	−2.70	−2.26	2.15
"	"	475°C	−0.97	−1.42	−0.90	+1.88	+1.42	−2.60	−1.97	1.88
"	G-71	1°/min.	+0.25	+0.17	+0.48	−0.49	−1.12	+0.62	+1.40	0.62
"	"	475°C	−0.39	−0.36	−0.15	+0.69	+0.29	−0.90	−0.38	0.69
Fernico	G-705 A J	1°/min.	−0.50	−0.49	−0.38	+1.18	+0.91	−1.48	−1.14	1.18
"	"	475°C	−0.63	−0.68	−0.66	+1.17	+1.18	−1.59	−1.60	1.17
"	G-71	1°/min.		+0.19	+0.55	−0.31	−0.90	+0.41	+1.18	0.41
"	"	475°C	0	−0.07	0	+0.13	0	−0.17	0	0.13
"	G-705 A O	1°/min.	+0.25	+0.23	+0.37	−0.39	−0.60	+0.52	+0.80	0.52
"	"	475°C		−0.04	−0.05	+0.09	+0.11	−0.11	−0.13	0.09
"	184	1°/min.		+0.08	+0.26	−0.19	−0.61	+0.23	+0.76	0.23
"	"	490°C		−0.13	0	+0.24	0	+0.33	0	0.24

in the glass, results when the coefficient of expansion of the glass is greater than that of the metal (cf. Eq. (3), Section 5). Hence, when the glass expands and contracts more rapidly than the metal, the seals are improved by the long annealing schedule b; but when the glass contracts less than the metal (deflection down), the seals are made worse by long annealing. Seals of the latter type, if used, should be cooled as quickly as is possible without introducing undue local strains in the glass. This difference in the effects of annealing has already been predicted (Sections 7, 8) from the expansion curves.

Table VII shows the numerical values of the stresses, both observed and calculated. Columns 6, 8 and 10 give the stresses calculated from the expansion curves of Fig. 8. In columns 4 and 5 are given the "observed" values of axial stress, obtained, respectively, by neutralizing the stress with a strip of glass under measured tension, and by measurement of the displacement of the dark lines in the photographs of Figs. 9 and 10. In all cases the stress which was directly measured was that parallel to the axis of the wire. From this the radial and tangential stresses at the surface of the wire were calculated, with the aid of Eqs. (1–3), Section 5, or Fig. 3. These stresses are maximum at the wire and decrease gradually (see Fig. 4), toward the surface of the glass, while the axial stress is uniform over the cross section.

It should be emphasized that these measurements, both "theoretical" and "experimental," apply to *annealed seals*. A more rapid rate of cooling, up to 50° per minute, is practical for seals of the size tested, without excessive local strain. We have not considered it worth while to make a detailed analysis of seals so cooled, since strains are of greatest importance in large seals which would of necessity require slow cooling. The general effect of rapid cooling can, however, be predicted from the curves of Fig. 8. It has already been noted that seals, in which the average coefficient of the glass up to the annealing temperature is lower than that of the metal, are better when cooled at the rate of 1°C per minute than when annealed for several hours, while the opposite is true of seals in which the expansion of the glass is greater than that of the metal. Thus, combinations of glass and metal, for which the photographs "a" of Figs. 9 and 10 show very bad *negative* (downward) stresses, may still be

used in some cases where the thickness of glass and metal is such as to allow rapid cooling.

13. Experimental Results

The agreement between the observed stresses and those predicted ("calculated") from the expansion curves is satisfactory, and within the limits of our knowledge of the annealing data, except possibly for tungsten and molybdenum, whose oxides appear to react slightly with the glass. The agreement is especially good for seals annealed for a long time at the "strain temperature." For seals cooled at 1° per minute there seems to be a small consistent error, in the same direction for all seals, *viz.*, an apparent lowering of the coefficient of expansion of the glass in the seals as compared with that shown by the curves.* It is to be emphasized that the seals, in the 1°C per min. annealing process, are cooled at exactly the same rate as the glass rods in the "contraction" measurements, and that these measurements are not affected by previous history. The effect in question is larger the higher the sealing temperature of the glass, and is such as would be accounted for if the glass in the seals is "hardened" by the sealing process. Some such hardening is to be expected from evaporation of alkali constituents of the glass. The glass is heated hotter and longer during the sealing process than in the drawing of the rods for expansion measurements. Evaporation would be greater the higher the sealing temperature of the glass, which is in the direction observed. It seems possible, however, that the "hardening" is the result of solution of metal oxides in the glass, either by directly lowering the coefficient of the glass, or by a catalytic action promoting chemical equilibrium in the under-cooled liquid glass. It is to be noted that the tungsten and molybdenum stress photographs in Fig. 10 are "peaked" near the wire, indicating that the glass nearer the wire is the more modified.

* The effect of a lower value of expansion of the glass in the seals than that shown by the curves would be to make the calculated stresses come out numerically too large for glasses whose expansion is greater than that of the metal, and too small for the glasses whose expansion is less than the metal. Such a difference is to be observed, without exception, in Table VII, for all seals cooled at a uniform rate of 1° per minute.

14. Discussion of Results

The relative merit of the different seals may be inferred directly from the stress-photographs of Figs. 9 and 10, in which the displacement of the dark lines is proportional to the stress, and from the numerical values of the stresses in Table VII. The important values are those of *maximum observed tension* (positive stress) for each type of seal, since it is generally accepted that glass will stand much greater compression than tension. These values are collected in the last column of Table VII. They are the radial stresses in those cases where the glass contracts less than the metal, and tangential (circumferential) stresses when it contracts more.

Table VII speaks for itself. If we accept the criterion that the *maximum safe stress is 1 kg/mm²* (Section 9), we may read off at once the glass-metal combinations that will make satisfactory seals under either of the annealing conditions studied, *viz.*, those combinations for which the *maximum tensile stress given in the last column is less than unity*. While these values apply specifically to cylindrical seals of a particular size, they do not differ greatly from those met with in practical seals of all types, including small wire seals (except Dumet). They do not apply to rapidly cooled seals, or seals deliberately strained by quenching.

The following comments may be added to the data given in the table.

Lead-glass seals

Of the three metals available for sealing to lead-glass, fernichrome is the only one that satisfies the stress requirements for a "safe" annealed seal. Fernichrome G-5 seals annealed at 1°/minute appear to be practically strain-free. We have made such seals in a variety of shapes and sizes, with the same result.

Chrome-iron and G-5 do not make safe seals with any kind of annealing tried; but the seals would be improved and probably be satisfactory if they could be quickly cooled, or the metal cooled more rapidly than the glass.

Dumet seals of the size tested, *viz.*, with 2 mm diameter wire, are very badly strained; in fact, we had difficulty in obtaining seals for test that did not break while cooling. But the stresses in

these seals, unlike all others, depend on the size of the wire, because of the limited flow-strength of the copper. The maximum tensile stress (radial) in the glass should be proportional to the cross section of the wire. Hence a wire of 1 mm diameter should show a stress of only 3.00/4 = 0.75 kg/mm², which is a "safe" value. This agrees with experience.

Lime-glass seals

Chrome-iron-G-6 seals are satisfactory if annealed at the "strain point," but not otherwise. They are worse the more rapid the cooling. Chrome-iron-G-8 (ordinary lime) seals are not satisfactory with any kind of annealing tried, but would be improved by rapid cooling. Fernichrome-G-8 seals barely pass when cooled at 1°/minute. They would be improved by more rapid cooling.

Tungsten seals

Tungsten-Nonex seals have been extensively used. The shrinkage, that is the fraction which breaks, has always been appreciable. The analysis shows that a long anneal (at the strain point) makes them worse, and that they are best when cooled as rapidly as practicable. When cooled at 1°/minute, which corresponds approximately to good lehr annealing, the stress is decidedly above the safe limit.

"Uranium" glass and tungsten make very satisfactory seals for lehr annealing. A rate more rapid than 1°/minute would make them still better, up to the highest rate allowed by the thickness of the glass.

Tungsten-Pyrex seals are entirely impractical. The enormous radial stress usually breaks the "cement" at the glass-metal interface, allowing air leakage along the interface.

Molybdenum seals

Molybdenum has been little used for seals, because of its oxidizability. But if oxygen is excluded as much as possible it makes excellent seals. It is evident from the table that G-71 has as nearly the right expansion to match molybdenum as can be found. The stresses are of opposite sign for the two types of annealing; hence the best anneal would be a rate between these two. G-71 is not a very common glass; but might become so, or some equivalent such as 705 A O be standardized, if sufficient use is found for it.

Fernico seals

Fernico has the unusual property that its expansion curve is bent, and runs parallel to glasses such as 705 A J *in the annealing range.* Hence seals like those with 705 A J, which are considerably strained and unsatisfactory, will be equally strained under all annealing conditions.

This same property, however, renders fernico seals with the proper glass *unstrained under all annealing conditions.* Inspection of Table VII shows that this is true of the combinations of fernico with G-71, G-705 A O, and 184* glasses. The expansion of 705 A O is slightly too high, but well within the "safe" limit. One other feature of fernico seals deserves mention, namely, that they are less stressed *during the cooling process,* due to small divergence of the glass and metal curves, than are seals made with "linear" metals and alloys.

(*Note*). The following table gives the official code designations of the Corning glasses referred to in this paper:

Descriptive Name	Code Designation
G-5 glass	Corning Glass 005
G-8 "	" " 008
G-6 "	" " 013
G-71 "	" " 771
Nonex Glass	Pyrex " 772
Pyrex "	" " 774
705 A J "	" " 705
705 A O "	" " 706
Uranium "	" " 332

* "184" is an experimental glass, made for us by Dr. Louis Navias of this laboratory, of the following composition: SiO_2—65, B_2O_3—23, Na_2O—7, Al_2O_3—5.

Analysis of Thermal Stresses in Sealed Cylinders and the Effect of Viscous Flow During Anneal

HILLEL PORITSKY, *Engineering General Department, General Electric Company, Schenectady, N. Y.*

(Received September 12, 1934)

Equations are derived for the thermal stresses in long sealed cylinders due to different coefficients of expansion, on the basis that the material of the cylinder is elastic. The optical retardation due to this stress distribution is computed for a ray traveling normal to the axis, and is found to depend upon the axial stress only. The modification in the stress distribution is then investigated for the case when plastic or viscous flow takes place during annealing.

1. THERMAL STRESSES IN SEALED CYLINDERS

THE case of long glass-metal seals, as well as the case of Dumet wire, may be idealized by imagining a long hollow cylinder of internal radius a and external radius b to be slipped over an equally long solid cylinder of radius a, the material of the two cylinders soldered or melted together at the junction at a temperature T_0, and the temperature then changed. The problem is what stresses develop in the cylinders at a temperature T, if the materials of the two cylinders possess different coefficients of thermal expansion.

In this section we shall suppose that no plastic flow or thermal creep occurs; that the substances of the cylinders are characterized by conventional elastic constants E, σ (E= Young's modulus, σ = Poisson's ratio); and that these are independent of temperature. We denote by k the coefficients of linear expansion, and distinguish constants and formulas pertaining to the inner cylinder from those relating to the outer one by using subscripts 1 in the former case, and 2 in the latter.

We shall assume that, due to the great length of the cylinders, the deflection, strains, and stresses are the same in various planes normal to the axis and that these planes, moreover, remain plane after the temperature change. The following calculations consequently do not apply to short cylinders where the "end correction" extends throughout the length of the axis.

Under these conditions the axial and radial directions are directions of principal stress. Introducing cylindrical coordinates r, θ, z, we shall denote the stress components in the directions of increasing r, θ, z by p_r, p_θ, p_z, respectively. Under the assumptions made there will be no shear components (such as p_{rz}), and p_r, p_θ, p_z will depend on r only.

We propose the following expressions for the stresses in the outer cylinder at temperature T:

$$p_r = A_2 + B_2/r^2; \quad p_\theta = A_2 - B_2/r^2; \quad p_z = C_2, \tag{1}$$

where A_2, B_2, C_2 are constants; and similar expressions with subscripts 2 changed to 1 for the inner cylinder, omitting, however, the B_1/r^2 term as this would become infinite at $r=0$:

$$p_r = A_1; \quad p_\theta = A_1; \quad p_z = C_1. \tag{2}$$

These expressions are of the same form as the Lamé solution for a cylinder subject to radial stress over the boundary.[1] To establish them we shall prove first that they satisfy the equations of equilibrium. Then we shall find the strains e_r, e_θ, e_z, by applying Young's law and taking the thermal expansions into account thus:

$$\begin{aligned} e_r &= p_r/E - \sigma(p_\theta + p_z)/E + k(T - T_0), \\ e_\theta &= p_\theta/E - \sigma(p_r + p_z)/E + k(T - T_0), \\ e_z &= p_z/E - \sigma(p_r + p_\theta)/E + k(T - T_0), \end{aligned} \tag{3}$$

and then establish the "compatibility relations" for the strains, namely, the condition that they can be derived from two displacement components u, w:

$$e_r = \partial u/\partial r, \quad e_\theta = u/r, \quad e_z = \partial w/\partial z, \tag{4}$$

where u is the radial displacement and w the axial one.

For the axial symmetry assumed, the equations of equilibrium reduce to

$$\partial(rp_r)/\partial r - p_\theta = 0; \quad \partial p_z/\partial z = 0.^2$$

[1] See, for instance, Love, *Theory of Elasticity*, 4th Ed., p. 144.

[2] See Love, reference 1, p. 143, Eq. (53).

The expressions will be found to satisfy these equations for arbitrary A_2, B_2, C_2. Eqs. (3) now yield (with E, σ, k, replaced by E_2, σ_2, k_2):

$$\begin{aligned} E_2e_r &= A_2(1-\sigma_2)+B_2(1+\sigma_2)/r^2-\sigma_2C_2 \\ &\quad +E_2k_2(T-T_0), \\ E_2e_\theta &= A_2(1-\sigma_2)-B_2(1+\sigma_2)/r^2-\sigma_2C_2 \\ &\quad +E_2k_2(T-T_0), \\ E_2e_z &= A_2(-2\sigma_2)+C_2+E_2k_2(T-T_0). \end{aligned} \tag{5}$$

These are compatible with (4), provided u is given by:

$$E_2u=[A_2(1-\sigma_2)-\sigma_2C_2+k_2E_2(T-T_0)]r -B_2(1+\sigma_2)/r.$$

While the above proof applies to (1) and to the outer cylinder, it can also be made to cover (2) and the inside cylinder, and expressions obtained for the extensions and u for it by changing the subscripts 2 to 1 and putting $B_1=0$.

With (1), (2) thus established as possible states of stress it remains to show that the arbitrary elements left, namely, the constants, A_2, B_2, C_2, A_1, C_1, can be made to take care of the interaction between the cylinders. First we equate p_r along the common boundary $r=a$:

$$A_2+B_2/a^2=A_1; \tag{7}$$

then we equate to zero the resultant of the axial stress p_z over a section $z=$constant of *both* cylinders:

$$C_2(b^2-a^2)+C_1a^2=0. \tag{8}$$

Again, since $r=b$ is a free boundary, p_r vanishes there:

$$A_2+B_2/b^2=0. \tag{9}$$

Solving (7), (8), (9) in terms of A_2, C_2 yields:

$$B_2=-A_2b^2, \quad A_1=A_2(1-b^2/a^2), \quad C_1=C_2(1-b^2/a^2). \tag{10}$$

Substituting in (1), (2), we obtain for the stresses:

$$\left.\begin{aligned} p_r &= A_2(1-b^2/r^2) \\ p_\theta &= A_2(1+b^2/r^2) \\ p_z &= C_2 \end{aligned}\right\} \text{for outer cylinder,} \tag{11}$$

$$\left.\begin{aligned} p_r &= p_\theta = A_2(1-b^2/a^2) \\ p_z &= C_2(1-b^2/a^2) \end{aligned}\right\} \text{for inner cylinder.} \tag{12}$$

To determine the two remaining constants A_2, C_2, we bring in the fact that along $r=a$ the displacements are the same. Equating e_z for both cylinders (e_z is independent of r), we obtain from (5) and the corresponding equation for the inner cylinder:

$$-A_2 2\sigma_2/E_2+C_2/E_2-(-A_1 2\sigma_1/E_1+C_1/E_1) =(k_1-k_2)(T-T_0),$$

and substituting from (10):

$$2A_2[\sigma_2/E_2-(1-b^2/a^2)\sigma_1/E_1]-C_2[1/E_2 -(1-b^2/a^2)/E_1]=(k_2-k_1)(T_2-T_1). \tag{13}$$

To equate u at $r=a$, it suffices to equate e_θ there; its value is given by the second of Eqs. (5) for the outer cylinder; and (omitting B and changing subscripts) by

$$E_1e_\theta=A_1(1-\sigma_1)-\sigma_1C_1+E_1k_1(T-T_0) \tag{14}$$

for the inner one. Utilizing (10), we transform the resulting equations into:

$$A_2[(1-\sigma_1)(1-b^2/a^2)/E_1-(1-\sigma_2)/E_2]-C_2[\sigma_1(1-b^2/a^2)/E_1-\sigma_2/E_2]=(k_2-k_1)(T-T_0). \tag{15}$$

Solving (13), (15) for A_2, C_2,

$$\begin{aligned} A_2 &= -(k_2-k_1)(T-T_0)[(1+\sigma_1)(1-b^2/a^2)/E_1+(1-\sigma_2)/E_2]/\Delta, \\ C_2 &= -(k_2-k_1)(T-T_0)[(1-\sigma_1)(1-b^2/a^2)/E_1-(1+\sigma_2)/E_2]/\Delta. \end{aligned} \tag{16}$$

where

$$\Delta=\begin{vmatrix} 2\sigma_2/E_2-(1-b^2/a^2)2\sigma_1/E_1 & -1/E_2+(1-b^2/a^2)/E_1 \\ (1-\sigma_1)(1-b^2/a^2)/E_1-(1-\sigma_2)/E_2 & \sigma_2/E_2-\sigma_1(1-b^2/a^2)/E_1 \end{vmatrix}.$$

This completes the determination of the stresses.

2. Photoelastic Determination of the Stresses

If, in the equations of the preceding section, we replace $T-T_0$ by unity, we obtain the effect per unit rise of temperature. The resulting u at $r=b$ and the extension e_z give the temperature coefficient of increase in radius and the axial coefficient of expansion, respectively. The experimental determination of these extensions furnishes a convenient check upon the applicability of the assumptions upon which the above calculation is based. For glass upon a metal the photoelastic method is available for stress determination. We now proceed to consider this method of stress determination.

For a long and uniform cylinder the optical retardation for a ray parallel to the axis would yield information about the stresses p_r and p_θ directly, except for the end effect correction. A more convenient procedure is to send a ray through in a direction normal to the axis. We proceed to show that the retardation for such a ray depends merely upon p_z and is given by

$$\beta p_z l, \tag{17}$$

where β is the Brewster constant (retardation per unit stress difference per unit length of path), and l is the geometric length of the path. Thus the stresses p_r, p_θ do not show up in this photoelastic test.

To prove this, introduce rectangular x, y coordinates in addition to the polar coordinates employed in the last section with the x-axis along $\theta=0$, and the y-axis at $\theta=\pi/2$. Let i_x, i_y be unit vectors in direction of positive x and y; i_r, i_θ unit vectors in directions of increasing r and θ, respectively. Then

$$\begin{aligned} i_r &= i_x \cos\theta + i_y \sin\theta, \\ i_\theta &= -i_x \sin\theta + i_y \cos\theta. \end{aligned} \tag{18}$$

The stress dyadic is given by

$$p_r i_r i_r + p_\theta i_\theta i_\theta + p_z i_z i_z, \tag{19}$$

where i_z is the unit vector in direction of positive z.

Imagine a plane-polarized ray of light traveling in the direction of the y-axis, at a distance c from the axis (see Fig. 1). The relative optical retardation of the two components of the light vector polarized along the x and z directions is given by

$$\beta \int (p_z - p_x)dy, \tag{20}$$

where p_x, p_z are the stress components in the direction of the x- and z-axes.

It will be recalled that p_z is constant throughout the outer cylinder; the first part of the integral in (20) consequently leads to (17). Consider the latter part, $-\beta \int p_x dy$. To find p_x, replace i_r, i_θ in (19) by their expressions (18) in terms of i_x, i_y and collect terms; the net coefficient of $i_x i_x$ is equal to p_x. In this way we obtain

$$p_x = p_r \cos^2\theta + p_\theta \sin^2\theta,$$

and, substituting from Eqs. (11),

$$\begin{aligned} p_x &= A_2 - A_2(b^2/r^2)(\cos^2\theta - \sin^2\theta) \\ &= A_2 - (A_2 b^2/r^2)\cos 2\theta. \end{aligned}$$

Now, from Fig. 1, $y = c\tan\theta$, $r = c\sec\theta$, and therefore $dy = c\sec^2\theta d\theta$. Thus

$$\begin{aligned} \int p_x dy &= A_2 \int dy - A_2 b^2 \int \frac{\cos 2\theta\, c\sec^2\theta d\theta}{c^2\sec^2\theta} \\ &= A_2 2c\tan\alpha - A_2 b^2(\sin 2\theta)/c2\Big|_{-\alpha}^{\alpha} \\ &= A_2[2c\tan\alpha - 2b^2(\sin\alpha\cos\alpha)/c]. \end{aligned}$$

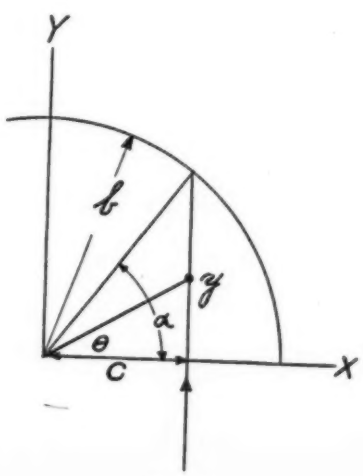

Fig. 1.

But (see Fig. 1), $b^2/c^2=\sec^2\alpha$; hence

$$[2c\tan\alpha-2b^2(\sin\alpha\cos\alpha)/c]$$
$$=2c[\tan\alpha-(b^2/c^2)\sin\alpha\cos\alpha]=0.$$

The above treatment has been simplified in that the stress p_x was treated as if it were a principal stress. Actually the principal stress directions at each point are along the directions of i_r, i_θ (and i_z), and one is confronted with the propagation of a ray in a direction oblique to the principal direction of stress and hence to the axes of the Fresnel quadric. Both the directions of the quadric, as well as the lengths of (two of) its semi-axes, vary along the ray path. As a result the planes of polarization are tilted in a somewhat complicated fashion. (The magnetic vector of a wave front coincides with semi-axes of the ellipse obtained by cutting the Fresnel ellipsoid by a central plane parallel to the wave front, while the wave velocity is inversely as the other semi-axis (see, for instance, Coker, *Photoelasticity*).

To avoid these complexities we note first that the change in the refractive indices due to the elastic stresses is very small, so that the actual deviation of the path of the ray from the assumed rectilinear one is negligible. Furthermore, the joint effect of two portions of the path symmetrically situated about the middle plane $y=0$ is the same as if the stresses were superposed. This would result in a stress distribution whose principal axes are along the x, y and z axes.

3. Effect of Viscous Flow During Anneal

We shall now assume that the material, while retaining its elasticity, also flows like a viscous fluid. Thus, in addition to the elastic extensions given by (3), we have further extensions whose *rates of change* are given by the ordinary viscosity equations of hydrodynamics for an incompressible fluid:

$$de_r/dt=(p_r-p)/2\mu,$$
$$de_\theta/dt=(p_\theta-p)/2\mu, \qquad (21)$$
$$de_z/dt=(p_z-p)/2\mu,$$

where p is the pressure defined by[3] $p=-(p_r+p_\theta+p_z)/3$, and μ the coefficient of viscosity.

The true extensions e_r are the sums of the elastic extensions given by (3) and of the viscous ones occurring in (21). Differentiating (3) and adding to (21), we obtain for the actual extensions

$$de_r/dt=p_r-p/2\mu+[p_r'-\sigma(p_\theta'+p_z')]/E+kT',$$
$$de_\theta/dt=p_\theta-p/2\mu+[p_\theta'-\sigma(p_r'+p_z')]/E+kT', \qquad (22)$$
$$de_z/dt=p_z-p/2\mu+[p_z'-\sigma(p_r'+p_\theta')]/E+kT',$$

where $'$ indicates time-differentiation. Here we have assumed that E, σ remain constant. The temperature T is supposed to be a known function, say decreasing linearly and assumed independent of position, while μ is assumed to be known as a function of temperature.

Eqs. (22) apply to the outside cylinder, which we suppose to be made of glass. For the inside cylinder we suppose that the viscous flow is negligible and thus apply equations (3) directly.

To solve, we assume that Eqs. (1), (2) still apply except that the constants A_2, $\cdots$, C_1 depend upon time. The equilibrium conditions obviously still apply. Furthermore, Eqs. (7), (8), (9) still apply, leading to (11) and (12). Substituting in (22), we obtain for the outer cylinder (with k_2, σ_2, E_2 in place of k, σ, E):

$$\frac{de_r}{dt}=\left(1-\frac{b^2}{r^2}\right)\left[\frac{1+\sigma_2}{E_2}A_2'+\frac{A_2}{2\mu}\right]-\frac{3\sigma_2}{E_2}\frac{2A_2'+C_2'}{3}$$
$$-\frac{2A_2+C_2}{2\mu}+k_2T', \qquad (23)$$
$$\frac{de_\theta}{dt}=\left(1+\frac{b^2}{r^2}\right)\left[\frac{1+\sigma_2}{E_2}A_2'+\frac{A_2}{2\mu}\right]-\frac{2A_2+C_2}{2\mu}+k_2T',$$
$$\frac{de_z}{dt}=\left[\frac{1+\sigma_2}{E_2}C_2'+\frac{C_2}{2\mu}\right]-\frac{2A_2+C_2}{2\mu}+k_2T'.$$

Recalling the second of (4), we may put

$$u'=\left(r+\frac{b^2}{r}\right)\left[\frac{1+\sigma_2}{E_2}A_2'+\frac{A_2}{2\mu}\right]$$
$$+r\left(k_2T'-\frac{3\sigma_2}{E_2}\frac{2A_2'+C_2'}{3}-\frac{2A_2+C_2}{2\mu}\right) \qquad (24)$$

[3] See Lamb, *Hydrodynamics*, 5th Ed., p. 542.

and observe that this checks with

$$\frac{de_r}{dt}=\frac{\partial}{\partial t}\left(\frac{\partial u}{\partial r}\right)=\frac{\partial}{\partial r}\left(\frac{\partial u}{\partial t}\right)=\frac{\partial u'}{\partial r}$$

as given by the first of Eqs. (4) and (23). The "compatibility conditions" are thus fulfilled.

For the inner cylinder the same equations hold as in Section 1. Thus

$$e_\theta=(1-b^2/a^2)[(1-\sigma_1)A_2-\sigma_1C_2]/E_1 +k_1(T-T_0), \quad (25)$$

$$e_z=(1-b^2/a^2)[-2\sigma_1A_2+C_2]/E_1+k_1(T-T_0).$$

Differentiating and equating to the right-hand members of the second Eq. (23) for $r=a$, and to the third Eq. (23), respectively, we obtain two simultaneous linear differential equations in the time functions A_2, C_2, namely:

$$\begin{aligned} a_{11}A_2'+\frac{a_{12}}{\mu}A_2+b_{11}C_2'+\frac{b_{12}}{\mu}C_2&=(k_2-k_1)\frac{dT}{dt},\\ a_{21}A_2'+\frac{a_{22}}{\mu}A_{22}+b_{21}C_2'+\frac{b_{22}}{\mu}C_2&=(k_2-k_1)\frac{dT}{dt}, \end{aligned} \quad (26)$$

where $a_{11}\cdots$ are constants defined by:

$$a_{11}=\left(1-\frac{b^2}{a^2}\right)\left(\frac{1-2\sigma_1}{E_1}\right)-\left(1+\frac{b^2}{a^2}\right)\frac{1+\sigma_2}{E_2}+\frac{\sigma_2}{E_2},$$

$$a_{12}=[(1+b^2/a^2)+4]/2,$$

$$b_{11}=[(1-b^2/a^2)(-\sigma_1/E_1)+\sigma_2/E_2],$$

$$b_{12}=2=a_{22},$$

$$a_{21}=(1-b^2/a^2)(-\sigma_1/E_1)+2\sigma_2/E_2,$$

$$b_{21}=(1-b^2/a^2)(1/E_1)-1/E_2,$$

$$b_{22}=1.$$

4. Solution of the Differential Eqs. (26)

The differential Eqs. (26) have to be solved subject to the initial conditions $A_2=C_2=0$ for $t=0$ and $T=T_0$. They admit of the following special treatment: multiply the second equation by λ and add to the first, where λ is as yet an undetermined constant multiplier. There results:

$$(a_{11}+\lambda a_{21})A_2'+\frac{a_{12}+\lambda a_{22}}{\mu}A_2+(b_{11}+\lambda b_{21})C_2' +\frac{b_{12}+\lambda b_{22}}{\mu}C_2=(1+\lambda)(k_2-k_1)\frac{dT}{dt}. \quad (27)$$

Now inquire whether there exist values of λ for which the coefficients of A_2', A_2 are proportional to those of C_2', C_2:

$$\frac{a_{11}+\lambda a_{21}}{b_{11}+\lambda b_{21}}=\frac{a_{12}+\lambda a_{22}}{b_{12}+\lambda b_{22}}=\text{say } \nu. \quad (28)$$

This leads to the quadratic in λ

$$\begin{vmatrix} a_{11}+\lambda a_{21} & b_{11}+\lambda b_{21} \\ a_{12}+\lambda a_{22} & b_{12}+\lambda b_{22} \end{vmatrix}=0.$$

Let λ_1, λ_2 be its roots and let ν_1, ν_2 be the corresponding value of either fraction in (28). Then for $\lambda=\lambda_1$, Eq. (27) can be put in the form

$$(b_{11}+\lambda_1b_{21})[A_2'+\nu_1C_2'] +[(b_{12}+\lambda_1b_{22})/\mu][A_2+\nu C_2] =(1+\lambda_1)(k_2-k_1)dT/dt.$$

This constitutes a first order differential equation for the function $A_2+\nu_1C_2$. Its solution, vanishing for $t=0$, is given by:

$$[A_2+\nu_1C_2]=\frac{(1+\lambda_1)(k_2-k_1)dT/dt}{b_{11}+\lambda_1b_{21}} =\frac{(1+\lambda_1)(k_2-k_1)}{b_{11}+\lambda_1b_{21}}\frac{dT}{dt}\times \int_0^t \exp\left(-\frac{b_{12}+\lambda_1b_{22}}{b_{11}+\lambda_1b_{21}}\int_s^t\frac{d\tau}{\mu[T(\tau)]}\right)ds. \quad (29)$$

A similar expression is obtained for $A_2+\nu_2C_2$ with λ_1 replaced by λ_2. From these equations A_2 and C_2 can be solved for and turn out to be proper linear combinations of the right-hand members of (29) and the similar expression with λ_2.

A similar treatment could be given for the case in which E is also assumed to depend on the temperature and in which flow in the inner cylinder is not neglected.

It has been assumed above that the viscosity is a function of temperature only. Now J. T. Littleton[4] and others claim that even at constant temperature viscosity changes with time, and ascribe it to the changing chemical composition of the glass. Obviously the above treatment can be applied once the viscosity has been determined as a time function for the particular mode of temperature variation employed, say from a simple tensile test specimen. Furthermore, extension of the solution is easily carried out to the case where the temperature coefficient of expansion k_2 is not constant but a known function of temperature.

Note Added November 2, 1934. The great simplicity of the conclusion arrived at in Section 2 concerning the vanishing of $\int p_x dy$ and its importance from the point of view of interpretation of photoelastic stress determination made it desirable to find out to what extent this conclusion can be generalized, for example for cases in which viscous flow has taken place during anneal and relieved some of the stress, and for glass rods strained by rapid cooling. The following proof is simpler than the one given in the text and shows that the conclusion still holds in very much more general circumstances.

Consider the integral or resultant of the stress X_x over the path of a ray in Fig. 1; it represents the net traction or resultant force in the direction of the x-axis that is applied by the material to the right of the ray upon that to its left, per unit length of z. If, now, no shearing stresses X_z are assumed to exist, and if the outer boundary is free from stresses, the net forces in the x-direction acting on the portion of the materiai to the right of the ray are equal to the negative of the above integral $\int p_x dy$. Since the portion of the material to the right of the ray is in equilibrium, this integral vanishes.

Applying this to the problem of optical retardation, we see that if the Brewster constant is really constant along the path of the ray the retardation will depend only upon the axial stress. This conclusion holds irrespective of how the stresses are produced, whether by temperature expansion, viscous flow, or otherwise. For instance, there may be several cylinders shrunk on one another with entirely different coefficients of thermal expansion and they may have been taken through any cycle of annealing operations. The condition $\int p_x dy$ still holds, provided the Brewster constant of their materials is the same. This is still true if the circular cylinder is replaced by a cylinder of any other shape just as long as there is symmetry about the middle plane perpendicular to the ray of light, the stresses are independent of z, and the shearing stress X_z vanishes.

To complete the above proof, one has to take into consideration the fact that the directions of principal stress would not coincide with the direction of the travel of the ray. This can be done by means of the same symmetry considerations that were employed in Section 2.

[4] Littleton, J. Am. Ceramic Soc. **17**, 47 (1934).

Fatigue and Crystal Recovery in Aluminum

HOWARD A. SMITH,* *Metals Research Laboratory, Carnegie Institute of Technology, Pittsburgh, Pennsylvania*

(Received August 18, 1934)

The previous x-ray work on fatigue in metals is reviewed. Such work has been confined to copper, silver and steel. The present note reports on the results of an investigation of service fatigue fractures in high voltage transmission cables made of commercially pure aluminum. The crystals composing the shallow surface layer of the fractures were found to have recovered sufficiently from the microscopic distorsion due to cold drawing that individual monochromatic diffraction spots could be identified. Two possible contributing causes are suggested to explain this crystalline recovery.

INTRODUCTION

X-RAY methods have been used to a limited extent only for investigating fatigue failures of metals. Dehlinger[1] and Pfarr[2] found a decrease of monochromatic diffraction line width in fatigued cold rolled copper and silver, and for hardened steel, respectively. The grain size and conditions of strain were such as to give continuous diffraction lines. Such behavior is characteristic of the first stages of microscopic recrystallization, i.e., recovery of the crystals from microscopic strain. Regler[3] found a definite increase in radial width of monochromatic diffraction spots following the fatigue of low carbon annealed steel. If the results of Dehlinger and Pfarr and of Regler seem contradictory it should be noted that the metals before fatigue were in very different conditions as regards grain size and internal strain. On cold working aluminum, tin, zinc and lead at room temperature Dehlinger[4] found negligible increase of diffraction line width, while Thomassen and Wilson[5] found an increase of line width in aluminum compressed at $-75°C$. Wood[6] reporting on an x-ray investigation of constantly increasing unidirectional torsion in fine grained copper and nickel finds that the most highly distorted crystals disrupt and tend to recrystallize adopting a new orientation in a less distorted state.

The present communication deals with an investigation of service fatigue failures in high voltage aluminum power transmission cables during which advanced stages of recovery from cold work were noticed at the fatigue breaks.

FATIGUE CONDITIONS

The all aluminum cables were made up of seven strands of commercially pure cold drawn aluminum, one centrally located, each 0.495 cm in diameter. The cables broke in service within the temperature range $-7°C$ to $49°C$ about 5 m from the support while being subjected to a direct tensile stress, due to the weight of the cable, of 880 kg per sq. cm. The elastic limit and ultimate tensile strength were, respectively, 985 and 1690 kg per sq. cm. These cable breaks occurred in the following manner: One or two strands broke throughout their cross section by fatigue and two or three partly across their section by fatigue. The stress thrown on the remaining section of the cable, two to four sound strands and the sections that remained of those strands partly broken by fatigue, then exceeded the tensile strength and the cable failed by direct tension. No matter from what material such cables be made there are many factors[7] which enter into the causes of such breaks. Of these factors, cycles of repeated stress due to vibration of the cable by wind forces is a major one. A 10.7 km per hour wind at $-7°C$ is considered the most unfavorable condition under which these cables operated.

RESULTS OF THE INVESTIGATION

These cables 15 cm from the fractures had a barely distinguishable zonal structure and a

* National Research Fellow.

[1] U. Dehlinger, Naturwiss. **17**, 545 (1929).

[2] B. Pfarr, Zeits. f. tech. Physik **14**, 220 (1933).

[3] F. Regler, Mitt. staatl. tech. Versuchsamt **21**, 31 (1932).

[4] U. Dehlinger, Zeits. f. Kristallographie **65**, 615 (1927).

[5] L. T. Thomassen and J. E. Wilson, Phys. Rev. **43**, 763 (1933).

[6] W. A. Wood, Nature **131**, 842 (1933).

[7] Committee Report, Zeits. f. Metallkunde **24**, 285 (1932).

fibered crystalline orientation of the normal type for aluminum ([111] parallel to the wire axis). X-ray transmission photograms showed intense radial asterism particularly when the beam was perpendicular to the wire and fiber axis. The grain size microscopically determined was 5–10μ. The (333), (224), (024) and (133) diffraction lines in back reflection photograms taken with copper radiation from the surface of the breaks reveal many distinct randomly arranged intensity maxima within the diffraction lines, due to individual diffraction spots from a layer of randomly oriented crystals. A composite line of similar appearance to that from the fatigue break was made by first obtaining a line from the normal structure and superimposing upon it the diffraction spots from the same structure after heating for 1 hour at 250°C. Microscopic examination of such an annealed sample gave no definite indication of macroscopic recrystallization. The diffraction lines from the normal structure and from the tension breaks were uniform in intensity throughout. Photograms taken after successive etchings indicated that the strain relieved crystals responsible for the intensity maxima formed a layer approximately one crystal thick. These advanced stages of crystal recovery were found to exist evenly over the breaks in those strands broken entirely by fatigue and to exist evenly up to the line of demarkation in the fractures of those strands broken partly by fatigue and partly by direct tension.

Precise lattice parameter measurements ($a_0 = 4.010$A) indicated that no appreciable quantities of foreign elements were present in solid solution. The presence of intermetallic compounds or other phases could not be detected. Spectrographic analyses showing very small quantities of silicon, iron and copper bore out the parameter measurements. These cable fatigue breaks, then are probably not complicated by the presence of several phases which may influence the failure[8, 9] of aluminum having larger quantities of alloying elements present.

[8] G. L. Clark and H. A. Smith, Phys. Rev. **43**, 305 (1933).
[9] L. W. Kempf, Phys. Rev. **43**, 942 (1933).

Discussion of Results

Since the transition from a strained metastable atomic arrangement to an unstrained state of equilibrium is accompanied by a decrease in entropy an acceleration of this process may be accomplished by supplying energy to the system. Of all the forms in which energy exhibits itself only those which are capable of directly increasing the atomic mobility can be considered as effective. Under the circumstances of the case here considered it seems likely that heat and work applied directly to the crystal lattice are the most effective in increasing atomic mobility. The possible sources of energy necessary for rapid return to the unstrained state of equilibrium may include, (a) heat from internal friction, (b) heat from the increased electrical load in the region of failure of the cable due to the fracture of strands and the resulting decrease in cross section, (c) heat from sparking between the two ends of the fractured strand, (d) work supplied to the crystals by plastic deformation from attrition, between the ends of a partially broken strand, due to cable vibration, and (e) heat and work supplied to the atoms[10, 11, 12] from the process of slip within the crystal, i.e., plastic deformation leading to rupture as a result of the high stress gradients at the van of the fatigue crack.

Heat from (a) and (b) effective in this microscopic recrystallization is improbable because of the very limited and well-defined region over which the effect was observed. Heat from (c) is probably just as ineffective because the potential difference between the ends of a fractured strand is very likely not sufficient to give a spark and because the strain relieved layer of crystals extended evenly over all sections broken in fatigue.

Often repeated cycles of small amounts of work and hence also of some heat from (d) may be considered as at least a contributing cause for the observed crystalline recovery. That such action may take place before complete rupture

[10] W. S. Farren and G. I. Taylor, Proc. Roy. Soc. (London) **A107**, 422 (1925).
[11] M. F. Sayre, Proc. Am. Soc. Test. Materials II, **32**, 548 (1932).
[12] A. W. Stepanow, Zeits. f. Physik **81**, 560 (1933).

of a member may be inferred from the often observed smooth and shiny appearance of a fatigue fracture.

In (e) we have a source of heat and work which while probably acting only momentarily supplies energy in large amounts over successive minute regions as the fatigue crack advances. If this source of energy is assumed to be effective the failure to find the localized region of low entropy in the tension breaks may be conceived to be due to the differences in stress gradients in the two types of failure and thus to differences in the rate of strain and the intensity of the energy available for returning the crystal system to equilibrium.

Whatever the forces causing this effect may be they must have been effective within a short period of time just preceding, during or immediately following crystalline rupture because of the very limited region within which the crystal recovery took place and because of the even distribution of the effect.

Author Index to Volume 5

Ambrose, H A. (see Loomis, A. G.)—207

Barnes, Colin. Diffusion through a membrane—4
Barton, Lois E. (see Parks, George S.)—193
Beeuwkes, R. Concerning the effect of strain and rate of strain on tensile tests at normal and elevated temperatures—135
Bingham, Eugene C. and Johns A. Geddes. Further studies on the relation between constitution and association: especially in reference to aromatic compounds—42
——— **and Robert A. Stephens.** Alternating stress method for the measurement of the consistency of very still materials—217
Bloomenthal, S. Nonmetallic conducting films—225
Botset, Holbrook G. Radium content of some connate waters—276
——— (see Wyckoff, R. D.)—265
Bozorth, R. M. (see Haworth, F. E.)—15
Bridgeman, Oscar C. What is oiliness?—125
Brown, Lawrence E. On the theory of an *N*-winding transformer—61
Browne, T. E., Jr. Dielectric recovery of a.c. arcs in turbulent gases—103
Burger, E. E. (see Hull, Albert W.)—384

Chapman, Seville. Charges on droplets produced by the spraying of liquids as revealed by the Millikan oil drop method—150
Clark, George L. and Julia Southard. Sorption on cotton fibers of dyes with varying molecular association in solution—95
Crary, A. P. (see Ewing, Maurice)—165; 181; 317

Dehlinger, Walter. Space charge grid tube with variable mu grid—173

Ewart, R. H. (see Mooney, M.)—350
Ewing, Maurice and A. P. Crary. Study of emergence angle and propagation paths of seismic waves—317
———, **A. P. Crary and A. M. Thorne, Jr.** Propagation of elastic waves in ice. Part I—165
——— **and A. P. Crary.** Propagation of elastic waves in ice. Part II—181

Fink, George A. (see Fox, Gerald W.)—302
Fox, Gerald W. and George A. Fink. Piezoelectric properties of quartz and tourmaline—302

Geddes, John A. (see Bingham, Eugene C.)—42
Gray, Marion C. Mutual impedance of grounded wires lying on the surface of the earth when the conductivity varies exponentially with depth—35

Hasler, M. F. Thermoelectric metal-crystal analyzer—9
Haworth, F. E. and R. M. Bozorth. Shot effect and electrical breakdown in insulators—15
Hickman, Roger W. Investigation of an alternating-current method of determining critical potentials—185
Hulburt, E. O. Absorption of heat rays by fog—101
Hull, Albert W. and E. E. Burger. Glass-to-metal seals—384
Hurst, William. Unsteady flow of fluids in oil reservoirs—20

Ingberg, S. H. Methods for calculating the volumetric composition of fluid mixtures—64

Jesse, William P. X-ray crystal measurements of nickel at high temperatures—147

Kelsall, G. A. Permeability changes in ferromagnetic materials heat treated in magnetic fields—169
Kennedy, H. T. (see Loomis, A. G.)—207
Kiehl, H. R. Electrical conductivity of glass. Part I. The formation of highly resistant layers—363; Part II. Current increase phenomena with highly resistant layers—370
Kuethe, A. M. (see Wattendorf, F. L.)—153

LaCoste, Lucien J. B., Jr. New type long period vertical seismograph—178
Loomis, A. G., H. A. Ambrose and H. T. Kennedy. Some rheologic aspects of petroleum production—207

MacGregor, C. W. Concerning the distribution of stress in a laterally compressed strip—140
Madge, E. W. Viscosities of liquids and their vapor pressures—39
Merkel, Wilhelm. Flow characteristics of sewage sludge and other thick materials—355
Meserve, Wilbur E. Behavior of a copper oxide photoelectrolytic cell when used with sinusoidally varying illumination—244
Mooney, M. and R. H. Ewart. Conicylindrical viscometer—350
Muskat, Morris. Flow of compressible fluids through porous media and some problems in heat conduction—71
——— Two fluid systems in porous media The encroachment of water into an oil sand—250

Neitzert, C. Thermal agitation voltages in resistors—292
Parks, George S., Lois E. Barton, Monroe E. Spaght and J. Wilfred Richardson. Viscosity of undercooled liquid glucose—193
Pearson, G. L. Fluctuation noise in vacuum tubes—233

Pekeris, Chaim L. Inverse boundary value problem in seismology—307
Pichot, M. Viscosity anomalies—200
Pittman, C. U. and R. N. Traxler. Rheological properties of asphalts. I. Effect of temperature—221

Poritsky, Hillel. Analysis of thermal stresses in sealed cylinders and the effect of viscous flow during anneal—406

Rashevsky, N. Mechanism of division of small liquid systems which are the seats of physico-chemical reactions—374
Reber, R. K. Effect of nascent hydrogen on the magnetic properties of iron—297
Reiner, Markus. Theory of non-Newtonian liquids—321
——— Viscometric studies of rubber solutions—342
Richardson, J. Wilfred (see Parks, George S.)—193
Richmond, W. O. Creep of wires at high temperature—131

Schilling, Harold K. Mosaic crystals of zinc—1
Smith, Howard A. Fatigue and crystal recovery in aluminum—412
Southard, Julia (see Clark, George L.)—95
Spaght, Monroe E. (see Parks, George S.)—193
Steinberger, R. L. Stress-strain relation in textile fibers—53
Stephens, Robert A. (see Bingham, Eugene C.)—217
Stevenson, A. F. On the theoretical determination of earth resistance from surface potential measurements—114
Suits, C. G. Stabilizing arcs by electrode surfacing—380

Thorne, A. M., Jr. (see Ewing, Maurice)—165
Traxler, R. N. (see Pittman, C. U.)—221

Wadell, Hakon. Some new sedimentation formulas—281
Wattendorf, F. L. and A. M. Kuethe. Investigations of turbulent flow by means of the hot-wire anemometer—153
Wissink, G. M. Magneto-optic method of determining the vitamin content of various substances—31
Wyckoff, R. D. and H. G. Botset. Experimental study of the motion of particles in systems of complex potential distribution—265

Analytic Subject Index to Volume 5

Absorption
Of dyes by cotton fibers, G. L. Clark, J. Southard—95
Absorption and reflection of light
Heat rays absorbed by fog, E. O. Hulburt—101
Acoustics
Elastic waves in ice, M. Ewing, A. P. Crary, A. M. Thorne, Jr.—165
Flexural and transverse waves in ice, M. Ewing, A. P. Crary—181
Aerodynamics (see also **Hydrodynamics**)
Turbulent flow measured by hot wire anemometer, F. L. Wattendorf, A. M. Kuethe—153
Volumetric composition of mixtures of gases, S. H. Ingberg—64
Arcs (see also **Discharge of electricity in gases**)
Extinction of a.c. arcs, T. E. Browne, Jr.—103
Stabilizing arcs by electrode surfacing, C. G. Suits—380

Conductivity, electrical (see **Electrical conductivity; Discharge of electricity in gases**)
Crystalline state
Creep of wires at high temperature, W. O. Richmond—131
Fatigue and crystal recovery in Al, H. A. Smith—412
Mosaic structure in Zn, H. K. Schilling—1
Nascent H_2 and magnetic properties of Fe, R. K. Reber—297
Permeability changes in magnetic alloys, G. A. Kelsall—169
Piezoelectric properties of quartz and tourmaline, G. W. Fox, G. A. Fink—302
Strain and rate of strain at various temperatures, R. Beeuwkes—135
Thermal expansion of Ni lattice, W. P. Jesse—147
Crystals, structure
Of Ni at high temperatures, W. P. Jesse—147

Diffusion
Of gases and volumetric composition of mixtures, S. H Ingberg—64
Of liquid through a membrane, C. Barnes—4
Discharge of electricity in gases (see also **Arcs**)
Stabilizing arcs by electrode surfacing, C. G. Suits—380

Elasticity
Creep of wires at high temperature, W. O. Richmond—131
Distribution of stress in a laterally compressed strip, C. W. MacGregor—140
Elastic waves in ice, M. Ewing, A. P. Crary, A. M. Thorne, Jr.—165
Emergence angle and paths of seismic waves, M. Ewing and A. P. Crary—317
Fatigue and crystal recovery in Al, H. A. Smith—412
Flexural and transverse waves in ice, M. Ewing and A. P. Crary—181
Inverse boundary value problem in seismology, C. L. Pekeris—307
Strain and rate of strain at various temperatures, R. Beeuwkes—135
Stress-strain relation in textile fibers, R. L. Steinberger—53
Thermal stresses in sealed cylinders, viscous flow during anneal, H. Poritsky—406
Electrical circuits
N-winding transformer, theory of, L. E. Brown—61
Thermal agitation voltages in resistors, C. Neitzert—292
Electrical conductivity and resistance
Breakdown in insulators, F. E. Haworth, R. M. Bozorth—15
Earth resistance from surface potential measurements, A. F. Stevenson—114
Of glass, current increase with highly resistant layers, H. R. Kiehl—370
Of glass, formation of highly resistant layers, H. R. Kiehl—363
Mutual impedance of wires on surface of earth, M. C. Gray—35
Of nonmetallic films, S. Bloomenthal—225
Electrons in metals
Thermal agitation voltages in resistors, C. Neitzert—292
Electron tubes (see **Vacuum tubes**)
Electrostatics
Charges on droplets produced by spraying, S. Chapman—150

Fluidity (see **Viscosity**)
Friction
What is oiliness? O. C. Bridgeman—125

Geophysics
Earth resistance from surface potential measurements, A. F. Stevenson—114
Elastic waves in ice, M. Ewing, A. P. Crary, A. M. Thorne, Jr.—165
Emergence angle and paths of seismic waves, M. Ewing, A. P. Crary—317
Inverse boundary value problem in seismology, C. L. Pekeris—307
Ra content of connate waters, H. G. Botset—276
Vertical seismograph, long period, L. J. B. LaCoste, Jr.—178

Hydrodynamics (see also **Aerodynamics**)
Flow characteristics of thick materials, W. Merkel—350
Flow of compressible fluids through porous media, M. Muskat—71
Motion of particles in systems of complex potential distribution, R. D. Wyckoff, H. G. Botset—265
New sedimentation formulas, H. Wadell—281
Theory of non-Newtonian liquids, M. Reiner—321
Two fluid systems in porous media, M. Muskat—250
Unsteady flow in oil reservoirs, W. Hurst—20

Instruments (see **Methods and instruments**)
Insulators
Shot effect and electrical breakdown, F. E. Haworth, R. M. Bozorth—15
Isotopes
Diffusion through a membrane, C. Barnes—4

Liquids (see also **Hydrodynamics**)
Division of small liquid systems, N. Rashevsky—374
Flow of compressible fluids through porous media, M. Muskat—71
Unsteady flow in oil reservoirs, W. Hurst—20

Magnetic properties
Alloys heat treated in magnetic fields, permeability changes, G. A. Kelsall—169
Effect of nascent H_2 on Fe, R. K. Reber—297
Magneto-optical effects
Determination of vitamin content, G. M. Wissink—31
Meteorology
Charges on droplets produced by spraying, S. Chapman —150
Methods and instruments
Alternating stress method for measurement of consistency of materials, E. C. Bingham, R. A. Stephens —217
Conicylindrical viscometer, M. Mooney, R. H. Ewart—350
Critical potentials, a.c. method, R. W. Hickman—185
Glass-to-metal seals, A. W. Hull, E. E. Burger—384
Motion of particles in systems of complex potential distribution, R. D. Wyckoff, H. G. Botset—265
N-winding transformer, theory of, L. E. Brown—61
Photoelectrolytic cell, characteristics, W. E. Meserve—244
Ra in waters, H. G. Botset—276
Rheologic aspects of petroleum production, A. G. Loomis, H. A. Ambrose, H. T. Kennedy—207
Solutions of heat conduction problems, M. Muskat—71
Thermoelectric metal-crystal analyzer, M. F. Hasler—9
Turbulent flow measured by hot wire anemometer, F. L. Wattendorf, A. M. Kuethe—153
Vertical seismograph, long period, L. J. B. LaCoste, Jr. —178

Petroleum production
Encroachment of water into an oil sand, M. Muskat—250
Flow of compressible fluids through porous media, M. Muskat—71
Motion of particles in systems of complex potential distribution, R. D. Wyckoff, H. G. Botset—265
Rheologic aspects of petroleum production, A. G. Loomis, H. A. Ambrose, H. T. Kennedy—207
Unsteady flow in oil reservoirs, W. Hurst—20
Photoelasticity
Distribution of stress in a laterally compressed strip, C. W. MacGregor—140

Photoelectric effect and properties; cells
CuO cell, varying illumination, W. E. Meserve—244
Plasticity
Theory of non-Newtonian liquids, M. Reiner—321
Polymerization
In aromatic compounds, E. C. Bingham, J. A. Geddes—42
Potentials, critical
a.c. method, R. W. Hickman—185

Radio
Fluctuation noise in vacuum tube, G. L. Pearson—233
Space charge grid tube with variable mu grid, W. Dehlinger—173
Radioactivity
Ra content of connate waters, H. G. Botset—276

Sedimentation
New sedimentation formulas, H. Wadell—281
Solid state (see **Crystalline state**)
Sorption (see **Absorption**)

Thermal conductivity
Solutions of problems in heat conduction, M. Muskat 71
Thermal expansion
Glass-to-metal seals, A. W. Hull, E. E. Burger—384 —
Of Ni, from x-ray data, W. P. Jesse—147
Thermal stresses in sealed cylinders, viscous flow during anneal, H. Poritsky—406
Thermoelectric effects
Metal-crystal analyzer, thermoelectric, M. F. Hasler—9

Vacuum tubes
Fluctuation noise, G. L. Pearson—233
Variable mu tube, space charge grid, W. Dehlinger—173
Vapor pressure
And viscosities of liquids, E. W. Madge—39
Viscosity
Alternating stress method for measurement of consistency of materials, E. C. Bingham, R. A. Stephens —217
Some anomalies, M. Pichot—200
Conicylindrical viscometer, M. Mooney, R. H. Ewart—350
Consistency of asphalt, effect of temperature, C. U. Pittman, R. N. Traxler—221
Factor in petroleum production, A. G. Loomis, H. A. Ambrose, H. T. Kennedy—207
Of 15 ortho, meta and para compounds, E. C. Bingham, J. A. Geddes—42
Flow characteristics of thick materials, W. Merkel—355
And "oiliness," O. C. Bridgeman—125
Of rubber solutions, M. Reiner—342
Theory of non-Newtonian liquids, M. Reiner—321
Of undercooled liquid glucose, G. S. Parks, L. E. Barton, M. E. Spaght, J. Wilfred—193
And vapor pressure, E. W. Madge—39